INVESTIGATION OF STRONG EARTHQUAKE

GROUND MOTION

Thesis by

Mihailo Dimitrije Trifunac

In Partial Fulfillment of the Requirements

For the Degree of

Doctor of Philosophy

California Institute of Technology

Pasadena, California

1969

(Submitted May 20, 1969)

ACKNOWLEDGEMENTS

ABSTRACT

The pattern of energy release during the Imperial Valley,
California, earthquake of 1940 is studied by analysing the El Centro
strong motion seismograph record and records from the Tinemaha
seismograph station, 546 km from the epicenter. The earthquake was
a multiple event sequence with at least 4 events recorded at El Centro
in the first 25 seconds, followed by 9 events recorded in the next 5
minutes. Clear P, S and surface waves were observed on the strong
motion record. Although the main part of the earthquake energy was
released during the first 15 seconds, some of the later events were as
large as M = 5.8 and thus are important for earthquake engineering
studies. The moment calculated using Fourier analysis of surface
waves agrees with the moment estimated from field measurements of
fault offset after the earthquake. The earthquake engineering sig-
nificance of the complex pattern of energy release is discussed. It is
concluded that a cumulative increase in amplitudes of building vibra-
tion resulting from the present sequence of shocks would be signifi-
cant only for structures with relatively long natural period of vibra-
tion. However, progressive weakening effects may also lead to
greater damage for multiple event earthquakes.

The model with surface Love waves propagating through a single
layer as a surface wave guide is studied. It is expected that the de-
rived properties for this simple model illustrate well several phe-
nomena associated with strong earthquake ground motion. First, it
is shown that a surface layer, or several layers, will cause the main

part of the high frequency energy, radiated from the nearby earthquake, to be confined to the layer as a wave guide. The existence of the surface layer will thus increase the rate of the energy transfer into the man-made structures on or near the surface of the layer. Secondly, the surface amplitude of the guided SH waves will decrease if the energy of the wave is essentially confined to the layer and if the wave propagates towards an increasing layer thickness. It is also shown that the constructive interference of SH waves will cause the zeroes and the peaks in the Fourier amplitude spectrum of the surface ground motion to be continuously displaced towards the longer periods as the distance from the source of the energy release increases.

TABLE OF CONTENTS

INTRODUCTION

The motivation for a detailed study of strong earthquake ground motion and the related problems which lead to the full understanding of these phenomena is clearly evident. The importance of a knowledge of the detailed properties and characteristics of strong earthquake ground motion at a given site is obvious to anyone concerned with construction of buildings or other structures which must meet "earthquake resistance" requirements. Consequently many studies in this field have been carried out in order to analyze the most important aspects of the problem.

It is convenient to consider a partition of the studies of strong earthquake ground motion and related phenomena into two groups, according to the order in which they occur in time and equivalently in space. The first group of these studies is concerned with the mechanism of earthquake generation. Here problems related to the pattern of energy release at the source of the seismic energy radiation, dimensions and a kind of source, multiplicity of the source, as well as the propagation and radiation patterns may be analyzed. In short one might think of these as the properties of the generalized forcing function, to be applied to the surrounding medium, together with the appropriate initial and boundary conditions.

The second group of the studies would be concerned with what happens to the seismic waves that are emitted from the source into the surrounding medium. Various properties of the medium along the path of the wave propagation such as velocities, nonhomogeneities of

the elastic constants, nonuniformity of the boundaries of the medium, etc., would be analyzed in order to predict their effect on the seismic wave propagation.

CHAPTER I

PATTERN OF ENERGY RELEASE DURING THE IMPERIAL VALLEY, CALIFORNIA, EARTHQUAKE OF 1940

NOMENCLATURE

A — area of the fault plane over which slip occurs

$A(t)$ — envelope of the vibration amplitude

$a(t)$ — window amplitude

A_L — Love wave amplitude factor

b — fault length

C — phase velocity

$F(\omega, t^*, \Delta t)$ — moving window Fourier spectrum

f — frequency

$f(t), f_{\Delta t}^*(t)$ — instrument record trace

M_o — seismic moment associated with a double couple source

$M_{0-SEISM}^i, M_{0-SEISM}^{TOT}, M_{0-field}$ — seismic moment of a single event, seismic moment of all events, and the total field moment, respectively

$M_L^{S.M.}$ — local magnitude estimated using the strong motion instrument

p — circular frequency of vibration of a one degree of freedom system

Q — attenuation constant

T — period ($= 2\pi/\omega$)

T_o — period at which moment is evaluated

t — time coordinate

t^* - center time of moving Fourier window

$t_{1/20}$ - time at which the vibration amplitude has decreased to 1/20 of the initial value

U   - group velocity

u_θ^{dc} - component of the displacement field in θ direction due to a double couple source

u   - spectral density determined from the record

$\bar{u}$ - weighted average of the fault slip

v   - velocity of source propagation

$W_{\Delta t}(t^*)$ - window amplitude

x   - characteristic coordinate describing the vibration of a one degree of freedom system

α - compressional wave velocity

β - shear wave velocity

δ - angle between u_θ^{dc} and EW component

θ - strike direction

Δ - source distance

Δt - window width

ζ - fraction of the critical damping

μ - rigidity

ρ - density

ω - circular frequency ($= 2\pi f$)

A. INTRODUCTION

In this study records of the Imperial Valley, California earthquake of 1940 are analyzed to obtain information about the complexity of the source function in time and space. The results of the study indicate that the Imperial Valley earthquake was characterized by multiple events that occurred in the first 15 seconds and several later events (in the next 5 minutes) which could be called aftershocks, but which, in some cases, were comparable in magnitude to the events in the main sequence. Thus this earthquake, which has often been described in earthquake engineering studies as a typical moderate-sized destructive earthquake, had a complicated pattern of energy release. Numerous examples of a complex pattern of energy release for larger earthquakes may be found in the literature (Florensov and Solonenko, 1963; Wyss and Brune, 1967; among others).[*]

The Imperial Valley earthquake centered along a well defined fault, and after the earthquake the fault offset was documented in detail (Buwalda, unpublished field notes; Richter, 1958). This allows estimation of the moment from field evidence, and thus gives an independent check on the results obtained from the instrumental records. The first portion of the El Centro strong motion accelerogram used in this study has a special significance for earthquake engineering, since, considering both duration and amplitude, it is the strongest earthquake ground motion yet recorded.

Documentation of the pattern of energy release is important for

---

[*]References are listed in alphabetical order at end of thesis.

engineering applications first because the duration and character of the shaking are the important factors controlling damage in structures. Secondly, the distance between the source of major energy release and a given structure is also closely related to damage.

B. DESCRIPTION OF THE IMPERIAL FAULT

The Imperial fault is a northwest trending fault of the San Andreas fault system in southern California. It was discovered as a result of the earthquake of 1940 (Buwalda and Richter, 1958) although the existence of a major structural break along this line is also indicated by geophysical evidence (Biehler et al., 1964) as well as by the existence of a pronounced scarp at the northwestern end.

The recent motion along the fault has been almost pure right lateral strike-slip. The fault trace is nearly straight (Figure 1.1a) except close to the northern end where the fault curves and branches and has a small amount of dip slip. The amount of right lateral motion for the Imperial Valley earthquake has been recorded in detail at various points along the fault (Figure 1.9; Buwalda, unpublished field notes; Richter, 1958). The maximum offset was 5.8 meters and the average offset along the 65 km fault trace was 1.25 m. Geodetic measurements of the rate of the decrease of displacement away from the fault indicate a depth of faulting of about 7 km (by fitting the data of Byerly and DeNoyer, 1958, with the theoretical curve obtained by Knopoff, 1958). A map and aerial photo of the fault
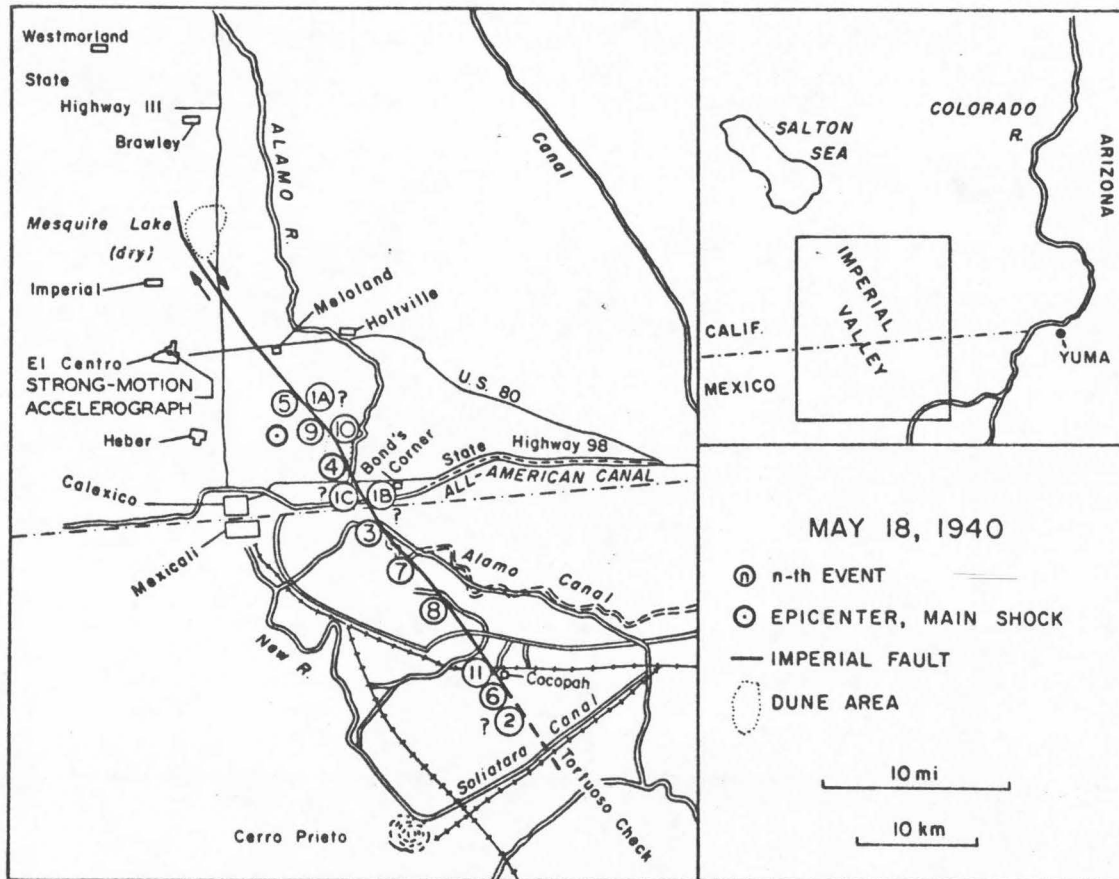
Figure 1. 1a.   Map (after Richter, 1958) indicating the location of
the Imperial fault and the epicenter of the main shock.
Locations of individual events studied here have been added.

Figure 1.1b. Aerial photo of the Imperial fault taken shortly after the 1940 earthquake. The orange grove in this photograph lies south of the Cole Road near the point on the fault nearest to Bonds Corner.

trace are given in Figures 1.1a and 1.1b. The map is modified after
Richter (1958). The aerial photo was taken shortly after the 1940
earthquake.

C. EPICENTER OF THE MAIN SHOCK AND AFTERSHOCKS

Because all close stations were on one side of the epicenter of
the main shock, the epicenter could not be determined very accurately.
The epicenter given in Richter (1958) is indicated in Figure 1.1a.
Concerning the epicenter of the aftershocks, Richter (1958) may be
quoted: ". . . the epicenter of the aftershock at 9:53 p.m. on May 18
cannot be located instrumentally with the desirable precision, nor
can any of the immediate aftershocks. Nearly all the large aftershocks
were later members of bursts of successive earthquakes, of which the
first were too small to be clearly recorded, while the later ones were
large enough to confuse the recording of the following largest shocks
in each group." The Quarterly Bulletin of Local Shocks of the Seis-
mological Laboratory of the California Institute of Technology lists
48 aftershocks in the period 19 May 1940, 4:36 (GCT) to the end of
1940. The first 29 of these recorded aftershocks, with magnitude
ranging from 2.0 to 5.5, occurred in the 4 days immediately after the
main shock. In this study the primary concern is with the sequence
of large events occurring in the first 6 minutes after the origin time
of the main event.

D. INTERPRETATION OF THE EL CENTRO
STRONG MOTION RECORD

In order to investigate the nature of energy release in this
earthquake the El Centro strong motion records for the first 6 minutes
after the instrument was triggered were studied. It is of interest to
note that the usually reproduced "standard" accelerogram used for
many engineering investigations (Figure 1.2a) consists only of the
first 30 seconds, including the first four shocks and omitting later
also significant events. The resolution of individual events in a
complicated pattern of energy release depends critically on the
distance of the recording station (because of dispersion) and the fre-
quency of the waves analyzed. For this reason the high frequency
strong motion recording close to the source of the energy release is
of great importance for this work. Clearly recorded P and S waves,
and in most cases, surface waves, were observed for several events.
These events are shown in Figure 1.2a to Figure 1.2k. The P wave
arrives with large amplitudes on the vertical component and is
followed a few seconds later by the S wave which arrives with strong
amplitudes on the NS and EW components. Several seconds after the
S wave a long period ($\sim$ 2 cps) surface wave can clearly be seen for
most events. The S wave amplitudes for events after the first 25
seconds are smaller than those for the earlier events, but when a
distance correction for amplitudes is made (distance is estimated
from the S-P times) it is found that the magnitudes of some of these
later events are only about 0.4 to 0.8 magnitude units less than the

EL CENTRO ACCELEROGRAM
MAY 13, 1940

b I0

11
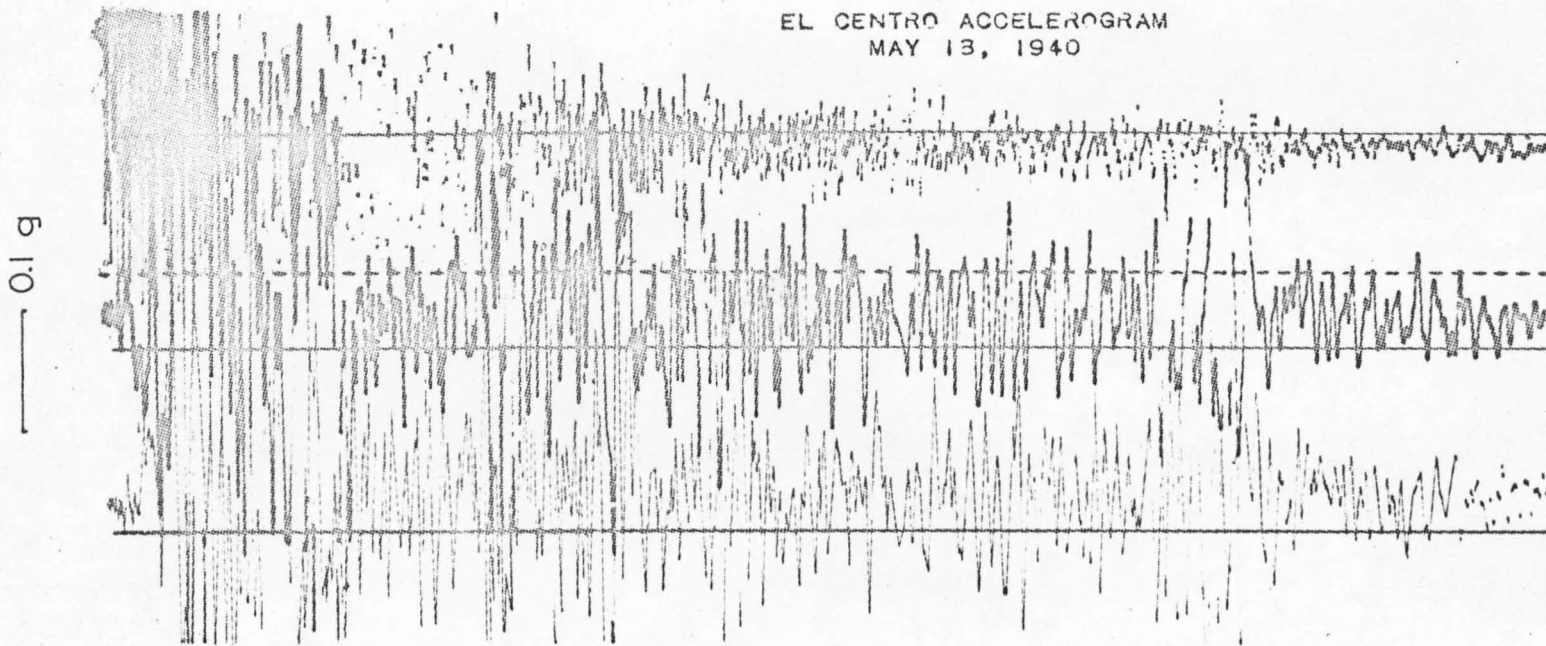
Figure 1.2a. El Centro strong motion accelerograph record for events
1A, 1B, 1C and 2. The time is given in seconds.

EL CENTRO ACCELEROGRAM

MAY 18 1940
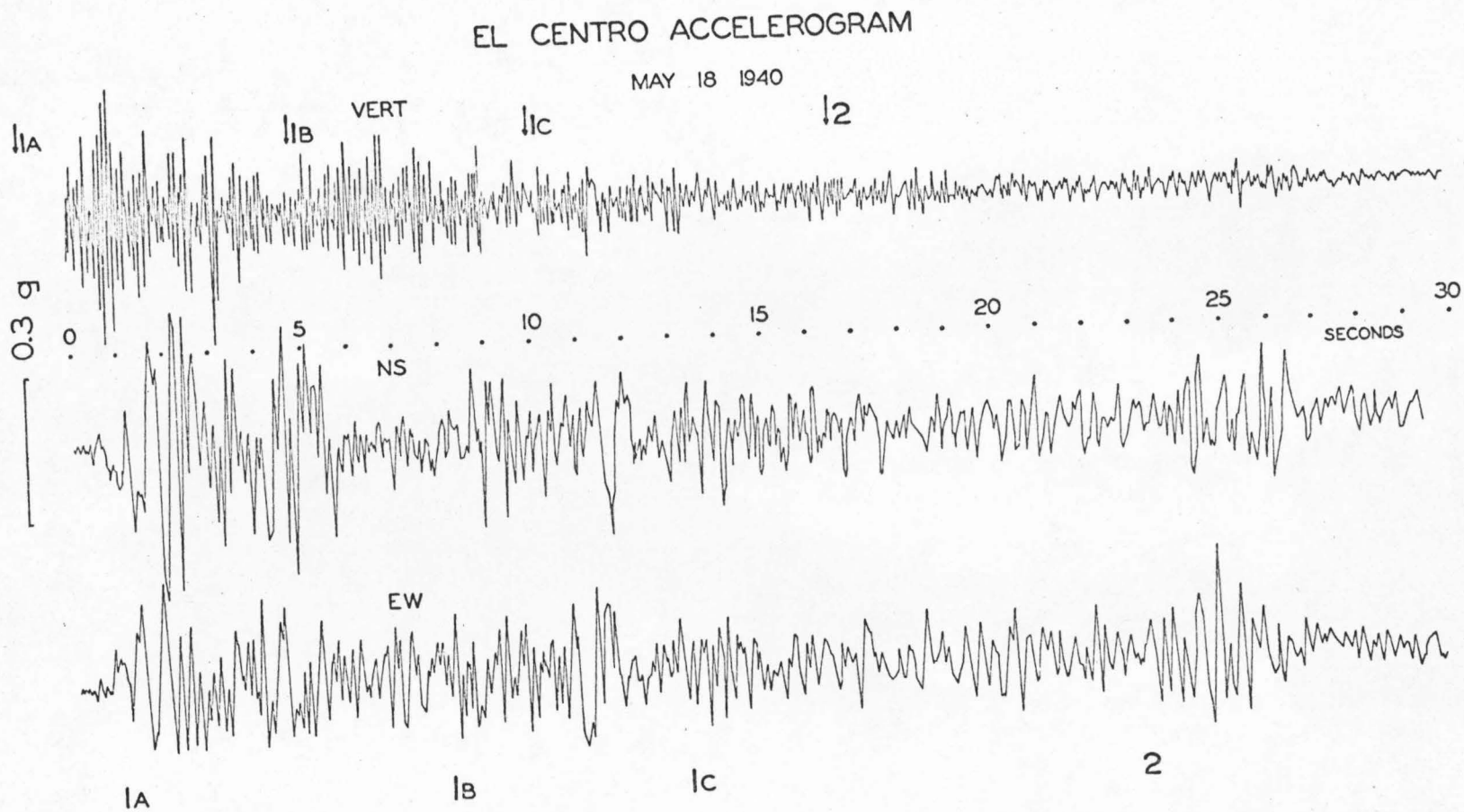
Figure 1.2b. Replotted El Centro strong motion accelerograph record for events 1A, 1B, 1C and 2. For better readability of the record the gain is reduced by the factor of 2.10.
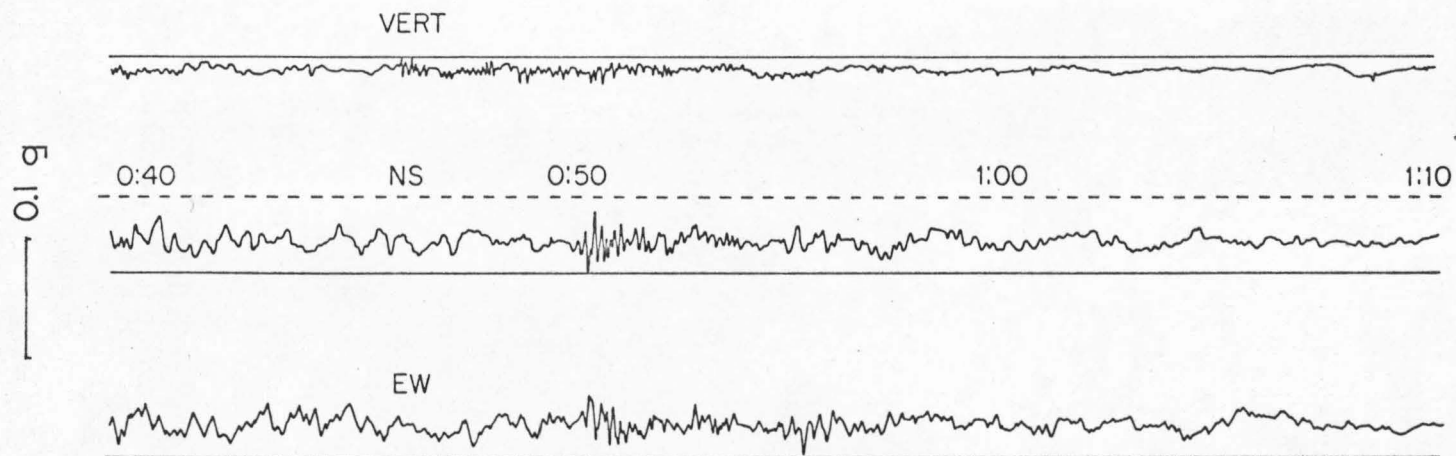
Figure 1.2c. El Centro strong motion accelerograph record for event 3.
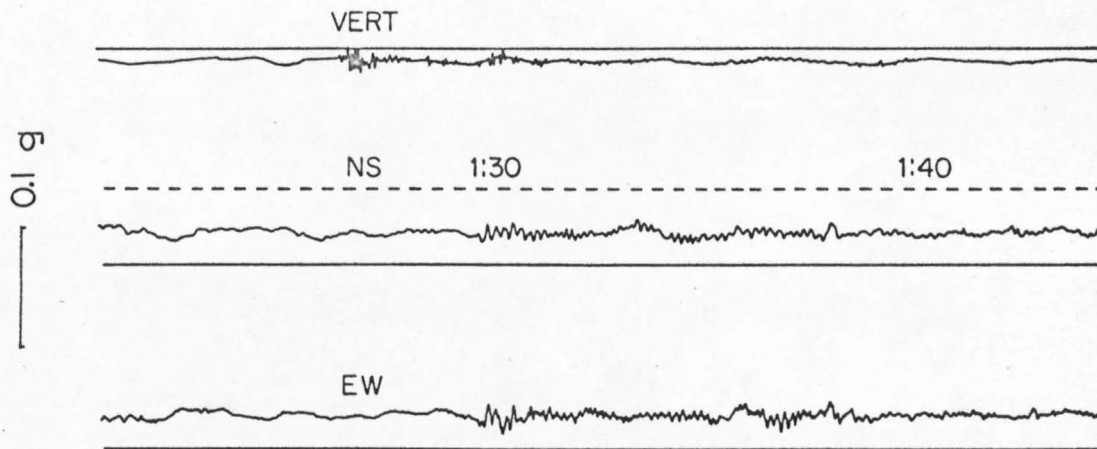
Figure 1.2d. El Centro strong motion accelerograph record for event 4.

VERT

0.10 g

1:40   NS   1:50   2:00

EW
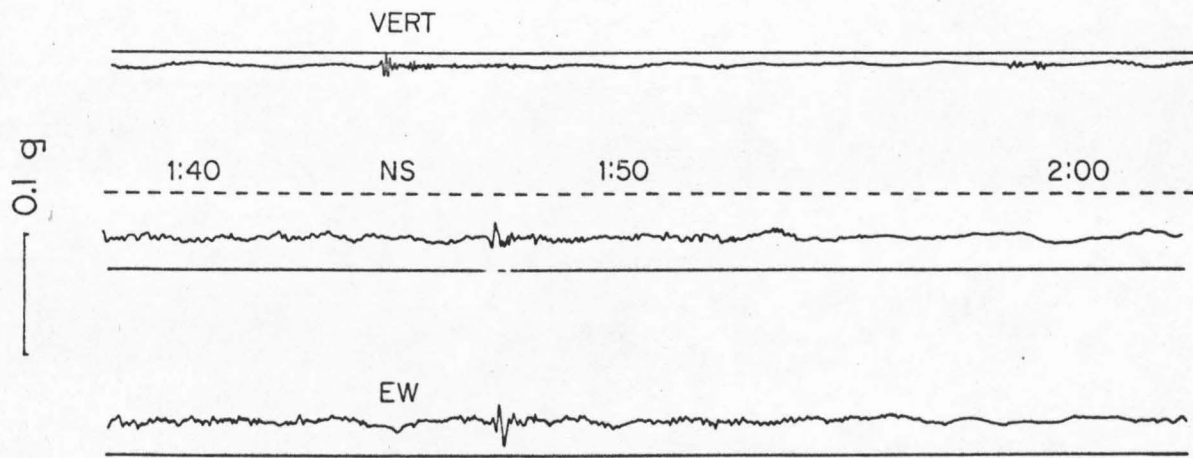
Figure 1.2e.   El Centro strong motion accelerograph record for
        event 5.

15

VERT

NS 2:10 2:20 2:30

EW

0.1 g
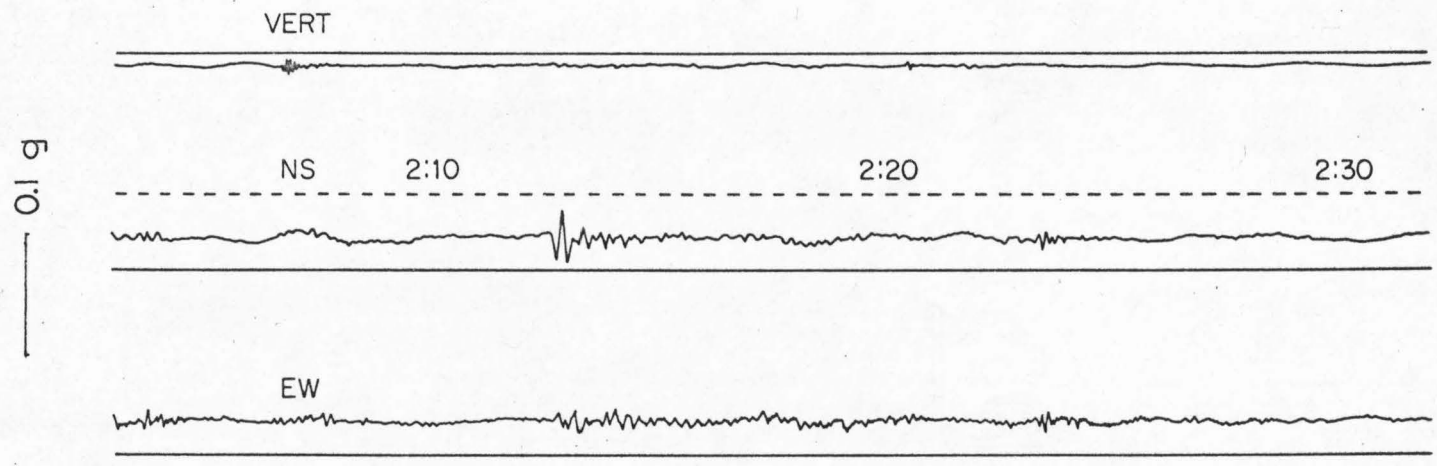
Figure 1.2f. El Centro strong motion accelerograph record for event 6.

VERT

5 10

NS   2:40   2:50   3:00

17

EW
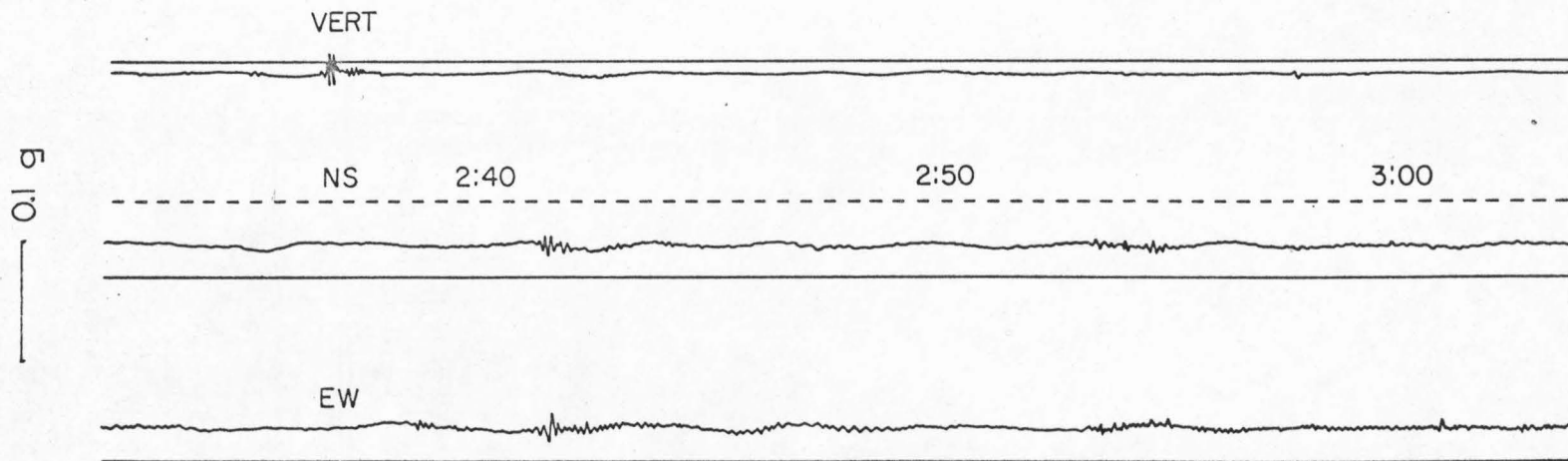
Figure 1.2g. El Centro strong motion accelerograph record for event 7.

VERT

NS   3:30   3:40   3:50

EW
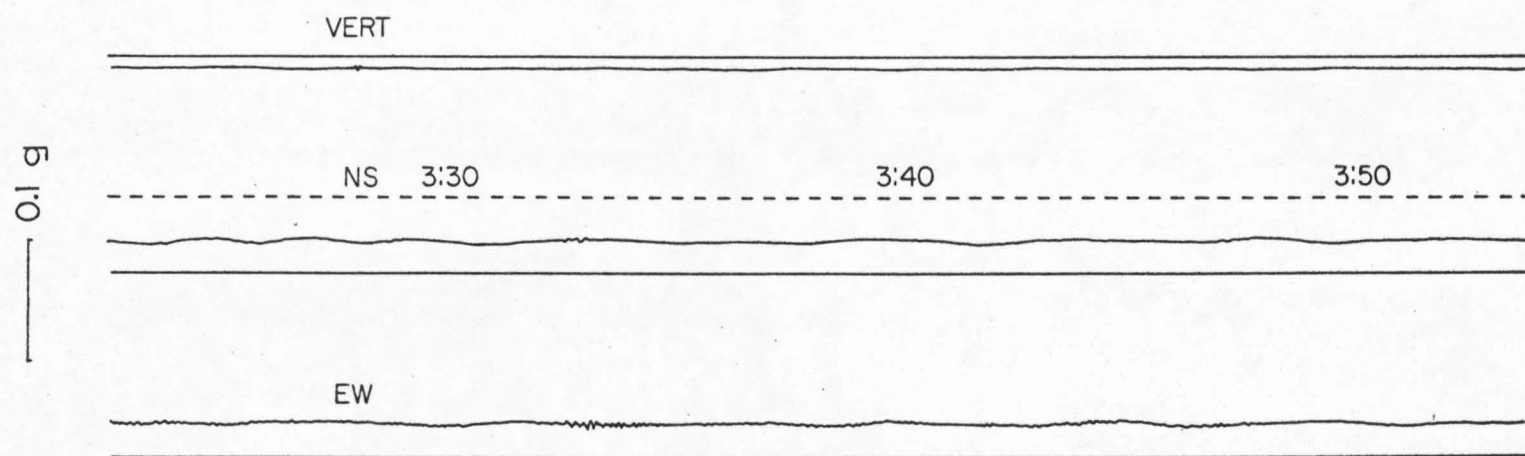
Figure 1.2h.   El Centro strong motion accelerograph record for event 8.

VERT

5 10

4:00   NS   4:10   4:20   4:30

19

EW
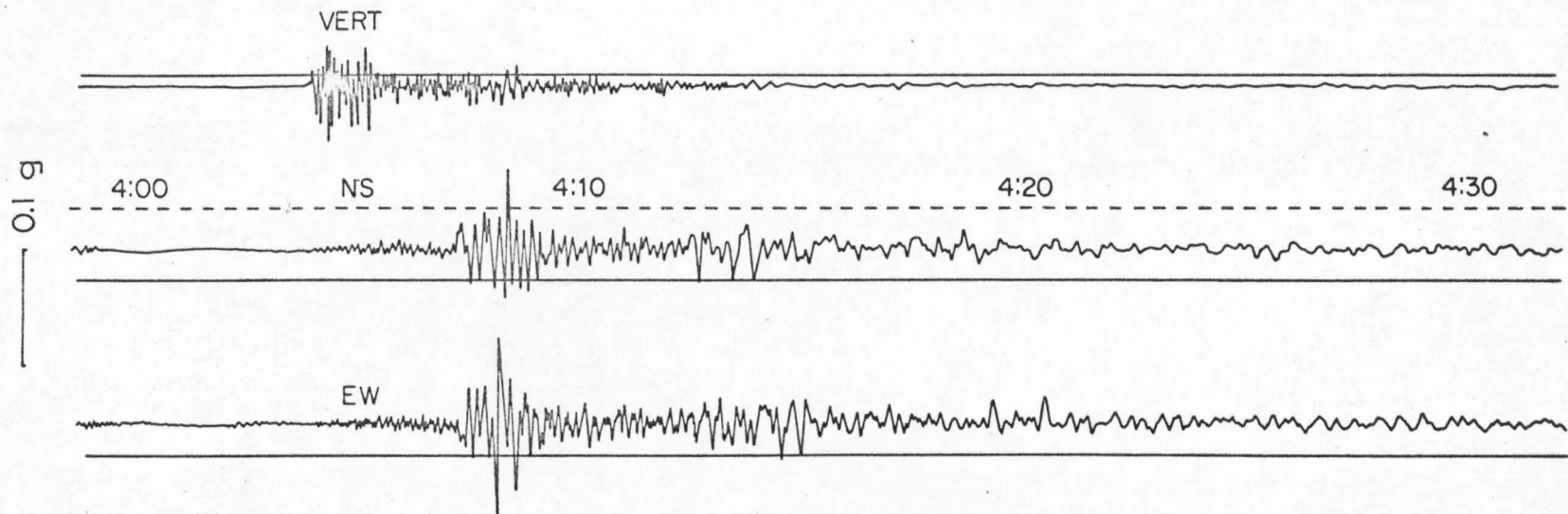
Figure 1.2i.   El Centro strong motion accelerograph record for event 9.

VERT

NS   4:50   5:00

EW

0.10 g
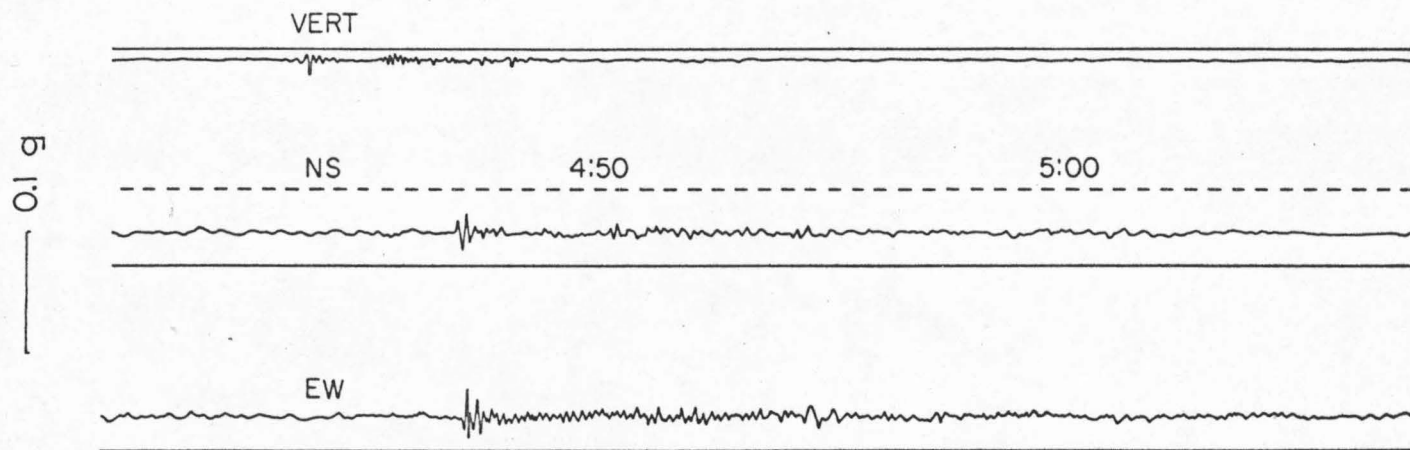
Figure 1.2j.   El Centro strong motion accelerograph record for event 10.
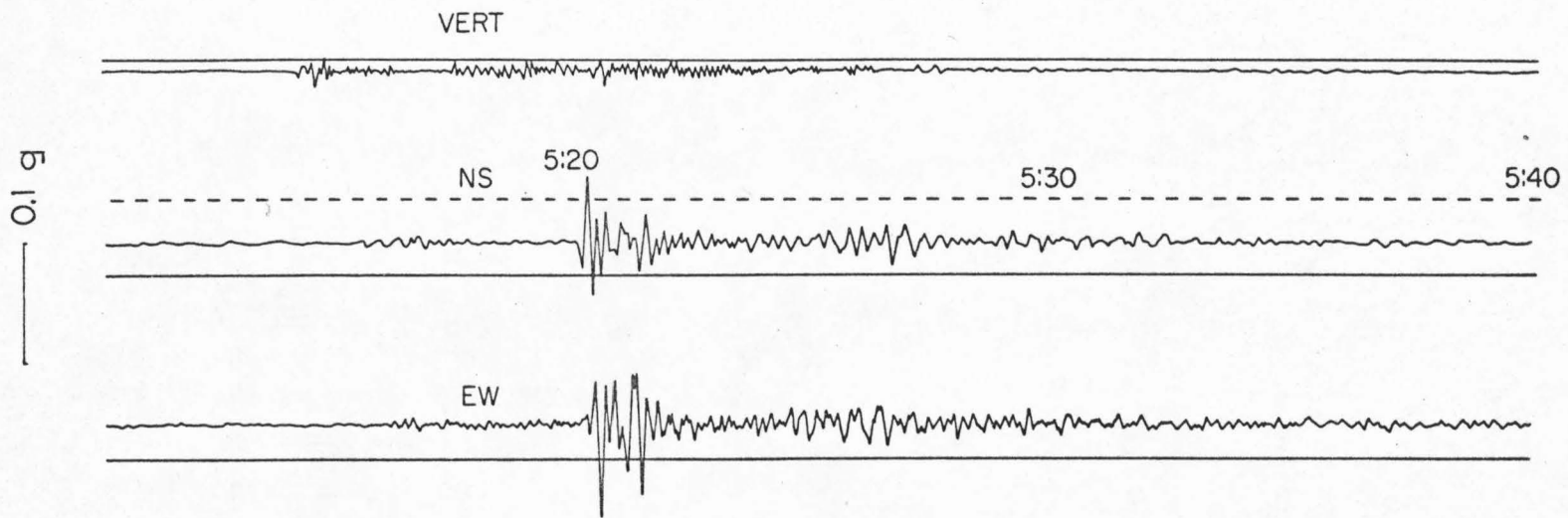
Figure 1.2k. El Centro strong motion accelerograph record for event 11.

largest event (event 2), and are thus important in earthquake engineering studies.

Because of large amplitudes, high frequency oscillations, and trace overlap, the original El Centro strong motion record (Fig. 1.2a) is confusing. To improve readability of this record all three traces were digitized and replotted at reduced gain in Figure 1.2b. Although this record appears complicated, when it is compared with aftershock events (e.g., event 9 in Fig. 1.2i), similar wave forms can be recognized. Higher frequency phases on EW and NS components represent S waves from the more or less distinct events. At least four S arrivals corresponding to events designated 1A, 1B, 1C and 2 can be seen in Figure 1.2b. Corresponding P wave arrivals for each of these events cannot be unequivocally identified because of the constant high level of the short period pulsations caused by all preceding events. Probable P wave arrivals for these events are indicated in Figure 1.2b by an arrow.

In order to interpret the phases recorded in Figure 1.2a to Figure 1.2k, travel time curves and dispersion curves were constructed from a five layer model of the Imperial Valley (Westmoreland profile, after Biehler, 1964). The travel time curves were used to estimate the distance of each event. To compute the surface wave dispersion curves, layer thicknesses, velocities, and densities were assumed as follows:

Layer	thickness (km)	α (km/sec)	β (km/sec)	ρ (gr/cm^3)
1	0.18	1.70	0.98	1.28
2	0.55	1.96	1.13	1.36
3	0.98	2.71	1.57	1.59
4	1.19	3.76	2.17	1.91
5	2.68	4.69	2.71	2.19
6	∞	6.40	3.70	2.71

Poisson's constant was taken to be 1/4. Densities in the last column were calculated using the empirical relationship of Birch (1961)

$$\rho = 0.770 + 0.302\,\alpha$$

Dispersion curves calculated for this model (Figure 1.3) show the group velocities for the first four Love and Rayleigh modes. The flat character of the fundamental mode curves indicate that most of the energy in the period range 0.5 to 5.0 seconds will travel with a velocity of about 1 km/sec.

The epicentral distances of each event were determined from the P and S wave arrival times on the El Centro strong motion seismogram. These distances were checked against the surface wave arrival times. Using only arrival times at one station it is not possible to determine the position of each event; however, if it is assumed that all events occurred along the observed surface trace of the fault southeast of El Centro, it is then possible to locate the relative position of these events along this surface trace. The
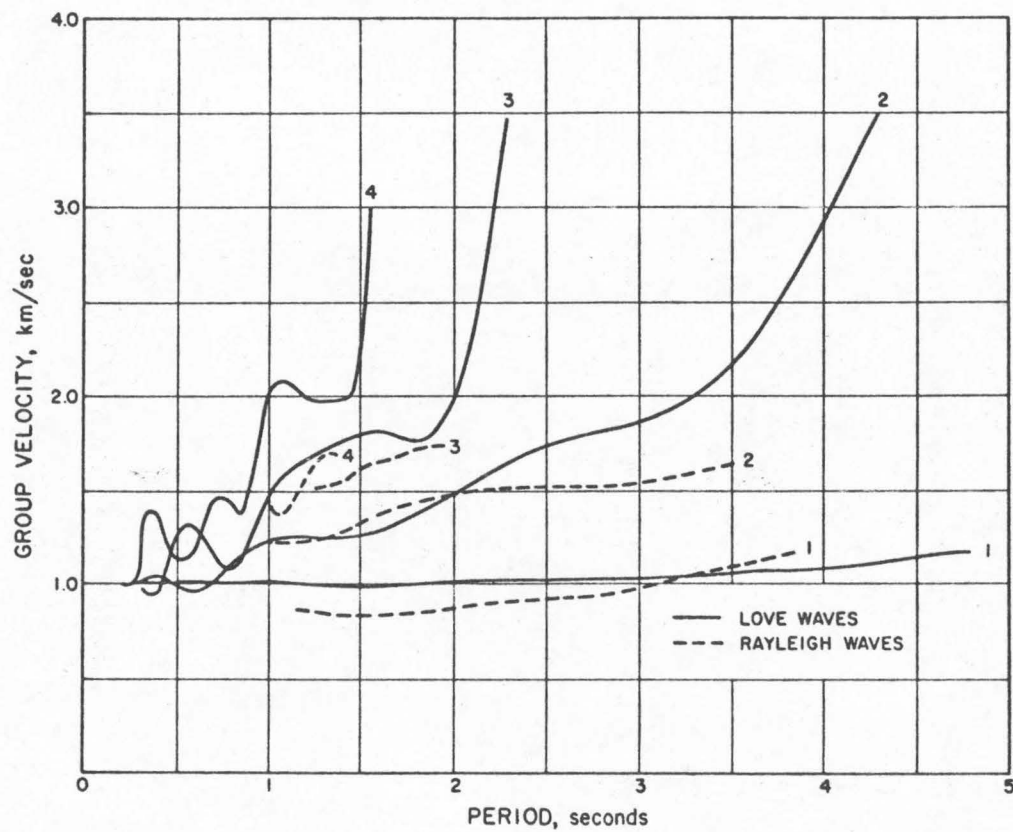
Figure 1.3. Love and Rayleigh wave dispersion curves for the structure corresponding to the Westmoreland profile (Biehler, 1964) in the Imperial Valley.

assumption that the epicenters of all events lie along the surface
trace of the fault to the southeast cannot be strictly justified, but
appears to be a reasonable first approximation. Certainly the locus
of the main energy release events must lie near the observed fault
trace. Aftershocks of large earthquakes also usually cluster around
the fault rupture and some recent studies of precisely located after-
shocks indicate that most of the events lie very close to the fault
trace (Parkfield, 1966; Eaton, 1967; Borrego Mountain Earthquake,
1968; Hamilton et al., 1969). The fact that the observed fault offset
(Figure 1.9) increased towards the southeast and that the biggest
displacements were recorded close to the international boundary sug-
gests that most of the energy release took place SE of El Centro.
The main energy release and fault rupture appears to be represented
by the first 25 seconds of the strong motion record (Figure 1.2a).
As mentioned earlier the identification of P wave arrivals for the 4
events on this section of the record is rather uncertain because the P
waves are less pulse-like than the S waves and are variable in relative
amplitude (e.g., compare the various events in Figure 1.2c to 1.2k).
Because of the complexity of this section of the record several other
smaller events could have occurred and not been identified. The
longer period pulses on the NS and EW components arriving at about
4 and 11 seconds are probably surface waves corresponding to events
1A and 1B, respectively. The excitation of 2 cps surface waves is
variable, in some cases a prominent surface wave pulse is observed
and in other cases not (Figure 1.2b to Figure 1.2k). This variability

is probably related to variations in the depth of the events. The S wave for event 2, probably the largest event of the series, arrived some 24 seconds after the first event. The P wave time and therefore the distance of this event is somewhat uncertain but is probably as indicated in Figure 1.2b, which would place the event at the southeasternmost part of the break, similar to event 6 (Figure 1.2f) and event 11 (Figure 1.2k). The El Centro strong motion record is interpreted to indicate that the main fault rupture occurred along a section of the fault from near the initial epicenter southeast to near Cocapah in a series of more or less discrete events which occurred in a time span of about 15 seconds and are represented on the first 25 seconds of the record.

Event 2 might be called a "stopping phase" in the sense that it probably represents the last event in a series of events successively further toward the southeast, but probably does not represent a stopping phase in the idealized sense for perfect interference as described by Savage (1965).

Magnitudes have been assigned to the various events using the definition of local earthquake magnitude (Richter, 1958) and the strong motion record (Figure 1.2a to Figure 1.2k). This is not a completely correct procedure for determining M_L because the local magnitude is defined in terms of the maximum amplitude on records from standard Wood-Anderson torsion seismometers rather than a strong motion instrument. Amplitudes were estimated for 2 cps waves which would give the maximum deflections on the Wood-Anderson instruments at these distances. Magnitudes measured in this way closely approxi-

mate the local magnitudes which would have been determined on a
Wood-Anderson type instrument at El Centro and are given in Table 1.

Table 1

Magnitudes for Events in the Imperial Valley Earthquake of 1940

Event	Distance (km)	$M_{L.}^{S.M.}$	M_L
1A	7-15 ?	5.7-5.9	-
1B	17-23 ?	5.6-5.8	-
1C	13-19 ?	5.4-5.6	-
2	35-44 ?	6.2-6.4	6.3
3	20-28	4.9-5.3	-
4	13-19	4.4-4.5	-
5	8-12	4.5	-
6	34-43	5.4-5.5	-
7	25-34	4.8-5.2	-
8	24-32	4.2-4.4	-
9	13-19	5.2-5.3	5.2
10	14-29	4.7-4.8	-
11	33-43	5.8-5.9	4.8

The local magnitude of M_L = 6.3 for the main shock was determined
by taking the grand average from EW and NS components of the Wood-
Anderson seismograph records at Tinemaha, Haiwee, Mt. Wilson,
Pasadena and Santa Barbara and EW component at Riverside (see
table 2) and agrees with the local magnitudes determined from the

strong motion instrument. Magnitudes M_L = 5.2 for event 9 and

M_L = 4.8 for event 11 were computed from the EW and NS records

from Mt. Wilson and the EW component from Riverside. M_L for

event 9 agrees closely with the determination from the strong motion

instrument; however event 11 gives a magnitude almost one unit

higher on the strong motion instrument than on the Wood-Anderson

instrument at large distances. The spectrum of this event is obviously

quite different than that of event 9.

E. ANALYSIS OF DISTANT RECORDS

Fourier Spectrum, $F(\omega, t^*, \Delta t)$, of the Tinemaha Records

In a simple Fourier analysis of the complete record, infor-

mation on the time dependence of the incoming wave forms, i.e., the

time of their arrivals, duration, and dispersion properties are not

directly displayed. Therefore, the following form of moving window

Fourier analysis is used:

$$F(\omega, t^* \Delta t) = \int_{-\infty}^{\infty} e^{-i\omega t} f^*_{\Delta t}(t) \ dt$$

where

$$f^*_{\Delta t}(t) = \begin{cases} 0 & ; \ t \leq t^* - \dfrac{\Delta t}{2} \\ f(t)a(t); & t^* - \dfrac{\Delta t}{2} \leq t \leq t^* + \dfrac{\Delta t}{2} \\ 0 & ; \ t \geq t^* + \dfrac{\Delta t}{2} \end{cases}$$

and $f(t)$ stands for the record trace as a function of the time. This

formulation is equivalent to taking the Fourier amplitude spectrum of

the function f(t) multiplied by the window of the form:

$$W_{\Delta t}(t^*) = \begin{cases} 0 & ; \ t \le t^* - \dfrac{\Delta t}{2} \\[2mm] a(t) & ; \ t^* - \dfrac{\Delta t}{2} \le t \le t^* + \dfrac{\Delta t}{2} \\[2mm] 0 & ; \ t \ge t^* + \dfrac{\Delta t}{2} \end{cases}$$

so that

$$f^*_{\Delta t}(t) = f(t)\, W_{\Delta t}(t^*)$$

It is evident that $F(\omega, t^*, \Delta t)$ can be used for several purposes. For example, if the time coordinate t^* is taken as the travel time, then for a given distance, $F(\omega, t^*, \Delta t)$ yields the dispersion properties of the incoming waves. In addition, for complicated records, in particular, records of multiple event earthquakes, $F(\omega, t^*, \Delta t)$ can be used to separate different events or different phases. The choice of Δt, i.e., the window width (as well as the window shape), depends on the particular needs of the analysis, and has to be chosen in each case to suit the physical character of the function f(t) to be analyzed.

In this work only a square window, $a(t) = 1.0$, is used. To analyze the record f(t), a discrete set of ω_i, $i = 1, 2, \ldots, n$ and t^*_j, $j = 1, 2, \ldots, m$, together with Δt are chosen. If ω_i are chosen, $F(\omega_i, t^*_j, \Delta t)_{i=1, \ldots, n; \ j=1, \ldots, m}$ for n and m large enough, will approximate a continuous function $F(\omega, t^*, \Delta t)$. Equally spaced ω_i's and t^*_j's and linearly interpolated $F(\omega, t^*, \Delta t)$ between the discrete points have been used. The records are digitized using a Benson-Lehner data reducer and the spectrum calculated on an IBM 7094.

Several Δt intervals were used during the course of the work in order to study the properties of $F(\omega, t^*, \Delta t)$. The final window width was chosen to be $\Delta t = 0.75$ min and increments in t^* were taken as 1/8 min. $F(\omega, t^*, \Delta t)$ was plotted using a Calcomp plotter (Figure 1.4a to Figure 1.5b). Each plot represents $F(\omega_i, t_j^*, \Delta t)_{i=1,\ldots,n; j=1,\ldots,m}$ for an interval of one minute and for the frequency range from 10 to 75 rad/min (periods 35 to 5 sec). All plots were normalized, each with respect to the maximum peak value that occurred in that 1 min time interval, so that spectral values range from 0 to 1.0 of that peak value. The interval from 0 to 1.0 was subdivided into 20 levels. Levels of value greater than 0.5 were connected with full contour lines in order to clearly display the peaks in the spectrum.

Figure 1.4a and 1.4b give the spectra obtained for the EW component at Tinemaha. The spectra are not corrected for the instrument response; however, such correction would not critically alter their appearance. Time on these figures corresponds to the time on Figure 1.6 and is measured in minutes from an arbitrary point at which the record digitization was initiated.

An aftershock, herein called the Brawley even (Figure 1.7, 19 May 1940, 5:51 GCT, M = 5.5), was used as an example of a simple event and the spectrum was computed and plotted (Figure 1.5a, Figure 1.5b) in the same manner as for the main event. As can be seen in Figure 1.5a and Figure 1.5b the spectrum corresponds to a slightly dispersed train of waves lasting for about 1/2 min with predominant periods between 7 and 20 seconds. A similar analysis

TINEMAHA EW COMPONENT

PEAK VALUE = 344.00 mm sec
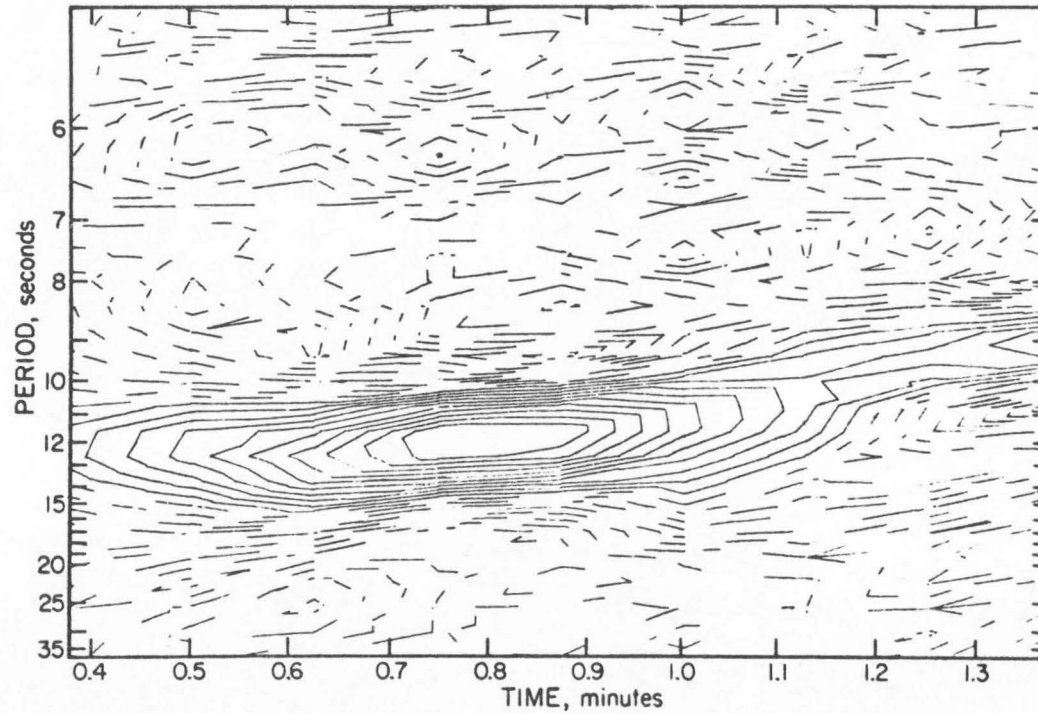
Figure 1.4a. Moving window Fourier spectrum $F(\omega, t^*, \Delta t)$ for the Tinemaha EW
seismogram of the Imperial Valley Earthquake of 1940.

TINEMAHA EW COMPONENT

PEAK VALUE = 343.50 mm sec
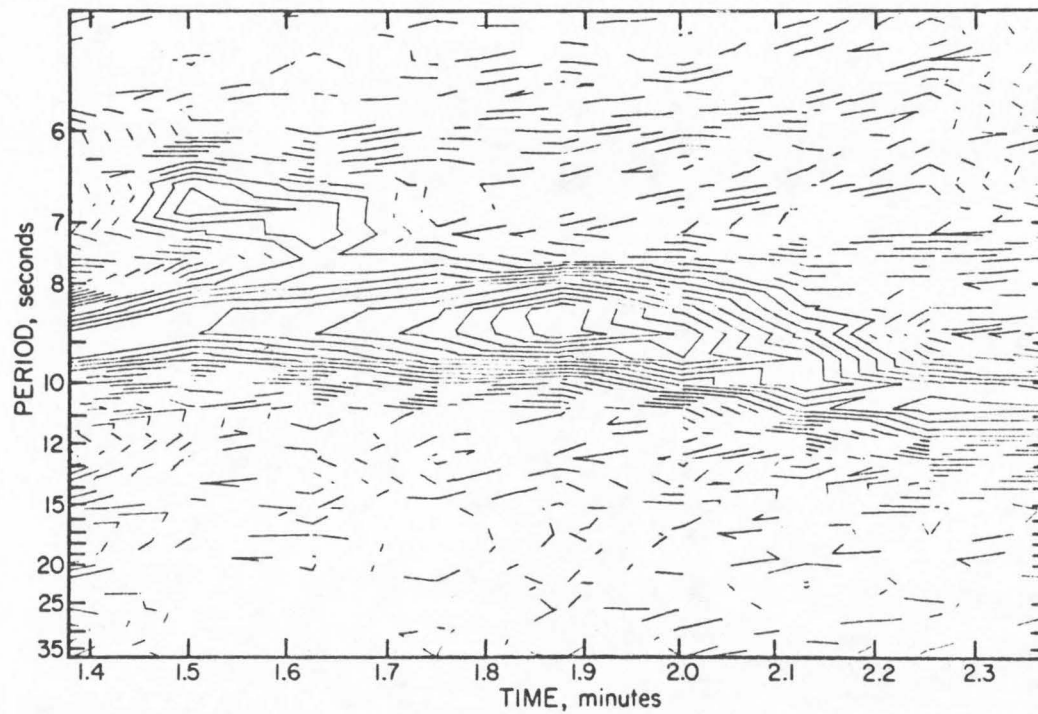
Figure 1.4b. Moving window Fourier spectrum $F(\omega, t^*, \Delta t)$ for the Tinemaha EW seismogram of the Imperial Valley Earthquake of 1940.

TINEMAHA EW COMPONENT

PEAK VALUE = 20.45 mm sec
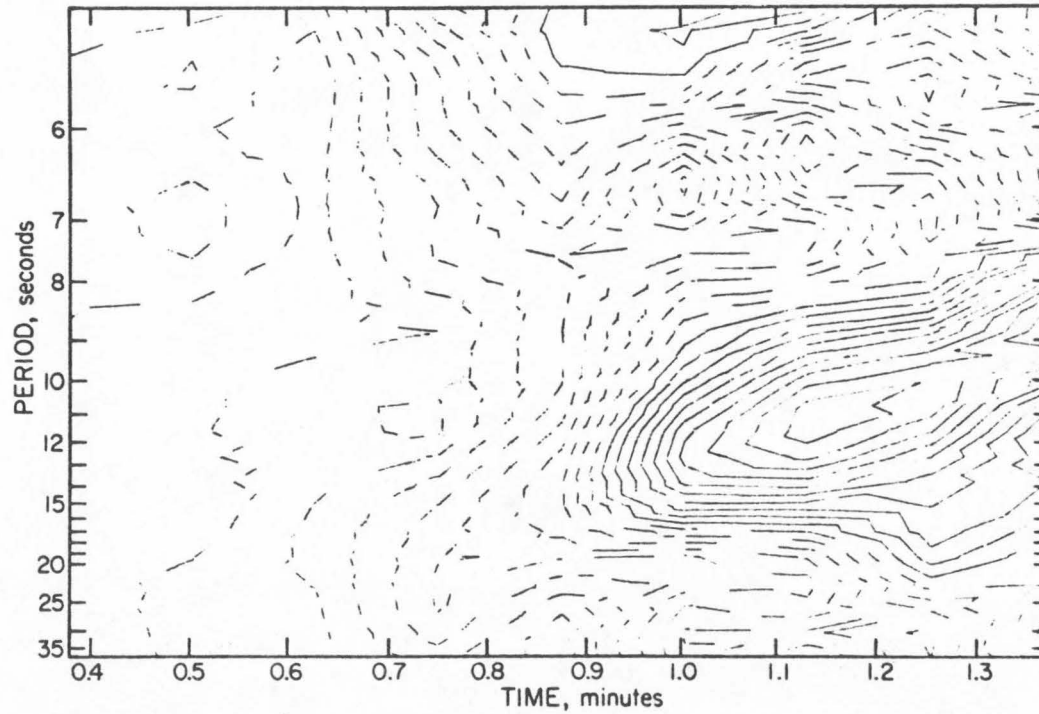
BRAWLEY EVENT

Figure 1.5a. Moving window Fourier spectrum $F(\omega, t^*, \Delta t)$ for the Tinemaha EW seismogram of the Brawley event (19 May 1940, 5:51 GCT).

TINEMAHA EW COMPONENT

PEAK VALUE = 20.45 mm sec
BRAWLEY EVENT
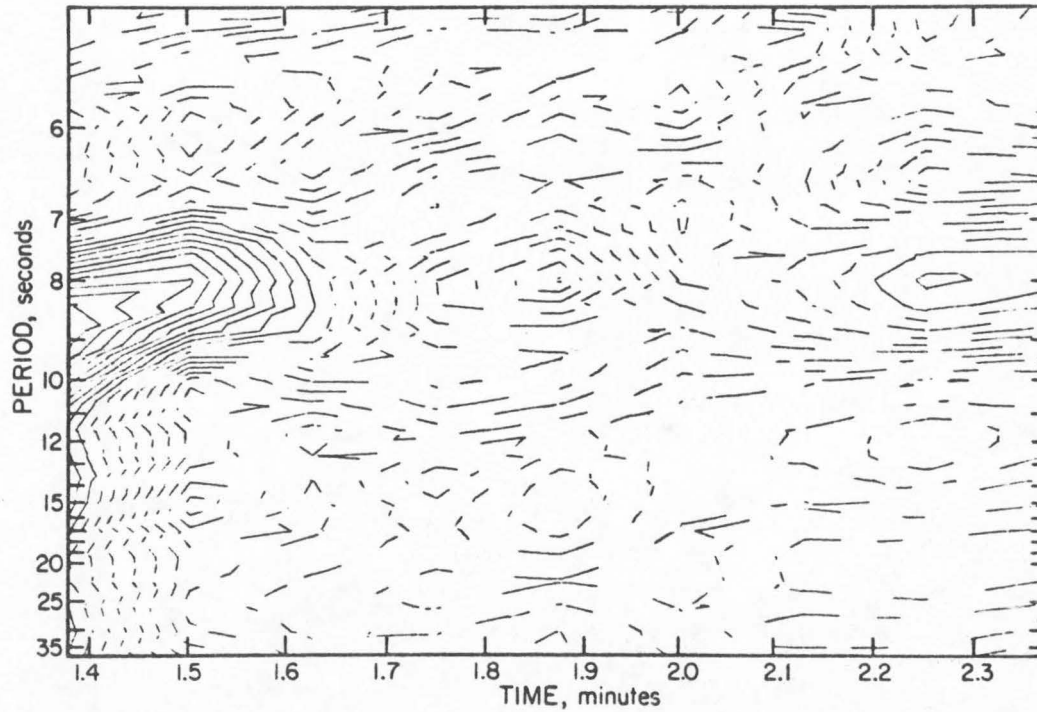
Figure 1.5b. Moving window Fourier spectrum $F(\omega, t^*, \Delta t)$ for the Tinemaha EW seismogram of the Brawley event (19 May 1940, 5:51 GCT).

34
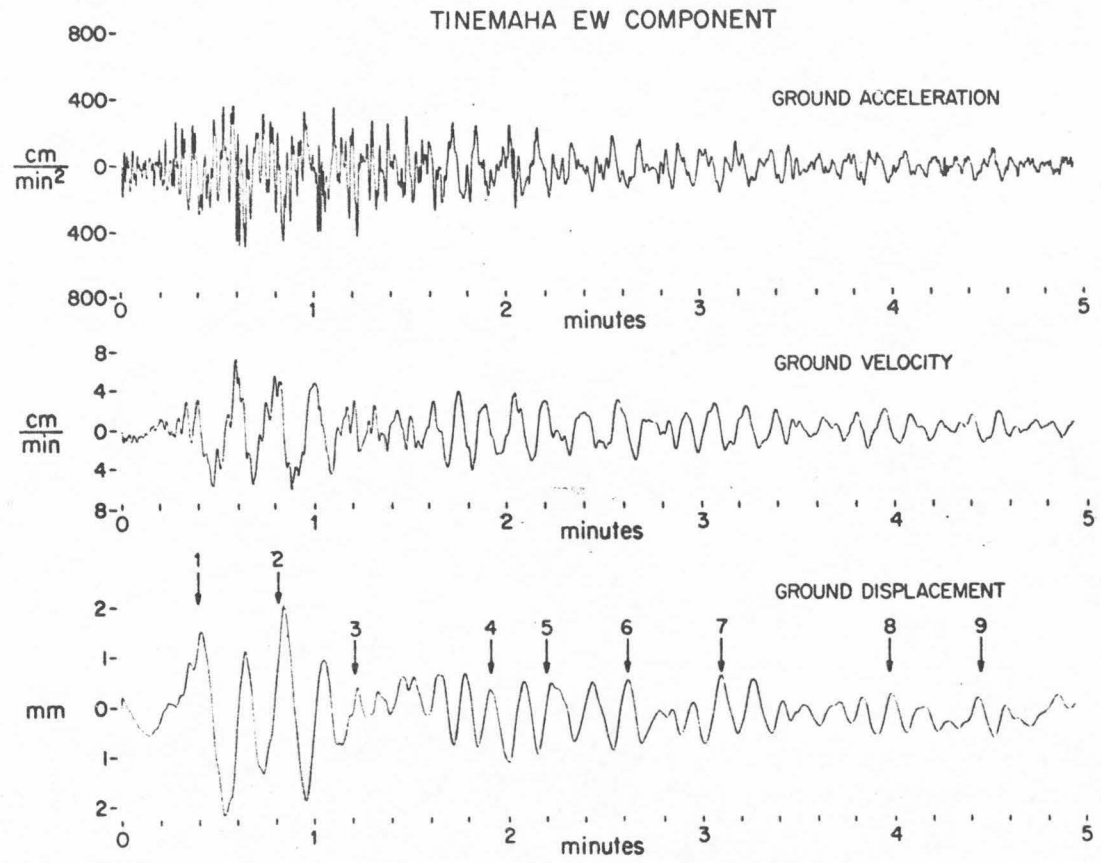
Figure 1.6. Calculated EW ground acceleration, velocity and displacements at Tinemaha for the Imperial Valley Earthquake, 1940. Arrows indicate expected arrival time for events as inferred from the El Centro strong motion seismogram.

36
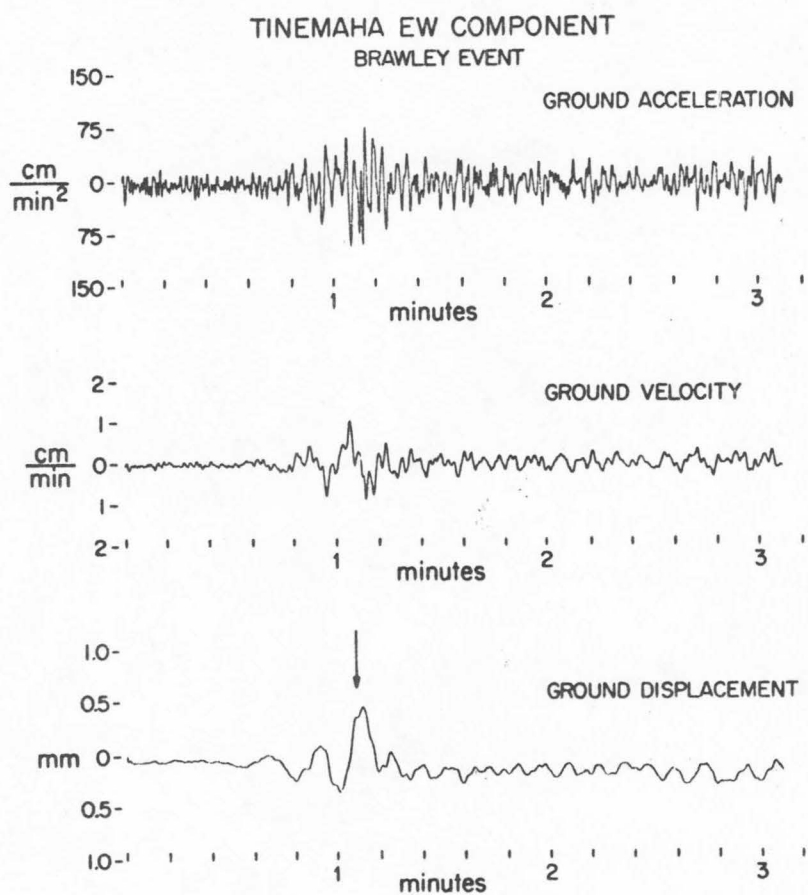
Figure 1.7. Calculated EW ground acceleration, velocity and
displacements for the Brawley (19 May 1940, 5:51 GCT)
event at Tinemaha.

made for a recording from the Haiwee Wood-Anderson instrument showed essentially the same features. The location of Tinemaha ($\theta = 8^\circ$) and Haiwee ($\theta = 4^\circ$) are such that EW motion represents essentially pure Love waves.

Integrated and Filtered Distant Records

The Tinemaha EW components of the Wood-Anderson records of both the Brawley event (Figure 1.7) and the main sequence (Figure 1.6) were corrected to give true ground acceleration as a function of time. The instrument constants used for the instrument correction were: $V_s = 2800$, $T = 0.8$ sec, and $\zeta = 1.0$. The corrected ground motion was then filtered to eliminate periods greater than approximately 30 sec. This was done because of possible uncertainties resulting from the data processing procedures and the large instrumental correction necessary.

The Wood-Anderson torsion seismograms at Tinemaha, Haiwee, Mt. Wilson and Riverside were also analyzed as a group using a simple running-mean low-pass filter to find whether there has been a coherent pattern to the waves in the coda at these stations. The corner period on the filter was about 15 seconds. Low-pass filter records from these four stations together with the EW record from a long-period torsion instrument at Pasadena are plotted in Figure 1.8.

Interpretation of Distant Records

Comparison of the Fourier amplitude spectra for the Brawley event (Figure 1.5a, Figure 1.5b) and the main sequence (Figure 1.4a and 1.4b) or a comparison of the calculated ground motion on Figure 1.6 and Figure 1.7 illustrates the complexity of the main earthquake. If all the source parameters associated with each of the multiple events were similar to the Brawley event and if there were sufficient time intervals between successive events so that interference would be negligible, it would be possible to identify all individual events on a long period ground motion record such as in Figure 1.6 by simply identifying a "characteristic" peak (e.g., indicated by an arrow in Figure 1.7). However, this is not the case for the Tinemaha record of the Imperial Valley Earthquake. As can be seen from the calculated ground motion (Figure 1.6, Figure 1.7) and Fourier spectra (Figure 1.4a and Figure 1.4b) the predominant period of waves recorded at Tinemaha was about 10 seconds. The duration of the surface wave train for a single event, e.g., the Brawley event is about 30 seconds or 3 cycles of a ten second period wave. This makes it difficult to resolve events separated by less than 30 seconds. Arrows numbered 1 to 9 in Figure 1.6 are spaced to represent the relative arrival times predicted at Tinemaha. The arrows on the basis of the approximate locations indicated by numbers 1A, 1B, ..., 11 (Figure 1.1a) have been time shifted as a group to give the best agreement with the first pulse of energy. Number 1 in Figure 1.6 stands for the group of events 1A, 1B, and 1C.

Because of the close spacing of events 1A through 2, they can-

not be resolved by the long period (~ 10 sec) surface waves recorded at Tinemaha. These waves thus combine to give approximately the effect of a source propagating to the southeast. The shape of the Fourier spectra corresponding to these events (Figures 1.4a and 1.4b) is consistent with this interpretation as is the Tinemaha ground motion record which can be explained as a superposition of several pulses shaped like the single pulse from the Brawley event. This interpretation is also supported by the difference of 0.8 on the Richter magnitude scale, between the local stations (M_L = 6.30) located mainly NW from El Centro and teleseismic stations (M_S = 7.1) located E and SE, suggesting independently that during the main energy release the source propagated towards the SE.

Local magnitudes $M_L^{S.M.}$, estimated above from the strong motion record at El Centro suggest that events 3, 6, 7, 9 and 11 might have been large enough to generate significant long-period energy. The prolonged train of surface waves on the EW component of ground motion at the Tinemaha station (Figure 1.6) show long-period (~ 10 sec) wave arrivals which might be associated with these events. However, filtered records from other local stations (Haiwee, Mt. Wilson, Pasadena, Riverside) show no coherent pattern associated with these events. This suggests that the prolonged train of surface waves consists of scattered reflections from crustal inhomogeneities that have been generated by the main events (first 15 seconds) but travelled indirect reflected paths to the seismograph station. Figure 1.8 gives low-pass filtered records (corner period approximately 15 sec) from these stations, time shifted according to distance
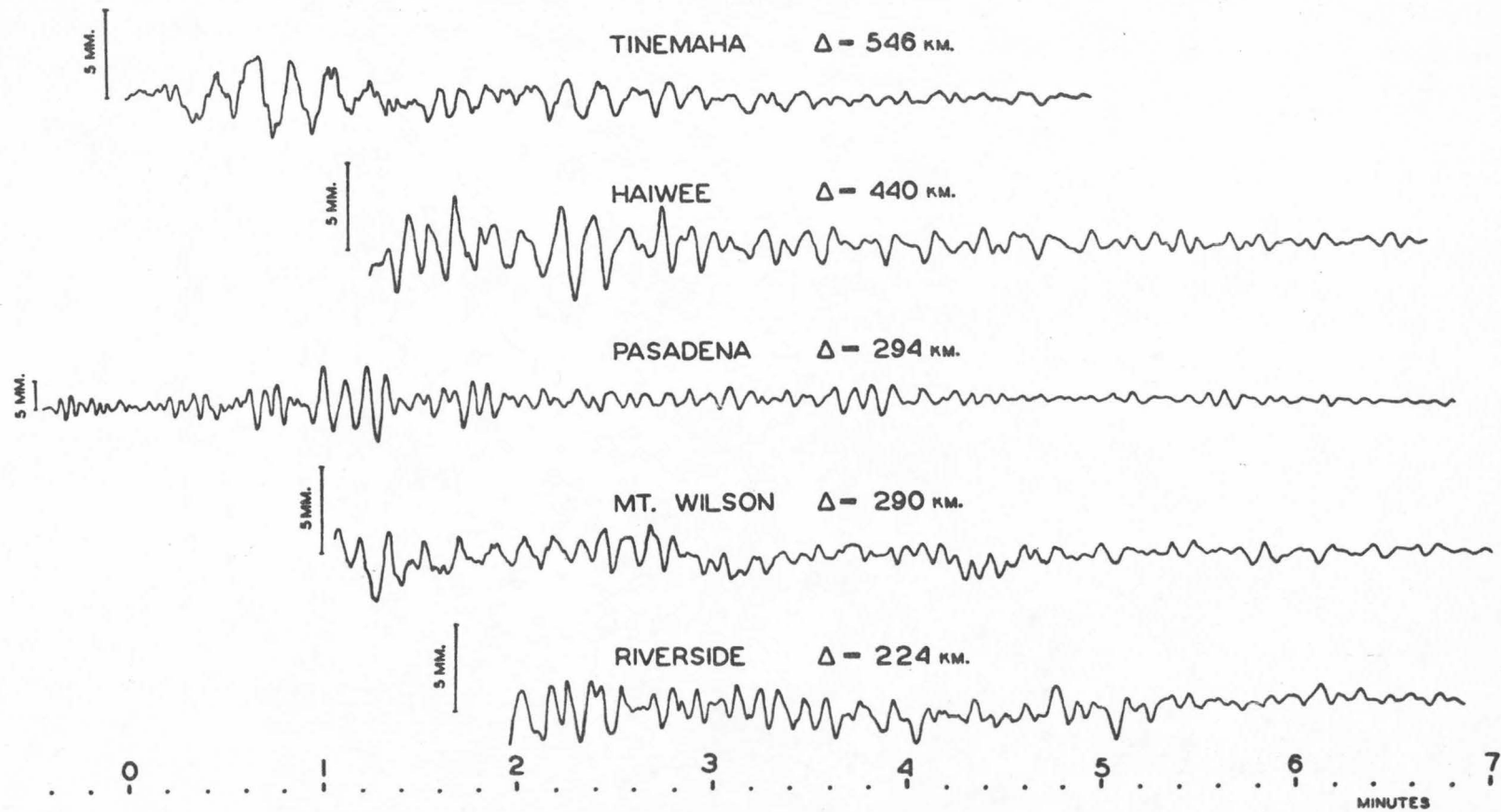
Figure 1.8. Surface waves from Imperial Valley Earthquake, California, 1940
recorded on low-pass filtered EW seismograms from Wood-Anderson
instrument at Tinemaha, Haiwee, Mt. Wilson and Riverside, and on
the low magnification long-period torsion record from Pasadena.

so that a surface wave traveling with a velocity of 3.5 km/sec arrives at the same time on all records. Although there is no coherent pattern, it is obvious that the "coda" of surface waves is longer and more complex than that following the Brawley (single-event) earthquake. This may have, in part, resulted from the greater relative excitation of long-period surface waves by the main events since the "coda" consists of primarily longer period waves. It is quite possible that the largest of these events (e.g., nos. 6, 9, and 11) generated surface waves that could have been clearly observed if it had not been for the large amplitudes of the scattered surface waves from the first part of the rupture. The magnitudes of these events were unusually large for ordinary aftershocks. According to Bath's law (Richter, 1958) the magnitude of the largest aftershock is usually about 1.2 less than the main event. Thus, although the main energy release during this earthquake probably occurred in the first 15 seconds, significant energy release occurred as late as event 11 some 5 minutes later. It is also possible that significant long-period energy continued to be radiated after the first 15 seconds in some complex manner not simply related to the inferred magnitudes of events 2 to 11. That there may be considerable variation in the ratio of long-period to short-period excitation is indicated by an inspection of the various aftershocks, in particular, events 9 and 11.

The relatively great excitation of high frequencies for event 9, suggests that it may have been deeper than events 6 and 11, assuming that deeper shocks occur under higher stress and thus generate higher frequencies. If this interpretation is correct, it would explain the

difference between $M_L^{S.M.} = 5.8 - 5.9$ and $M_L = 4.8$ for event 11.

F. FIELD OBSERVATIONS OF FAULT OFFSET

Figure 1.9 shows the amount of right lateral offset along the Imperial fault as it was observed in the field shortly after the May 19, 1940 earthquake (Buwalda, unpublished field notes). The pattern of these offsets indicates that the main part of the displacement took place along a surface fracture some 20 to 25 km long extending approximately from the instrumentally determined epicenter of the main shock SE some 5 km past Cocopah (Figure 1.1a). Tentative location of the main sequence of the events 1A, 1B, 1C and 2 (Figure 1.1a), or an "equivalent" propagating rupture towards SE along the same section of the fault, are in agreement with the observed surface displacement (Figure 1.9). In addition, the distribution of the set of nine aftershocks (Figure 1.1a) also supports the conclusion that the main energy release took place along the same 20 to 25 km section of the fault. The observed fault offset (Figure 1.9) NW of the instrumentally determined epicenter (Figure 1.1a) is probably associated with the Brawley event, as suggested by Richter (1958). Repeated surveying of the Imperial fault since 1940 indicates (Brune and Allen, 1967) that there has been creep along the northwestern part of the fault trace. On March 4, 1966 there was a low-magnitude earthquake (M = 3.6) with surface faulting along 10 km of the fault trace, centered about the point nearest to El Centro, the same northwestern part of the Imperial fault which was fractured during the 1940 sequence
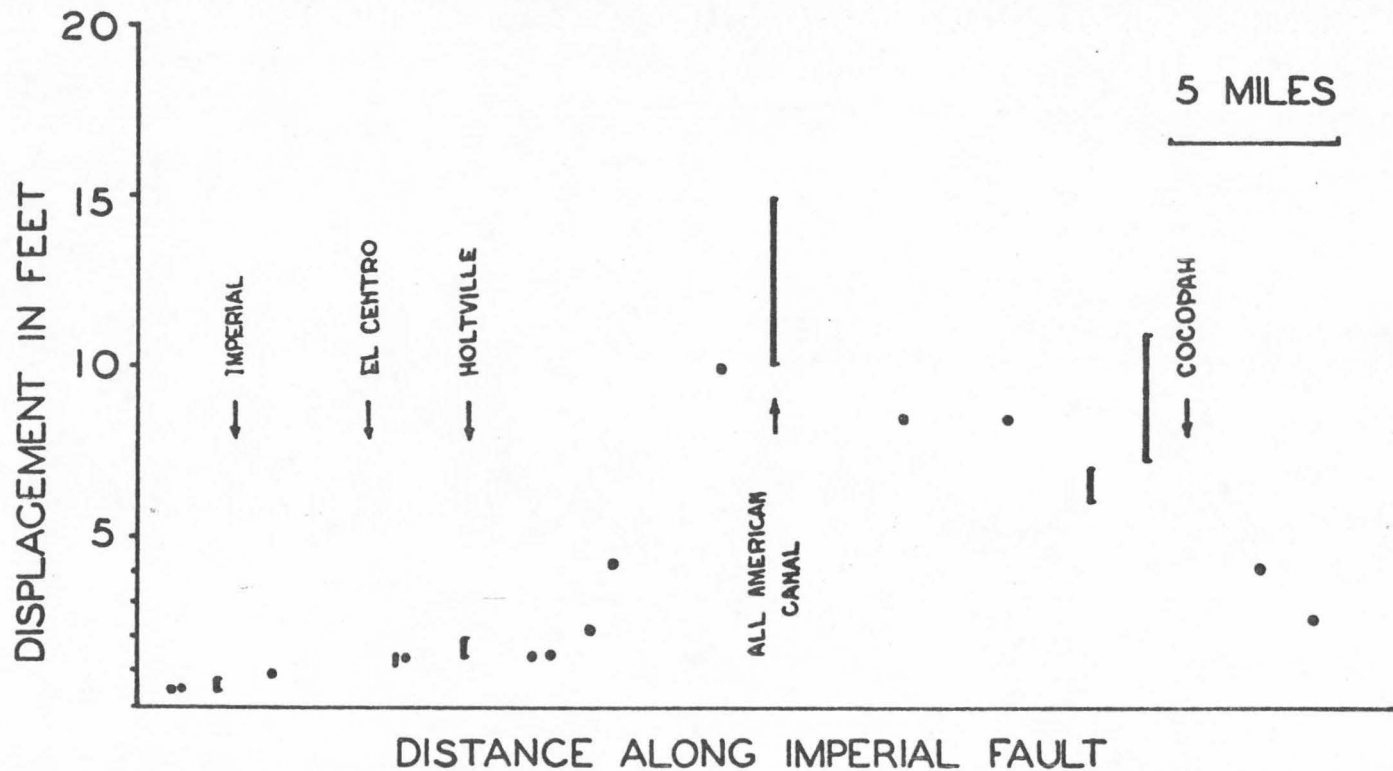
HORIZONTAL DISPLACEMENTS ON IMPERIAL FAULT - MAY 18, 1940

Figure 1.9. Plot of the relative displacements along the fault trace as measured in the field by J. P. Buwalda (original notebook and some additional data were kindly supplied by Prof. C. R. Allen). Vertical lines indicate the range of the observed displacements at essentially same locality.

(Brune and Allen, 1967). The Borrego mountain, California, earth-
quake of 9 April 1968 (M = 6.5) triggered creep episodes on several
fault systems including the Imperial fault. Theodolite resurveys
(Allen, et al., 1968) indicate 1.2 cm cumulative right lateral dis-
placement at the point where highway 80 crosses the Imperial fault
(Figure 1.1a), 1.1 cm 6 km northwest, and 1.3 cm 11 km northwest
from the same locality. These new triggered breaks along the
Imperial fault extended for more than 20 km in the same region as
the small earthquake of 1966 (Brune and Allen, 1967). Allen, Brune
and Lomnitz (personal communication) did not find any evidence of
recent fault slippage at either the locality of the All American Canal
(Figure 1.1a) or in the vicinity of Cocopah as of January 1969. The
recent activity along the northwestern part of the Imperial fault sug-
gests that it is behaving at present differently than the section south-
east of the epicenter of the 1940 earthquake. This difference could
perhaps be related to the fact that the NW part of the fault did not
slip as much as the SE section during the May 19, 1940 earthquake,
but was rather fractured by the later aftershock activity, fault creep
or both, and remained in a higher state of strain.

G. COMPUTATION OF SOURCE MOMENT USING SEISMIC WAVES

Seismic moment was calculated using relations from Ben-
Menahem and Harkrider (1964) for a vertical strike-slip surface
fault and including a correction for directivity function, i.e.,

$$M_o = \frac{u_\theta^{dc}}{A_L \cos 2\theta} \cdot \sqrt{2\pi\Delta C\omega} \cdot \left| \frac{\chi}{\sin \chi} \right|$$

where

$$\chi = \frac{\pi b}{CT_o} \left(\frac{C}{v} - \cos \theta \right)$$

To take into account the attenuation of the waves due to scattering and anelasticity (together with other sources of the energy loss), and to correct for the angle δ of the EW component relative to the u_θ^{dc} direction, the following expression can be written:

$$u_\theta^{dc} = ue^{\frac{\pi\Delta}{QUT_o}} \frac{1}{\cos \delta}$$

where u is the spectral density determined from the record.

In the case of a multiple event earthquake where the individual events are sufficiently separated in time, the moment may be calculated as the sum of the moments associated with each event. If each such moment is denoted by $M_{0\text{-SEISM}}^i$,

$$M_{0\text{-SEISM}}^{TOT} = \sum_i M_{0\text{-SEISM}}^i$$

The sequence of 4 events that occurred in the first 25 seconds of the onset of the strong motion record were too closely spaced for this condition to apply to waves of about 10 seconds period recorded at Tinemaha. For these waves, the multiple events behave more like a propagating source.

To correct for directivity it is necessary to know the rupture

length and the propagation velocity. From the plot of displacements
(Figure 1.9) and the distribution of aftershocks shown in Figure 1.1a,
the main rupture appears to have extended from the epicenter to
Cocopah, a distance of about 20-25 km. The rupture velocity is
approximately given by the fault length divided by the time difference
between the triggering of the strong motion instrument and the origin
time of the last event, about 15 seconds. This gives an effective
rupture velocity of about 2 km/sec. Estimates of the source param-
eters (b = 20 - 25 km, v ≈ 2 km/sec, C ≈ 3.4 km/sec at T_o = 11 sec,
and cos θ = - 0.99) give an approximate value for χ to be 4.5 to
5.0 and $\left| \frac{\sin \chi}{\chi} \right|$ ~ 0.20 which is in approximate agreement with the
shape of the spectrum given in Figure 1.4a as indicated by spectral
gaps at periods of about 9 and 15 seconds. With the above assump-
tions one obtains

$$\text{at Tinemaha:} \quad M_{0\text{-SEISM}} \approx 1.1 * 10^{26} \text{ dyne-cm}$$

$$\text{at Haiwee:} \quad M_{0\text{-SEISM}} \approx 1.3 * 10^{26} \text{ dyne-cm}$$

In these calculations the following values were used: $Q \approx 200$;
$A_L = 0.91 * 10^{-18}$ cm/dyne; T_o = 11 sec; R_{T_o} = ground amplitude
in microns/trace amplitude in millimeters = 60; C = 3.7 km/sec;
Δ = 546 km for Tinemaha; Δ = 440 km for Haiwee; δ_{HAIWEE} = 31°;
$\delta_{TINEM.}$ = 27°. These two determinations are regarded to be in
good agreement considering the difficulty in the interpretation and
the accuracy of the necessary assumptions.

H. COMPUTATION OF MOMENT FROM FIELD OBSERVATIONS

The computation of the moment from field observations was performed using the well known relation (Maruyama, 1963; Aki, 1966; Brune and Allen, 1967):

$$M_{0-field} = \bar{u}\mu A$$

From the field evidence the average displacement along the complete fault length measured on the surface of the ground was 1.25 m. The fault length was about 65 km (Richter, 1958). The depth of the faulting was estimated to be about 7 km by fitting the geodetic data given by Byerly and DeNoyer (1958) with the theoretical curve for a strike-slip fault taken from Knopoff (1958). With $\mu = 3.3 \times 10^{11}$ dyne/cm^2, one obtains for the whole fault plane

$$M_{0-field} = \frac{3}{4} \times 1.25 \times 3.3 \times 0.7 \times 6.5 \times 10^{25} = 1.4 \times 10^{26} \text{ dyne-cm}$$

However, if the northwestern section of the fault did not slip during the main event, but later during the Brawley event as suggested above, then the field moment for the main event should be calculated from the southern section only.

Taking the length of the fault section corresponding to the main propagating rupture to be about 25 km fault depth of 7 km and the average displacement of 2.7 meters corresponding to the fault section between the All American Canal and Cocopah, one obtains essentially the same moment:

$$M_{0-field} = \frac{3}{4} \times 2.7 \times 3.3 \times 0.7 \times 2.5 \times 10^{25} = 1.2 \times 10^{26} \text{ dyne-cm}$$

The moment estimated from the field evidence would be expected to be somewhat larger than that estimated from the seismic results because the field observations include fault slippage occurring during later aftershocks as well as creep. Considering the uncertainties involved in both the field data and the seismic analysis, the agreement is remarkable.

I. MAGNITUDE AND MOMENT

The published magnitude for the Imperial Valley earthquake of 1940 is 6.7 (Richter, 1958). However, a strictly objective determination of magnitude using Wood-Anderson torsion seismometer records gives a value of 6.3. The magnitude indicated from the strong motion instrument is also 6.3. It was originally felt that more weight should be given to distant stations in the assignment of 6.7 as the magnitude. The magnitude M_L^* = 6.3 is obtained from the average of magnitudes determined using maximum deflections on EW and NS Wood-Anderson components at stations Tinemaha, Haiwee, Mt. Wilson, Pasadena, Santa Barbara, and Riverside as shown in Table 2. The period of these deflections is about 1 sec.

---

[*]By definition, $M_L = \log A - \log A_0$ where A is the amplitude in mm of the trace recorded by a standard Wood-Anderson torsion seismometer ($V = 2800$, $T = 0.8$ sec, $\zeta = 0.8$) at a distance of 100 km from the epicenter, and A_0 is the amplitude with which the same instrument would record an earthquake of magnitude zero, at this distance. The magnitude defined in this way is a measure of the largest amplitude of ground motion at a given distance. Determination of magnitude in this manner is not considered reliable at distances greater than about 600 km.

TABLE 2

Data Used in Determining the Local Magnitude M_L

For the Imperial Valley Earthquake of 1940

Station	Direction	Distance (km)	Distance Correction	Station Correction	max A (mm)	log A	M
Tinemaha	EW	546	4.8	-0.2	50.5	1.70	6.3
	NS				79	1.90	6.5
Haiwee	EW	440	4.6	0.	~110	2.04	6.6
	NS				~125	2.1	6.7
Riverside	EW				103	2.02	5.9
	NS	224	3.7	+0.2	-	-	
Mt. Wilson	EW	290	4.0	-	<143	2.16	6.2
	NS				<149	2.17	6.2
Pasadena	EW	294	4.0	+0.2	90.5	1.96	6.2
	NS				?> 79.5	1.90	6.1
Santa Barbara	EW	435	4.6	-0.2	> 85	1.92	6.3
	NS				91	1.96	6.4

Subsequently, Gutenberg increased the magnitude to 7.1 on the basis of determinations of 20 second surface wave magnitudes for stations La Plata, Uppsala, DeBilt, Stuttgart, and Helwan (Richter, personal communication) and on the basis of the field evidence of extensive faulting.

In the case of multiple event earthquakes, obviously the magnitude versus moment relationship need not be single valued since an increase in the number of events will increase the total moment but not necessarily the maximum amplitude. The magnitude calculated from the moment (long-period waves) will tend to be larger than the magnitude determined from the record of the short-period waves. The magnitude directly determined from the record of the short-period waves will correspond more closely to the moment for the single event which generated the biggest short-period waves. Stated otherwise, a series of events propagating in space will constructively interfere for wave lengths large compared to the source dimensions, but not constructively interfere for shorter wave lengths (Brune and King, 1967).

J. DESTRUCTIVENESS OF MULTIPLE EVENT SOURCES

As can be seen in Figure 1.2a to Figure 1.2k at least 13 events occurred in the period of approximately 6 minutes, one large event every 5 to 10 seconds during the first 25 seconds and about one clearly recorded event every 25 to 30 seconds during the next 5 minutes. The shortest resolved time interval between two distinct

events was close to 4 seconds and the longest 50 seconds. However, other events not resolved could have occurred at shorter intervals. The interval between relatively large events during the latter 5 minutes was of the order of 1 minute.

The effect of a given ground motion on typical engineering structures is commonly investigated by calculating the response spectrum. This has been done in the engineering literature for the first 30 seconds of the Imperial Valley, 1940 earthquake, including the first four events (Alford, et al., 1951). It is now of interest to investigate the additional effects on structures that might be associated with the later events.

If the building is represented by a one degree of freedom simple oscillator with a natural frequency of vibration p and a fraction of critical damping ζ, transient response to a given initial velocity and displacement is

$$x = e^{-p\zeta t} [c_1 \sin p \sqrt{1 - \zeta^2} t + c_2 \cos p \sqrt{1 - \zeta^2} t]$$

where c_1 and c_2 depend on the initial velocity and displacement. This is an oscillatory motion with an amplitude given by

$$A(t) = e^{-p\zeta t}$$

Many buildings have a small equivalent viscous damping, not exceeding 2% if vibration is in the elastic range or perhaps 5% to 8% if the vibration level is in the plastic range. The natural period of the vibration of most buildings would fall in the range from $T = 0.05$ sec, for small stiff structures to $T = 4.0$ sec or greater for tall and

flexible structures.

If it is supposed that the excitation of the building vibration is small between the successively arriving events, the vibration will die out during the "quiet" interval of time as $e^{-p\zeta t}$. When $p\zeta t$ becomes close to 3.0 the amplitude of the oscillatory motion will be 20 times smaller than at the beginning of the quiet interval ($t = 0$) i.e., at the moment when the excitation caused by the m-th event has just ceased to be significant. This qualitative argument gives

$$t_{1/20} = \frac{3}{\zeta p} \quad \text{or} \quad t_{1/20} = \frac{3}{2\pi} \frac{T}{\zeta}$$

Taking $T = 1.0$ sec and $\zeta = 0.02$, $t_{1/20} = 24$ sec. Thus for most buildings excited by a sequence of events similar to the Imperial Valley earthquake, the vibration will nearly die out between most of the individual events. Buildings with relatively short natural periods of vibration (say 1 sec or smaller) will respond to a sequence of events such as the Imperial Valley earthquake as if there were 13 or more different earthquakes each with duration of 3 to 30 sec. For such buildings the time build up of the amplitude of the vibration will depend on the duration of each single event and the occurrence of a new event every 30 sec or so will not be important for response amplitude, although it might be important if progressive weakening is involved.

For buildings whose natural period of vibration is longer, amplitudes may be cumulatively increased by the sequence of events. The actual rate at which building vibrations grow will depend on the

effects of the interference of the waves coming from the successive events, on the number and duration of events, on the distance between the structure and each event, and on the elapsed time between events. It is clear that for a sequence of events with similar long-period wave amplitudes, the response amplitude could increase with the total number of events in the multiple sequence. In this case, there might well be a good correlation between destructiveness and seismic moment (or, equivalently to the amplitudes of very long-period waves, e.g., mantle wave magnitude, Brune and Engen, 1968).

Presently, there are increasing numbers of tall buildings and other structures with long natural periods of vibration which may be subject to vibration with cumulatively increasing amplitudes if excited by a sequence of events similar in character to the Imperial Valley earthquake of 1940. In order to accumulate necessary data for analysis of such structures calculation of the relative velocity spectra should be extended to longer natural periods of vibration, say up to 10 sec. In addition, much longer portions of the available strong motion accelerogram records should be used as an input.

K. CONCLUSIONS

1. Analysis of the P, S and short-period surface waves recorded on the El Centro strong motion accelerometer indicates that the Imperial Valley earthquake of May 19, 1940, consisted of a

series of at least 13 distinct events occurring during the period of about 6 minutes and distributed over a distance of about 25 km SE along the fault from the initial epicenter. Most of the energy and seismic moment was produced in the main sequence of about 4 events which occurred in the first 15 seconds and were distributed over the same section of the fault. Events recorded in the 5 minutes after the main sequence were important for engineering studies of strong earthquake ground motion, since their magnitudes ranged as high as 5.8, only 0.5 magnitude units smaller than the largest event in the main sequence. The rupture of the NW section of the fault may have taken place during an aftershock herein called the Brawley event, in agreement with an earlier suggestion by Richter (1958). The Tinemaha record of surface waves generated by the Brawley event, one hour and 17 minutes after the first event, illustrates the difference between surface waves from a simple event and those from the complicated main event.

2. The seismic moment calculated for the main sequence of events, about 10^{26} dyne-cm, agrees well with the moment inferred from field observations of the fault offset.

3. Two lines of evidence indicate that the seismic energy released in the first 15 seconds was generated by a series of events propagating SE from the vicinity of the initial epicenter along a section of the fault 25 km long:

a. The Richter magnitude, $M_L = 6.3$, determined from stations NW of the epicenter was 0.8 magnitude units less

than the surface wave magnitude, $M_s = 7.1$, determined from surface waves recorded SE and E of the epicenter. This suggests a focusing of energy toward the SE such as would be the expected for a rupture propagating in that direction.

b. The distortion of the seismogram and moving window Fourier spectrum of surface waves at Tinemaha is consistent with a rupture propagating toward the SE.

4. For the Imperial Valley earthquake, buildings with a relatively short fundamental period of oscillation (say, 1 sec and shorter) would respond as if the individual aftershock events were completely separate in time whereas buildings with a relatively long fundamental period of oscillation (say, 2 sec or longer) might vibrate with gradually increasing amplitude and thus the amount of damage could be closely related to the duration of the energy release in the whole sequence.

CHAPTER II

RELATIVE AMPLITUDES AND SPECTRAL PROPERTIES OF
STRONG EARTHQUAKE GROUND MOTION ASSOCIATED
WITH HORIZONTALLY PROPAGATING SEISMIC WAVES

NOMENCLATURE

A	bound on θ and η, also used as A_θ^η in Appendix I
$A_{1,2}$	constants representing initial conditions for the $T(t)$ function
$A(x)$	amplitude of $X(x)$ function
a	left limiting point of the x interval
$a\left(\begin{smallmatrix}H\\f\end{smallmatrix}\right)$	function defined and used in Appendix I (evaluated at H or f)
b	right limiting point of the x interval
$b\left(\begin{smallmatrix}H\\f\end{smallmatrix}\right)$	function defined and used in Appendix I (evaluated at H or f)
C, $C(x)$	phase velocity, also used as a constant in $Z(x,z)$ solution
$c\left(\begin{smallmatrix}H\\f\end{smallmatrix}\right)$	function defined and used in Appendix I (evaluated at H or f)
D	constant in $Z(x,z)$ solution
F	constant in $Z(x,z)$ solution
f	frequency of vibration (cps)
$f(\alpha)$	numerical function
H_0	constant layer thickness
H, $H(x)$	variable layer thickness along x direction
ℓ	wave length ($\ell = cT$) along the boundary plane
M	constant

N, $N(\omega)$	constant
n	integer, number
P_1, P_2	frequency parameter in the modal function $Z(x,z)$
$p(x)$	function $\left(p(x) \equiv 1/C^2(x)\right)$
$R_{1,2}$	rate of the energy flux, also used as a numerical constant
r	ratio of the energy flux $(r \equiv R_2/R_1)$ in the infinite medium and the surface layer
$r(t)$	function defined by $p(x)$ and its derivatives
$S_{F/\eta}(T)$, $S_{F/0}(T)$	Fourier amplitude spectrum at distance η and $\eta = 0$ respectively
SH	horizontally polarized S (shear) waves
s	coordinate along the normal to the boundary surface
T	period of vibration $(T = 2\pi/\omega)$, used also as a limit of the interval for the variable t
$T(t)$	function defining the time dependence of $v(x,z,t)$
t	time coordinate
U	group velocity
u	component of motion in x direction
$v_{1,2}$	displacement in y direction in the layer (1) and in infinite medium (2) respectively
w	component of motion in z direction
x	coordinate axis
y	coordinate axis
α	numerical constant
$\alpha(x)$	dimensionless function defining the boundary between the surface layer and the infinite medium

$\beta_{1,2}$	shear wave velocity, (1) in the layer and (2) in the infinite medium
δ	group velocity ratio $(\delta \equiv \beta_1/U)$
$\delta\begin{pmatrix}H\\f\end{pmatrix}$	function defined and used in Appendix I (evaluated at H or f)
$\epsilon, \epsilon(x)$	phase velocity ratio $\left(\epsilon(x) \equiv \beta_1/C(x)\right)$
$\epsilon\begin{pmatrix}H\\f\end{pmatrix}$	function defined and used in Appendix I (evaluated at H or f)
$\eta(t,\omega)$	normalized $X(x)$ function
η	angle of the layer surface inclination along x, also used as the dimensionless distance along x direction $(\eta = x/H_0)$
θ	incidence angle (in Appendix II interchangeable with φ), inclination of the boundary between the layer and the infinite medium, also used as the divergence of the vector field u
θ_c	critical incidence angle
$\varkappa$	dimensionless constant $(\varkappa = \rho_2/\rho)$
λ	dimensionless constant $(\lambda = \omega H_0/\beta)$ used in Appendix I, also used for the Lamé constant
$\mu_{1,2}$	Lamé constants in the layer and in the infinite medium respectively
ξ	dimensionless ratio $(\xi = \mu_2/\mu_1)$, also used as a variable of integration
π	numerical constant $(\pi = 3.14159)$
$\rho_{1,2}$	densities of the layer and infinite medium respectively
$\rho(f)$	function used in Appendix I
τ	variable of integration
Φ_0, Φ_0'	function used in the period equation
φ	phase shift, also used as an incidence angle in Appendix I

χ dimensionless constant $(\chi = \beta_2/\beta_1)$

$\psi(x)$ dimensionless function defining the surface of the layer

ω mathematical frequency of vibration $(\omega = 2\pi f)$

Other symbols not defined here are given in the text with an appropriate explanation.

A. MODEL WITH HORIZONTALLY PROPAGATING ENERGY

Most of the past theoretical work to determine the effects of the ground on the amplitudes of earthquake strong motion was mainly concerned with the effects of a uniformly stratified layer, or a set of layers, on a vertically propagating plane front of shear waves. Studies were made on the amplification of the wave amplitudes because of successive reflections and refractions through one or several layers. The results were used to determine the natural periods of layer vibrations, their distribution in the frequency space and consequently their effect on response spectra. The justification for applying such a model was that waves at distant stations essentially propagate vertically because of the decreasing velocity of the wave propagation towards the surface of the ground. One major objection to such an assumption is that strong motion, significant to earthquake engineering studies, occurs very close to the source of the earthquake energy release, in fact so close that it is difficult to imagine that the most significant part of the wave energy would be represented by only one vertically incoming ray. It seems more

natural to think of the motion caused by the superposition of many rays, generated by the reflections and refractions as well as scattering through the ground and also emitted from the different locations along the fault surface, with each ray having in general a different incidence angle. Of course, an exception to this would be the case when the source is beneath the surface point at which the motion is recorded.

It seems therefore that the model with vertically incoming waves towards the stratified surface of the ground could be appropriate for studying the influence of the surface layers on the amplitudes of P and S waves from distant earthquakes and teleseisms. Such a model could probably also be used for the near but sufficiently deep-focus earthquakes, but not always for the analysis of the close fields of the ground motion caused by shallow and surface faulting.

Classical observational treatments of elastic waves, generated by the energy released from earthquakes, distinguish four principal wave groups: P, S, L and R. Symbols P and S stand for the compressional and shear waves while L and R stand for Love and Rayleigh surface waves respectively. P and S are also often called body waves, and in fact are the two basic types of motion that can exist in the homogeneous elastic and infinite medium. Boundaries of the elastic solid, together with discontinuities of the material properties, cause transformation of original P and S motions into the two basic surface wave groups, here called L and R. The energies belonging to each of the four groups propagate

with different velocities, the velocity of P being the biggest. The resulting motion at great distances may be recorded as clear and distinct pulses (P and S) or a train of dispersed waves (L and R). Recent observations have shown that there are many other phases and wave forms but most of them may be included in one of the four generalized P, S, L or R groups of motion.

The motion close to the source of the energy release can not be described by the above simple wave groups. It is composed of essentially the same four basic types of waves but often not clearly separated because of the source proximity. In addition the high frequency terms whose amplitudes decay rapidly with distance and so can not be observed on most of the teleseismic records, are now present together with other effects some of which are caused by the source mechanism. Also, source size relative to the distance to the station, the spatial and temporal distribution of the pattern of the energy release, the radiation pattern and properties of the medium along the wave propagation path between the source and the recording station, are important.

In order to study strong earthquake ground motion close to the source of the energy release, it is proposed here to consider a model in which seismic energy is propagated along the surface of the ground or a "model with horizontally propagating energy." From mathematical considerations it may be seen that for the existence of surface Love waves, the velocity of the SH wave propagation must increase as a function of the depth, or in the simplest case there

must exist at least one layer. This, however, does not seem to be a serious restriction for the existence of surface waves along the plane boundary, because actual ground is so non-uniform that in all practical cases it can be represented by a model with a variable velocity. Rayleigh surface waves may exist also in the absence of a surface layer, i.e., along the surface of the infinite uniform half space, and in that case there is no dispersion of the wave form.

To give some immediate motivation for the model with horizontally propagating energy, one may consider a simple idealized case consisting of one layer on top of an infinite and uniform half space. To simplify the discussion further, it may be supposed that the source consists of a line s (Fig. 2.1 and Fig. 2.2) which extends to infinity in y direction. Further it may be assumed that this line represents a source which emits seismic energy radially and uniformly in all directions $0 \le \theta \le 2\pi$ and at a constant rate. Because of the elastic properties of the layer and the infinite medium welded together at $z = 0$, all of the energy transmitted in directions such that $|\theta'| \le \frac{\Theta}{2}$ (Fig. 2.1), when the source is in the layer, will be conserved in the layer for all subsequent times. On the assumption that the line source is generating SH waves, a simple application of Snell's law gives.

$$\Theta = \pi - 2 \sin^{-1}\left(\frac{\beta_1}{\beta_2}\right) \tag{1}$$

when the source is in the layer, and

$$\Theta = \frac{\pi}{2} - \sin^{-1}\left(\frac{\beta_2}{\beta_1} \sin \theta_c\right) = 0 \tag{2}$$

LINE SOURCE IN THE LAYER
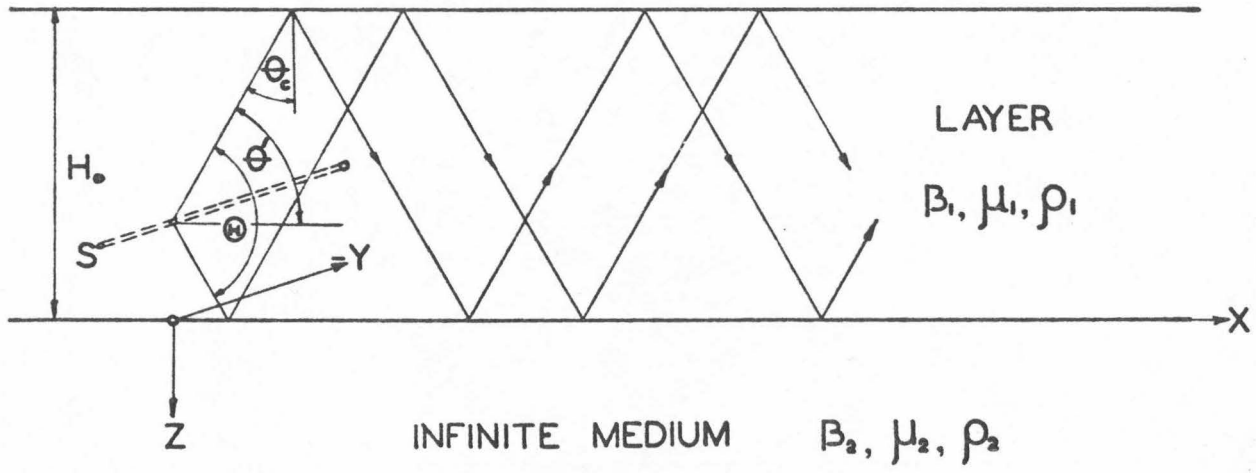
Figure 2.1. Line source in the layer

LINE SOURCE IN THE INFINITE MEDIUM
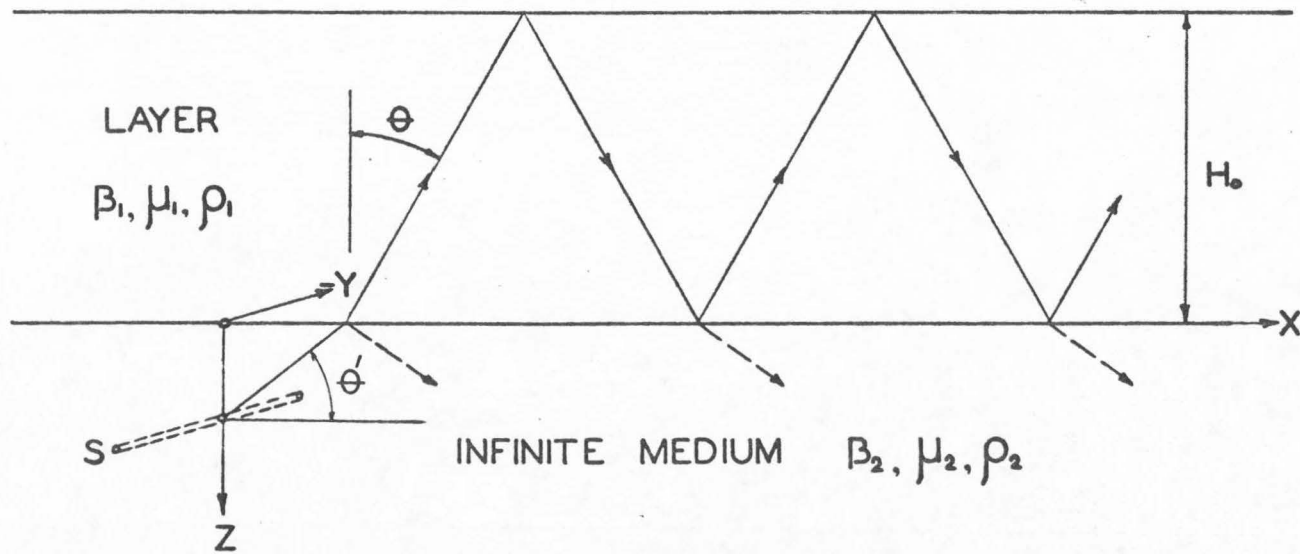
Figure 2.2.   Line source in the infinite medium

when the source is in the infinite medium; β_1 and β_2 are the velocities of the SH waves in the layer and in the infinite medium respectively. Waves in the directions $\Theta/2 \leq |\theta'| \leq \pi/2$ for the source in the layer (Fig. 2.1) and $0 \leq \theta' \leq \pi/2$ for the source in the underlying infinite medium (Fig. 2.2) will initially bounce in the layer but will loose a certain fraction of their amplitude at each point of the reflection and refraction along the boundary $z = 0$. Their contribution to the total amplitude of the ground motion at the surface will tend to zero as the distance from the source increases indefinitely. The above representation is of course symmetric in the negative x direction from the source s.

Many destructive strong earthquake ground motions are generated near fault systems often extending to the surface of the ground. In such cases energy is not radiated from a single and infinitely long line, but from portions of the two surfaces along which the ground slips. From the analogy with the preceding qualitative discussion of the line source it is clear that if the fracture extends to the surface and is not much deeper than the thickness of the layer, most of the seismic energy will be preserved in the layer provided that the velocity contrast between the layer and the infinite medium is great enough. That portion of the energy which is conserved in the layer will represent a superposition of the successively bouncing P, SH and SV waves which travel along the x direction (Fig. 2.1 and Fig. 2.2). Constructive interference of these waves leads to the Love and Rayleigh surface waves. The analysis presented in the following sections is concerned with Love waves only. In

principle, a similar analysis may be carried out for Rayleigh surface waves as well.

Attempts to decipher the record of strong earthquake ground motion close to the causative fault in terms of simple wave groups can often be only tentative. This is because most of the observed bursts of energy on the records are the result of superposition of many various waves generated by reflections and scattering through the non-homogeneous medium, and do not necessarily display the separation into the four basic groups P, S, L and R characteristic of distant seismological records.

The record of strong earthquake ground motion is almost always in the form of an accelerogram. The nature of this recording is such that higher frequency motions of the ground are recorded with greater emphasis than the lower frequencies. Seismological records on the other hand, because of the variety of instrument characteristics, may be accelerometers, displacement-meters, or something in between depending on the natural period of the instrument as compared to the period of the measured wave motion. Typical strong motion accelerometers usually give information on the waves of periods ranging from less than 0.1 seconds to the order of 10 seconds. Most seismological instruments cover longer periods of ground motion. Since they are usually located far from the energy release, they do not record high frequency vibrations in detail because those have been much attenuated and filtered out along the

propagation path. Since higher frequency seismic waves are more sensitive to various inhomogeneities and discontinuities of the ground properties, they can hopefully yield more information on the local geology and the details of energy release. Such high frequency waves will of course need to be recorded sufficiently close to the source to avoid significant attenuation.

P waves on the strong motion record can be recognized by distinct high frequency pulses on the vertical component of the instrument record. S waves will show predominantly on the two horizontal components, also in the form of high frequency pulses, but usually with somewhat longer periods of vibration than the P group. Depending on the distance from the source, the S waves will be near the beginning of a dispersed group or train of waves which continuously merges into the L and R waves of longer periods. The duration of P and S groups on the strong motion accelerogram, close to the source, will be of the order of several seconds each, depending on the source mechanism. The following surface wave motion will last much longer, up to ten seconds and more, depending on distance. Because of the emphasis of the higher frequencies on the accelerogram record, surface waves may not appear with big acceleration amplitudes although their wave displacement amplitudes may be quite significant. On distant seismological records on the other hand most of the biggest recorded amplitudes of vibration, and also the long lasting trains of waves, will be surface Love and Rayleigh waves for the majority of surface or shallow shocks. P and S phases, well separated in time and arriving much earlier

than the train of surface waves, will be usually represented by a few pulses of small amplitude. This short outline of the difference between strong motion and the distant seismological records is only an illustration of some qualitative features and depends very much on the characteristics of the instruments that are used.

The mechanism of seismic wave generation is not yet completely understood. It is closely related to the mechanics of faulting, the amount of the released potential energy which was stored before the fracturing, and the manner in which the fracture takes place. Since the greatest part of the present knowledge of the earthquake mechanism is derived from a study of radiated elastic waves, attempts have been made to define equivalent source forces or systems of forces which would produce the same elastic waves as those which are observed after the earthquake.

A simplified source representation by a model with forces acting essentially at a point is useful and sufficiently accurate when the observing station is far from the source and when the recorded waves are sufficiently long compared to the source dimensions. Strong earthquake ground motion, as already mentioned, occurs close to the locus of the energy release, which is often a surface fault. Since the wave lengths which are of interest to earthquake engineering are relatively short, corresponding roughly to the periods of 0.1 to 10 sec, and since distances from the locus of energy release are small compared to the source dimensions, the source can not be represented by a simple model with forces acting only at one point. An alternative representation could consist of

many small sources distributed in time and space and scaled appropriately to account for the total integral effect. If motion occurs along a well defined vertical strike slip fault, a model based on the horizontally guided SH waves may be a fair representation of the predominant motions in directions parallel and perpendicular to the orientation of the fault plane.

Some observations of earthquake ground motion are difficult to explain by the simple theory of a vertically incident infinite train of S waves upon the set of the uniform horizontal layers, or even contradict some of the qualitative conclusions based on that theory. A few of such observations will be pointed out here. For example (see Gutenberg, 1957, p. 238, Fig. 16) for nearby earthquakes there is an increase of the intensity of shaking at locations where seismic waves emerge from the rock into the alluvium, but then as waves proceed into the deeper alluvium amplitudes decay. Similarly, for earthquakes originating north of the Imperial Valley, it was observed that the intensity of shaking rapidly decays southwards in the valley (Richter, 1958). A simplified case illustrating such a situation is presented in the qualitative manner in Fig. 2.3. Most of the wave energy generated by a nearby fault enters the valley along its boundary AB and less along BC. A typical wave is refracted into the layer at α and reflected once from the surface at β. By the time the wave approaches γ, the orientation of the lower interface has sufficiently changed so that most of the energy originally contained in that ray is reflected back into the layer. From that point
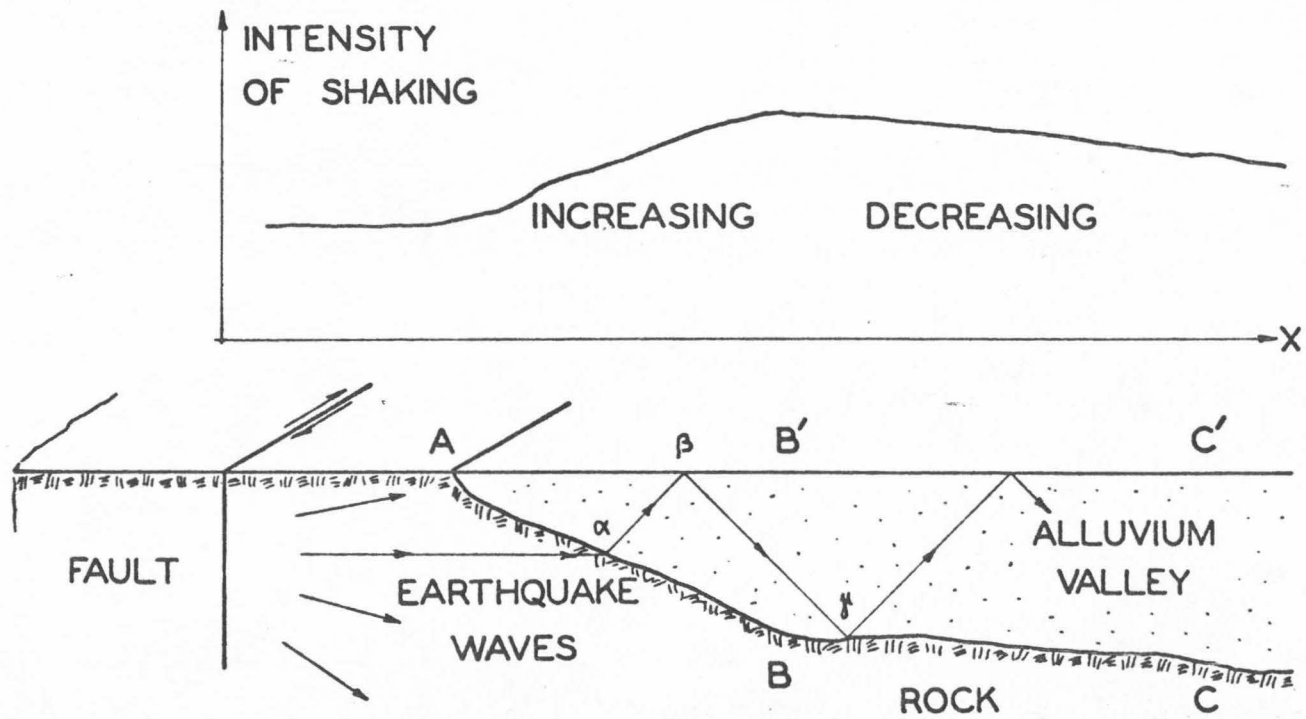
Figure 2.3. Influence of the underlying soil on the intensity of ground shaking.

on the wave bounces in the layer generating a surface wave. If the boundaries are sufficiently smooth so that the predominant part of the motion of the SH type can be explained by the theory of Love waves, and if the thickness of the alluvium gradually increases, simplified theory indeed predicts that wave amplitudes will decrease as the wave energy progresses into the deeper alluvium. Although the boundaries here are very complicated it may be pointed out that the intensity of shaking increases between A and B' in the manner probably similar to that predicted by the model with vertically incoming shear waves although the process is quite different. On the other hand from C' to the right, the functional behavior of the intensity of shaking is predominantly related to the properties of the surface waves.

A consideration of the one layer problem and vertically and steadily propagating shear waves predicts that the interference may lead to amplitude build up at the surface of the ground. The one-dimensional nature of this model implies that for the given layer thickness H_0 and shear wave velocity β_1, and for the same excitation, periods T of the layer vibration for which the amplitudes are a maximum are fixed for all points of the surface and are the same for all x. Instrumental studies to analyze x-distributions of ground motion are almost entirely lacking. There is an indication, however, based on the observed ground motion, that for different locations

along the x direction spectrum peaks may occur at different periods (Housner and Trifunac, 1967).

It should be pointed out here that neither model with vertically propagating shear waves nor the model with horizontally propagating energy can be used alone and in all circumstances. The reason for this is that both models are based on idealizations which are very restrictive and almost never satisfied in full. The assumptions that the materials of the layer and the underlying infinite medium are homogeneous, isotropic and elastic are probably not the most sensitive. The most serious violations in any comparisons with the real alluvium valleys are the boundary conditions. Both models are based on a layer that is uniform in the y direction (Fig. 2.4) and is either of uniform thickness H_0 or of variable thickness $H(x)$ along the x direction. Thus when applying some of the conclusions based on the theoretical model analysis to real cases, special attention has to be given to the consequences of the violated boundary conditions. Furthermore both models are based on stationary and continuous input of wave energy with a few exceptional treatments (e. g., Whitman, 1968; Tsai, 1969 among others). Since strong earthquake ground motion is of a transient character this is another serious simplification.

It may be noted here that the difference between the stationary and transient wave motion is particularly significant when considered

LAYER WITH A VARIABLE THICKNESS
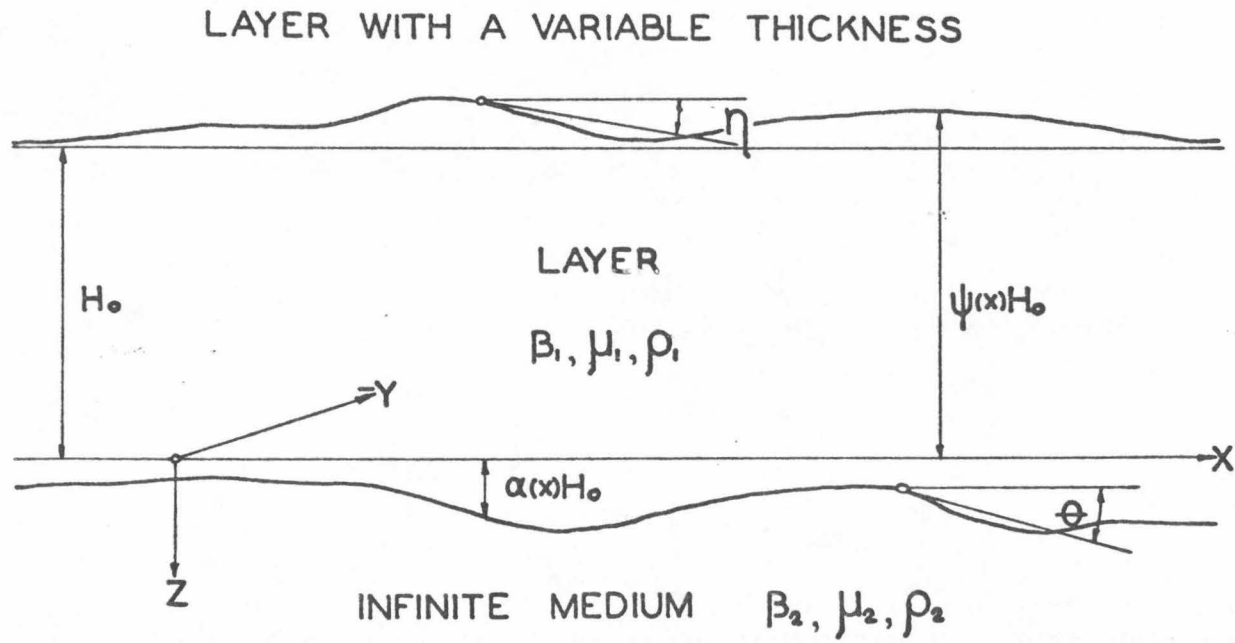
Figure 2.4. Surface layer with a variable thickness

from the point of view of the rate at which the energy propagates as a function of time. Transient wave motion is characterized by the fact that before the energy generation at the source is initiated there is no motion throughout the medium and that subsequently the velocities of the propagation are finite. These two statements are equivalent to saying that there is no motion beyond a certain distance $\Delta = v_{max}(t-t_0)$ from a point source in an infinite homogeneous elastic medium. Here Δ is the radial distance measured away from the source, v_{max} is the biggest velocity that can exist in the medium, t is the time and $t = t_0$ is the time at which the source was initiated. If the pattern of the energy release at the source is nonstationary in time, the rate of energy flux at any point of observation will also be nonstationary and in addition further complicated by the filtering effects of the ground. Simple models that assume stationary and constant rate of energy input, as is done in many treatments on the vertically incoming shear waves as well as the present analysis of horizontally propagating energy, are therefore violating the transient nature of earthquake motions. The stationary assumption often allows a simple treatment of certain properties of stationary trains of waves which are similar for transient waves. The reason for the simplicity of the stationary wave problem is the fact that the initial conditions do not have to be considered.

When the geology of the site in question is simple and close to the case of one or several layers of sediments, so that both models could be used, the question arises as to which is most appropriate.

The answer is that both should be considered. This is because both body and surface waves are to be expected. A statistical study of the seismicity of the region and the existing active faults may suggest the most probable direction and the distance of the origin of a future earthquake. Knowing the distances and the geology of the area will hopefully allow an estimation of the character of the shaking resulted by P, S and surface waves.

Because P and S waves show practically no dispersion it suffices to associate with them fixed velocity of propagation. Surface waves are all dispersed and propagate with the velocities which are in the interval between the maximum C_{max} and the minimum C_{min} phase velocities. Therefore, if the source is at the distance Δ from the recording station surface wave motion will last for

$$\Delta \left(\frac{1}{C_{min}} - \frac{1}{C_{max}} \right)$$

time units, while the body wave motion will be almost instantaneous. Of course, in real nature their duration will be even more extended because of reflection and scattering effects caused by irregularities of the medium through which the waves propagate. Since the duration of shaking plays an important role in structural response to strong earthquake ground motion, the importance of studying surface waves involving horizontally guided energy seems obvious.

The analysis which is presented in the following sections treats only some of the simple and immediate consequences of the concept of horizontally propagating energy under stationary conditions.

Other results based on the same model but subject to different boundary conditions can be derived also.

B. ON THE SIGNIFICANCE OF THE EXISTENCE OF THE LOW VELOCITY SURFACE LAYER ON THE INTENSITY OF SHAKING

Numerous investigations of the problem of the influence of the ground on the intensity of shaking have been carried out, both theoretically and experimentally. The experimental approach is often based on the correlations of known ground properties of the ground response to both major destructive earthquakes and explosions, as well as to smaller disturbances such as teleseisms, microseisms, microtremors, etc. The theoretical approach appears to be more difficult and solutions to only a few simple models are known and understood. This is because practically all theoretical models are founded on very restrictive and often unrealistic assumptions to facilitate the mathematical treatment.

An important problem is how the intensity of shaking of the ground depends on the properties of the underlying soil. In particular does the existence of a "soft surface layer, or of several layers" necessarily imply that the intensity of shaking will be increased, and how could surface shaking depend on the material and the elastic properties of the layer and the underlying medium.

To answer qualitatively this question it may be useful to think in terms of the steady energy flux of waves along the x direction (Fig. 2.6). First the case of a layer with a constant thickness H_0,

and in which this energy travels in the x direction in the layer and in the underlying infinite medium will be considered. To begin with, some of the results given by J. A. Hudson (1961) on the internal reflection of SH waves will be reproduced.

Taking H_0 to be

$$H_0 = \frac{\beta_1}{\omega \cos \theta} (\alpha + n\pi), \quad n = 0, 1, 2, \ldots \tag{1}$$

where β_1 is the velocity of the propagation of SH waves in the layer, ω the circular frequency, θ the angle of incidence and $0 \leq \alpha \leq \pi/2$, a real variable, n being associated with fundamental, first and higher modes, the stress-free surface can be defined by

$$z = - H_0 \tag{2}$$

The motion of the layer v_1 and the underlying medium v_2 respectively can be written as

$$v_1 = 2 \cdot \cos \left[\omega \left(t - \frac{x \sin \theta}{\beta_1} \right) + \alpha \right] \cos \left(\frac{z \omega \cos \theta}{\beta_1} + \alpha \right) \tag{3a}$$

$$v_2 = 2 \cdot \cos \alpha \cdot \cos \left[\omega \left(t - \frac{x \sin \theta}{\beta_1} \right) + \alpha \right] \cdot e^{-\omega \sigma z} \tag{3b}$$

where

$$\sigma \equiv \sqrt{\frac{\sin^2 \theta}{\beta_1^2} - \frac{1}{\beta_2^2}} \quad , \quad \text{and} \quad \omega \sigma > 0 \tag{4}$$

The motion described by v_1 and v_2 represents Love waves whose character is oscillatory in the layer and exponentially decaying in the infinite medium. The number of zeros in the modeshape is given by n, period of the vibration $2\pi/\omega$, and the velocity of the

propagation in x direction $C = \beta_1/\sin \theta$ (Fig. 2.6). The necessary condition for the existence of the Love waves is that $\omega\sigma > 0$ which is satisfied provided $\beta_1 < \beta_2$ and $\pi/2 > \theta > \theta_c$, and where the critical angle θ_c is given by

$$\sin \theta_c = \frac{\beta_1}{\beta_2} \tag{5}$$

The physical significance of the imposed limiting values of θ, $\pi/2$ and θ_c will be indicated later.

One can consider the rate of the mechanical work R or power which may be taken as the rate at which work is done by one side of the plane $x^- = $ const. on the other plane $x^+ = $ const. Rates in the layer R_1 and in the underlying infinite medium R_2 are given by

$$R_1 = \int_{-H_0}^{0} \left(-\mu_1 \frac{\partial v_1}{\partial x}\right) \frac{\partial v_1}{\partial t} \, dz \tag{6a}$$

$$R_2 = \int_{0}^{\infty} \left(-\mu_2 \frac{\partial v_2}{\partial x}\right) \frac{\partial v_2}{\partial t} \, dz \tag{6b}$$

where μ_1 and μ_2 stand for the rigidities of the layer and the infinite medium respectively.

Using the expressions (3a) and (3b) for the displacements v_1 and v_2 in the equations (6a) and (6b) one obtains,

$$R_1 = \mu_1 \omega \tan \theta \left[2(\alpha + n\pi) + \sin 2\alpha \right] \sin^2 \left[\omega \left(t - \frac{x \sin \theta}{\beta_1} \right) + \alpha \right] \tag{7a}$$

$$R_2 = \frac{4\pi\mu_2}{\ell\sigma} \cos^2 \alpha \cdot \sin^2 \left[\omega \left(t - \frac{x \sin \theta}{\beta_1} \right) + \alpha \right] \tag{7b}$$

where

$$\ell \equiv \frac{2\pi\beta_1}{\omega \sin\theta} \tag{8}$$

is the wave length of the displacement along the free surface $z = -H_0$. Defining r to be the ratio of the rate R_1 in the layer and the rate R_2 in the underlying medium, and using the period equation for the Love waves, r becomes

$$r \equiv \frac{R_2}{R_1} = \left(\frac{\mu_2}{\mu_1}\right)^2 \frac{1}{f(\alpha)} \tag{9}$$

where

$$f(\alpha) \equiv \tan\alpha \left[\frac{2(\alpha+n\pi)+\sin 2\alpha}{2\cdot\cos^2\alpha}\right] \tag{10}$$

and α is given by (1) as

$$\alpha = \frac{H_0\omega}{\beta_1}\cos\theta - n\pi$$

This concludes the short outline of some results on the internal re-fraction of SH waves as given by J. A. Hudson (1961). Since $\sin\theta = \beta_1/C$ (see section C-(26)) one can write

$$\alpha = \frac{H_0\omega}{\beta_1}\sqrt{1-\frac{\beta_1^2}{C^2}} - n\pi \;\; ; \;\; n = 0,1,\ldots \tag{11}$$

From the behavior of the phase velocity as a function of α (See Appendix I) if $\beta_1 < \beta_2$ it follows that $\beta_1 < C < \beta_2$ and also when $\alpha \to \pi/2$, the phase velocity C approaches β_1 and $\omega \to \infty$. Also when $\alpha \to 0$, $C \to \beta_2$ and $\omega \to 0$. In other words when $\alpha \to 0$,

the resulting Love waves represent vibrations of long periods and "penetrate" deeply into the underlying infinite medium. At that point the effect of the surface layer on the behavior of waves propagating with velocity C almost equal to β_2 along the x direction becomes negligible. This also means that the amplitude of the mode shape is very slowly decaying as $z \rightarrow \infty$, which in turn implies that most of the energy of the wave vibration is contained in the underlying infinite medium. Thus it might be expected, from this argument, that the ratio r as it is given by equation (9), would be very large and in fact tend to infinity. Examination of the expression (9) shows that this is the case, because when $\alpha \rightarrow 0$, $f(\alpha) \rightarrow 0$ and so $r \rightarrow \infty$. In the other extreme case, when $\alpha \rightarrow \pi/2$ and Love wave lengths ℓ become very short, corresponding to the high frequencies of vibration $f(\alpha) \rightarrow \infty$ and $r \rightarrow 0$. Fig. 2.5 shows the behavior of the normalized ratio r/ξ^2 as a function of α and for the first six mode shapes (defining $\xi \equiv \mu_2/\mu_1$).

As may be seen in Fig. 2.5, the normalized ratio r/ξ^2 is essentially zero for all values of α greater than say 1.0. This means that when

$$\alpha = \frac{\omega H_0}{\beta_1} \sqrt{1 - \frac{\beta_1^2}{C^2}} - n\pi \, \tilde{>} \, 1.0 \tag{11'}$$

all energy which is associated with the frequencies that satisfy the inequality (11') is being "transported" through the surface layer only.

The ratio r depends on the material and elastic constants ρ_1, μ_1, β_1 and ρ_2, μ_2, β_2 and of course on the dimensionless
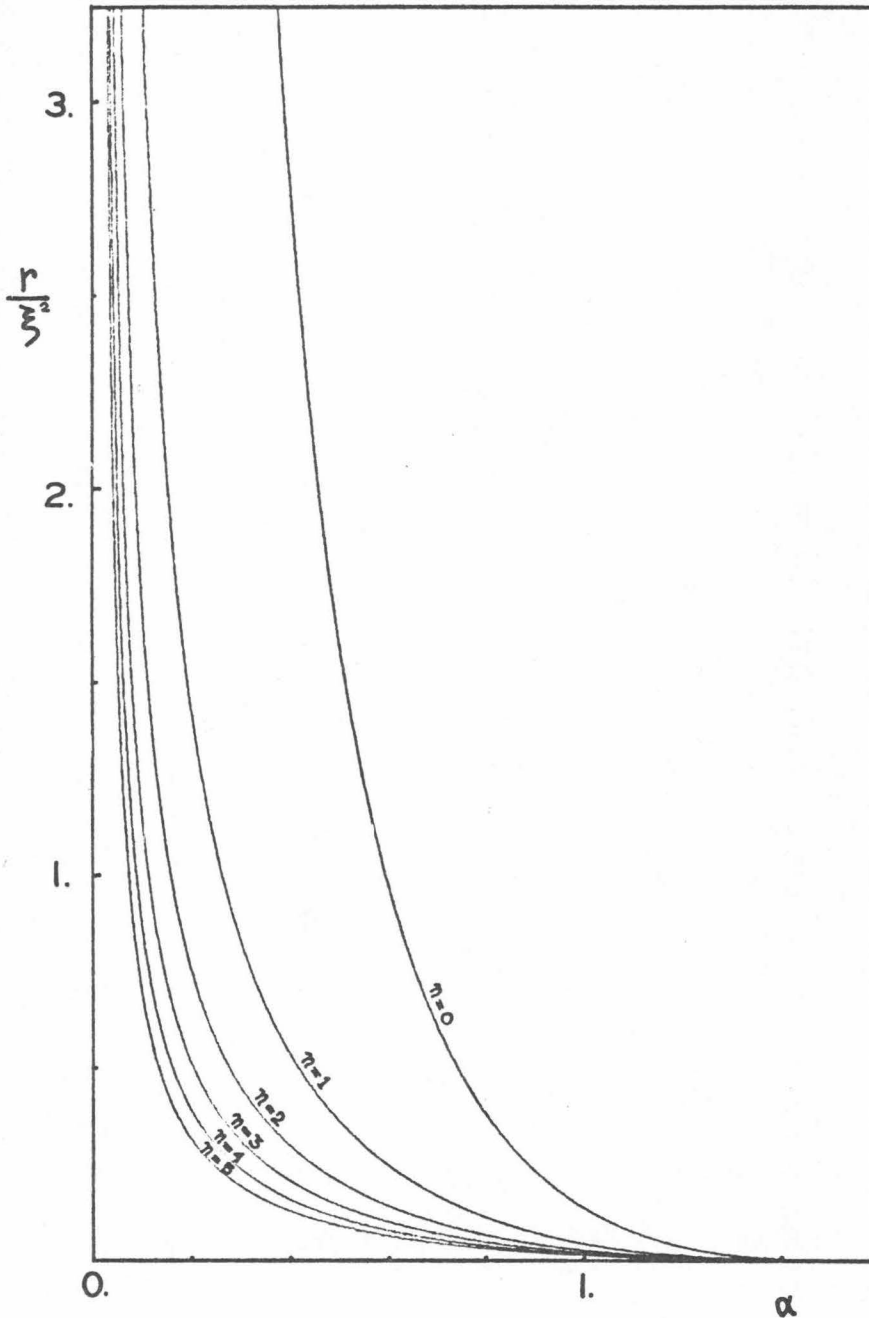
Figure 2.5. The normalized ratio $R_2/R_1\xi^2$ of the rate at which the Love wave energy travels in the infinite medium to the rate at which it travels in the layer, for the first six modes.

parameter $\omega H_0/\beta$. It may be immediately seen that the greater the ratio $\xi = \mu_2/\mu_1$ the greater will be r. Dependence of r on the other constants enters through the dependence of r on α. Since

$$\alpha = \frac{\omega H_0}{\beta_1} \sqrt{1 - \frac{\beta_1^2}{C^2}} - n\pi$$

and

$$\beta_1 \equiv \sqrt{\frac{\mu_1}{\rho}}$$

it is obvious that when ω or H_0 increases, and other parameters and constants are held fixed, r decreases. Also when β_1 decreases α increases and then r again decreases. From such a behavior of the ratio r one can conclude that the part of the total energy of the strong earthquake ground motion which comes from high frequency SH waves will be almost completely contained in the layer if the layer thickness is big, and the velocity in the surface layer, and the ratio $\xi = \mu_2/\mu_1$ are relatively small.

The above analysis of the behavior of the ratio r and its dependence on the material and elastic constants of the media in question as well as the frequency of vibration, offers a basis for the qualitative answer to questions posed at the beginning of this section. Thinking only about that part of the earthquake energy that is transmitted into the surrounding medium in the form of seismic SH waves one can conclude that in the case of a homogeneous iso-tropic infinite elastic medium in the form of the half space, without any surface layer, energy would be transmitted away from the

source in a "uniform" way in all directions. This is of course true if the source of the energy release generates the same amount of energy in all directions in the xz plane.

In the other extreme case when there exists a layer of considerable thickness H_0 and with low velocity of SH waves β_1 and in addition if source of the energy release is in the layer itself or predominantly in the layer, a big part of the total radiated energy will be confined to the layer. In this case the surface layer will act as a "wave guide" or a "wave canal." This second extreme case is of special interest to earthquake engineering in particular to the studies of strong earthquake ground motion. The existence of a surface layer with r close to zero for sufficiently high frequencies indicates that the amount of the energy which is traveling through the layer is big. A part of that energy is directly fed into buildings and other structures that are on the surface of the layer and it is apparent that the presence of the layer increases the intensity of ground motion for the same energy generated by the earthquake. Equivalently, the presence of the surface layer leads to the high concentration of the high frequency energy flux through the layer and in this way causes more energy to be fed into buildings. If there were no surface layer all of this energy would be more uniformly distributed over the whole half space and the intensity of the energy flux per unit volume at the ground surface would be smaller, for the same total energy released. In this work only SH waves are studied in some detail. Similar qualitative conclusions probably hold for other guided waves as well.

C. LOVE WAVES IN A SINGLE SURFACE LAYER

Some consequences of surface wave transmission through a perfectly elastic medium will be investigated. The medium to be analyzed consists of a surface layer, in general of a variable thickness along the x coordinate direction, but with a constant thickness and uniform properties in the y direction, for $-\infty < y < \infty$ (Fig. 2.4). The thickness of the surface layer will be given by $H(x) = H_0\big(\psi(x) - \alpha(x)\big)$ where H_0 is a constant. $H_0\alpha(x)$ defines a lower layer boundary, and $H_0\psi(x)$ defines another cylindrical surface which represents the free surface of the layer. The coordinate system will consist of the three mutually perpendicular axes x, y and z with positive z pointing downward and measured from the horizontal plane defined by $H_0\alpha(x) \equiv 0$.

The most general form of the infinitesimal wave motion in a three-dimensional medium is described by the set of three differential equations (see Ewing, Jardetsky, Press, 1957)

$$\rho\frac{\partial^2 u}{\partial t^2} = \rho X + \frac{\partial}{\partial x}[(\lambda+2\mu)\theta] + \mu\nabla^2 u - \mu\frac{\partial\theta}{\partial x} - 2\frac{\partial\mu}{\partial x}\theta$$

$$+ 2\frac{\partial\mu}{\partial x}\frac{\partial u}{\partial x} + \frac{\partial\mu}{\partial y}\left(\frac{\partial u}{\partial y}+\frac{\partial v}{\partial x}\right) + \frac{\partial\mu}{\partial z}\left(\frac{\partial w}{\partial x}+\frac{\partial u}{\partial z}\right)$$

$$\rho\frac{\partial^2 v}{\partial t^2} = \rho Y + \frac{\partial}{\partial y}[(\lambda+2\mu)\theta] + \mu\nabla^2 v - \mu\frac{\partial\theta}{\partial y} - 2\frac{\partial\mu}{\partial y}\theta$$

$$+ \frac{\partial\mu}{\partial y}\left(\frac{\partial u}{\partial y}+\frac{\partial v}{\partial x}\right) + 2\frac{\partial\mu}{\partial y}\frac{\partial v}{\partial y} + \frac{\partial\mu}{\partial z}\left(\frac{\partial v}{\partial z}+\frac{\partial w}{\partial y}\right)$$

$$\rho\frac{\partial^2 w}{\partial t^2} = \rho Z + \frac{\partial}{\partial z}[(\lambda+2\mu)\theta] + \mu\nabla^2 w - \mu\frac{\partial\theta}{\partial z} - 2\frac{\partial\mu}{\partial z}\theta$$

$$+ \frac{\partial\mu}{\partial x}\left(\frac{\partial w}{\partial x}+\frac{\partial u}{\partial z}\right) + \frac{\partial\mu}{\partial y}\left(\frac{\partial v}{\partial z}+\frac{\partial w}{\partial y}\right) + 2\frac{\partial\mu}{\partial z}\frac{\partial w}{\partial z}$$

(1)

where u, v and w are the components of motion in the x, y and z directions, density ρ and rigidity μ depend on the space co-ordinates and X, Y and Z are the components of the body force in the x, y and z directions. θ is given by

$$\theta = \frac{\partial u}{\partial x} + \frac{\partial v}{\partial y} + \frac{\partial w}{\partial z} \tag{2}$$

In this work only a special kind of motion that is associated with propagation of SH waves, rather than the most general solution of the equation (1), will be considered. The symbol SH stands for horizontally polarized shear waves. For this special case, the components u and w are identically equal to zero. The only nonzero component of the ground motion is v in the y direction which is parallel to the displacement vector of the SH waves. The amplitudes of the waves to be analyzed will depend only on the x and z coordinates. Taking u = 0 and w = 0 into the equation (1) and assuming that the body forces are zero it reduces to

$$\rho \frac{\partial^2 v}{\partial t^2} = \frac{\partial}{\partial x}\left(\mu \frac{\partial v}{\partial x}\right) + \frac{\partial}{\partial z}\left(\mu \frac{\partial v}{\partial z}\right) \tag{3}$$

This is the most general form of the Love wave equation for μ = μ(x,z) and ρ = ρ(x,z). In the special case where μ = μ(z) and ρ = ρ(z), with μ and ρ varying only in z direction, the solution to the above equation may be sought in the form

$$v(x,z,t) = Z(z)X(x)T(t) \tag{4}$$

where X(x) and T(t) are harmonic functions of their arguments. Substitution of this trial solution into the differential equation (3)

shows that the functions $T(t)$, $X(x)$ and $Z(z)$ have to satisfy the following ordinary differential equations

$$\ddot{T}(t) + \omega^2 T(t) = 0 \tag{5a}$$

$$X_{xx}(x) + \frac{\omega^2}{C^2} X(x) = 0 \tag{5b}$$

and

$$Z_{zz}(z) + \frac{\mu_z(z)}{\mu(z)} Z_z(z) + \omega^2 \left(\frac{1}{\beta^2(z)} - \frac{1}{C^2} \right) Z(z) = 0 \tag{5c}$$

where ω is real and positive constant representing the frequency of vibration ($\omega = 2\pi f$), C is the phase velocity which is the eigenvalue of this problem and $\beta(z) \equiv \sqrt{\mu(z)/\rho(z)}$ is the velocity of propagation of SH waves in the medium with the gradually increasing $\beta(z)$ along the increasing z or in the medium defined by the $H_0 \psi(x)$ and $H_0 \alpha(x)$ as above.

The requirements that the surface of the layer $z = H_0 \psi(z)$ is free of any stress, that the layer and the underlying medium are welded together along the surface $H_0 \alpha(x)$, and hence that the displacements and stresses along that surface must be continuous, and that the amplitudes of the wave motion decay monotonically approaching zero as z tends to $+\infty$, provide sufficient conditions to determine $Z(z)$ for given ω and C belonging to that ω. The last requirement to be imposed, i.e., that $Z(z) \rightarrow 0$ as $z \rightarrow +\infty$ demands that the motion be confined to the proximity of the surface layer and the layer itself which is a necessary condition that such motion be a "surface wave." If one calls v_1 and v_2 solutions of

equation (3) for media 1 (in the layer) and 2 (underlying medium) respectively, the boundary conditions described above can be summarized as follows:

1. $\quad \dfrac{\partial v_1}{\partial s} = 0$ $\qquad$ at $\quad z = H_0 \psi(x)$ $\hfill$ (6a)

2. $\quad v_1 = v_2$ $\qquad$ at $\quad z = H_0 \alpha(x)$ $\hfill$ (6b)

3. $\quad \mu_1 \dfrac{\partial v_1}{\partial s} = \mu_2 \dfrac{\partial v_2}{\partial s}$ $\qquad$ at $\quad z = H_0 \alpha(x)$ $\hfill$ (6c)

4. $\quad v_2 \rightarrow 0$ $\qquad$ when $z \rightarrow +\infty$ $\hfill$ (6d)

where $\partial/\partial s$ denotes a dreivative along the normal to the cylindrical surface $z = H_0(x)$ or $z = H_0 \psi(x)$ at a given value of x. In the simple case when $\psi(x) \equiv -1$ and $\alpha(x) \equiv 0$ for all x, $\partial/\partial s$ becomes $\partial/\partial z$.

Writing $v_i = X Z_i T$, $i = 1, 2$, applying condition (6d) and then substituting v_i into the first three conditions (6a), (6b) and (6c) leads to a transcendental equation which gives a denumerable set of C's corresponding to each chosen value of ω and where C is an eigenvalue of the ordinary differential equation (5c) defining $Z(z)$. This transcendental equation is frequently called the period equation for Love waves because for a given C it produces an infinite discrete set of frequencies ω and therefore also periods of vibration $T = 2\pi/\omega$ (for the detailed treatment of the derivation of the period equation see Appendix I).

In the case of a surface layer of uniform thickness H_0, $(\alpha(x) \equiv 0, \psi(x) \equiv -1)$ the solution of the partial differential equation (3)

reduces to the solution of three uncoupled ordinary differential equations. Given the appropriate initial conditions for X_k and T_k and normalizing all $Z_k(z)$ such that $Z_k(-H_0) = 1$, $v(x,z,t)$ corresponding to a given frequency ω is determined for the whole half space $z \geq -H_0$ and for all x, belonging to the phase velocities C_k, $k = 1,2,...,N$, where $N = N(\omega)$. The most general SH type of motion in the y direction can be written then as a superposition of all $v_k(x,z,t)$ for all C_k, $k = 1,2,...,N(\omega)$ and over all frequencies ω.

In the present work the layer thickness is changing in some prescribed way, along the x direction. In particular, the behavior of the wave amplitudes along the surface of the layer as a function of the layer thickness is studied. The general solution to the layer problem when $H = H(x)$ has not yet been found. An attempt will be made to approximate that solution by "reasonable" trial functions that suggest themselves by the simple limiting case when $H(x) = H_0 = $ const. It might be expected that when $H(x)$ is "nearly" constant over a given interval in x, that the solution will be "closely" approximated by some solution which is of the same form as the solution for the case $H(x) = H_0$, but with some parameters possibly slightly perturbed in accordance with the perturbation of $H(x)$ away from H_0. Specifically, one could try the solution of the form

$$v(x,z,t) = X(x)Z(x,z)T(t) \tag{7}$$

such that

$$X_{xx}(x) + \frac{\omega^2}{C^2(x)}X(x) = 0 \tag{8a}$$

$$Z_{zz}(x,z) + \omega^2 \left(\frac{1}{\beta_i^2} - \frac{\omega^2}{C^2(x)} \right) Z(x,z) = 0, \quad i = 1,2 \qquad (8b)$$

and

$$\ddot{T}(t) + \omega^2 T(t) = 0 \qquad (8c)$$

for the case when μ_i and β_i, $i = 1,2$, are constants in the layer and the underlying infinite medium respectively. The more general case in which $\mu = \mu(z)$ and $\beta = \beta(z)$ will not be analyzed here. The approach to the solution of the problem is in general the same, but the solution cannot be expressed in closed form for arbitrary variations of μ and β with z. In principle, such a problem can be solved only by numerical integration of the differential equation.

At this stage one can only hope that a set of differential equations (8a), (8b) and (8c) will generate X, Z and T whose product will satisfy the partial differential equation (3). At worst, one might hope that if (3) is not satisfied identically by the product XZT then the errors represented by the difference of the correct solution v and the appropriate solution $v_A = XZT$ will be small.

Consider now solutions $T(t)$, $X(x)$ and $Z(x,z)$ to the set of equations (8a), (8b) and (8c). Differential equation (8c)

$$\ddot{T}(t) + \omega^2 T(t) = 0 \qquad (8c)$$

for ω real and positive does not give any difficulties and can be immediately solved by

$$T(t) = A_1 \sin \omega t + A_2 \cos \omega t \qquad (9)$$

where A_1 and A_2 are to be determined from the given initial conditions.

Differential equation (8a) for $X(x)$ is not quite so simple and the fact that the phase velocity $C = C(x)$ depends on x does not permit a simple solution in closed form. One can however examine this equation for a special case when ω is "large" using a standard technique (Courant and Hilbert, 1931). Let $1/C^2(x) \equiv p(x)$ so that

$$X_{xx}(x) + \omega^2 p(x) X(x) = 0 \tag{8a'}$$

Now, a new independent variable t can be introduced such that

$$t \equiv \int_a^x [p(\xi)]^{1/2} d\xi \tag{10}$$

where $p(\xi) > 0$ for all $x, \xi, \in [a,b]$ and where $[a,b]$ is a finite interval on x. Then let

$$\eta(t,\omega) \equiv [p(x)]^{1/4} X(x,\omega) \tag{11}$$

where ω indicates dependence of the solution on the parameter ω. Transforming (8a') one obtains

$$\frac{d^2\eta}{dt^2} + [\omega^2 - r(t)]\eta = 0 \tag{12}$$

on

$$0 \le t \le T = \int_a^b [p(\xi)]^{1/2} d\xi \tag{10'}$$

and where

$$r(t) = \frac{1}{4}\frac{p''(x)}{p^2(x)} - \frac{5}{16}\frac{[p'(x)]^2}{p^3(x)} \tag{13}$$

For the initial conditions $\eta(0,\omega) = 1$ and $\frac{d\eta}{dt}(0,\omega) = 0$ solution to (12) is given by the integral equation

$$\eta(t) = \cos \omega t + \frac{1}{\omega}\int_0^t \sin \omega(t-\tau)r(\tau)\eta(\tau)\ d\tau \qquad (14)$$

One may use successive approximations to solve equation (14). Denoting η_i to be the ith approximation, and choosing

$$\eta_0 \equiv \cos \omega t$$

the ith iterate becomes

$$\eta_i(t) = \cos \omega t + \frac{1}{\omega}\int_0^t \sin \omega(t-\tau)r(\tau)\eta_{i-1}(\tau)\ d\tau \qquad (15)$$

In particular for $i = 1$

$$\eta_1(t) = \cos \omega t + \frac{1}{\omega}\int_0^t \sin \omega(t-\tau)r(\tau)\cos \omega\tau\ d\tau$$

$$= \cos \omega t + \frac{\sin \omega t}{\omega}\int_0^t \cos^2\omega\tau r(\tau)\ d\tau$$

$$- \frac{\cos \omega t}{\omega}\int_0^t \sin \omega\tau \cos \omega\tau\ r(\tau)\ d\tau \qquad (15')$$

It is not difficult to show, by repeating iteration (15), that the difference between the true solution $\eta(t)$ and $\eta_n(t)$ tends to zero when $n \to \infty$ and for ω large. That is

$$|\eta(t) - \eta_n(t)| \leq \frac{e^{RT}}{\omega^{n+1}} \qquad (16)$$

where $R \geq |r(t)|$ is a constant for $0 \leq t \leq T$. Therefore when ω is large one can write

$$\eta(t) \approx \cos \omega t + \frac{\sin \omega t}{\omega} \int_0^t \cos^2 \omega\tau \, r(\tau) \, d\tau$$

$$- \frac{\cos \omega t}{\omega} \int_0^t \sin \omega\tau \cos \omega\tau \, r(\tau) \, d\tau + O(1/\omega^2) \qquad (17)$$

In order to obtain the amplitude of the oscillatory $X(x)$ function first note that

$$X(x) \approx C^{1/2}(x) \left\{ \cos \omega t + \frac{\sin \omega t}{\omega} \int_0^t \cos^2 \omega\tau \, r(\tau) \, d\tau \right.$$

$$\left. - \frac{\cos \omega t}{\omega} \int_0^t \sin \omega\tau \cos \omega\tau \, r(\tau) \, d\tau + O(1/\omega^2) \right\} \qquad (18)$$

which is immediately obtained from (17) and (11). It is also easy to observe that

$$|X(x)| \leq A(x) \equiv C^{1/2}(x) \left\{ 1 + \frac{1}{\omega} \left[\left(\int_0^t \cos^2 \omega\tau \, r(\tau) \, d\tau \right)^2 \right. \right.$$

$$\left. \left. + \left(\int_0^t \sin \omega\tau \cos \omega\tau \, r(\tau) \, d\tau \right)^2 \right]^{1/2} + O\left(\frac{1}{\omega^2} \right) \right\} \qquad (19)$$

Here, $A(x)$ as defined by (19) is the amplitude of $X(x)$ on $x \in [a,b]$. Thus if ω is large the solution $X(x)$ of the differential equation (8a) will be well approximated by the first few terms in the asymptotic expansion for $X(x)$, given by (18).

Consider now the differential equation (8b) which defines $Z(x,z)$.

$$Z_{zz}(x,z) + \omega^2 \left(\frac{1}{\beta^2} - \frac{1}{C^2(x)} \right) Z(x,z) = 0 \qquad (8b)$$

When $\left(\frac{1}{\beta^2} - \frac{1}{C^2(x)} \right) \geq 0$ one has $\omega^2 \left(\frac{1}{\beta^2} - \frac{1}{C^2(x)} \right) \geq 0$. For the fixed

value of x and for $H_0 \alpha(x) \geq z \geq H_0 \psi(x)$, and $\beta = \beta_1$, the solution of (8b) is oscillatory in character with "frequency"

$$\omega \sqrt{\frac{1}{\beta_1^2} - \frac{1}{C^2(x)}}$$

For the case of the single surface layer over the infinite underlying medium it can be shown (see Appendix I) that $\beta_1 < C < \beta_2$ if $\beta_1 < \beta_2$. For any value of $C(x)$ in this interval define

$$p_1 \equiv \omega \sqrt{\frac{1}{\beta_1^2} - \frac{1}{C^2(x)}} \tag{20}$$

and

$$p_2 \equiv \omega \sqrt{\frac{1}{C^2(x)} - \frac{1}{\beta_2^2}} \tag{21}$$

Thus, whenever $H_0 \alpha(x) \geq z \geq H_0 \psi(x)$ solution $Z(x,z)$ will be oscillatory with "frequency" p_1. Now when $z \geq H_0 \alpha(x)$ and $\beta = \beta_2$,

$$\omega \sqrt{\frac{1}{\beta^2} - \frac{1}{C^2(x)}}$$

becomes $\pm ip_2$ and the solution of (8b) either exponentially decreases or exponentially increases, depending on which of the two independent solutions is taken associated with positive or negative p_2. Recalling the fourth boundary condition given by (6d), i.e., that the motion is confined to the neighborhood of the layer, the choice of the sign of p_2 has to be such that the solution exponentially decays when $z \to \infty$.

Therefore

$$Z(x,z) = \begin{cases} C \sin p_1 z + D \cos p_1 z \; ; & \text{in the layer} \\ \\ Fe^{-p_2 z} \; ; & p_2 > 0, \text{ in the infinite medium} \end{cases} \qquad (22)$$

Two "constants" from the three C, D and F will be determined for fixed x from the first three boundary conditions (6a), (6b) and (6c). The function $Z(x,z)$ describes the variation of the amplitude of the particle motion in y direction due to the SH waves which constructively interfere to form Love waves. It is also called the modal function.

After the form of the solution to equation (3) is established, it is useful to consider some requirements that are necessary for the existence of Love waves in the surface layer. Figure 2.6 shows SH wave propagation according to ray theory representation. The normal to the plane front of the SH waves 1, 2, 3, 4 indicates a path of one portion of the long planar wave front bouncing in the layer. The first obvious requirement for the existence of surface waves is that the energy associated with the wave motion be confined to the layer. An equivalent requirement is that the incidence angles θ for each ray be such that there is no refracted energy into the infinite medium below. Snell's law states that

$$\frac{\sin \theta_1}{\beta_1} = \frac{\sin \theta_2}{\beta_2} \qquad (24)$$

The condition that there is no refraction at points 1, 3, ..., etc., is the same as the requirement that θ_2 is imaginary or that
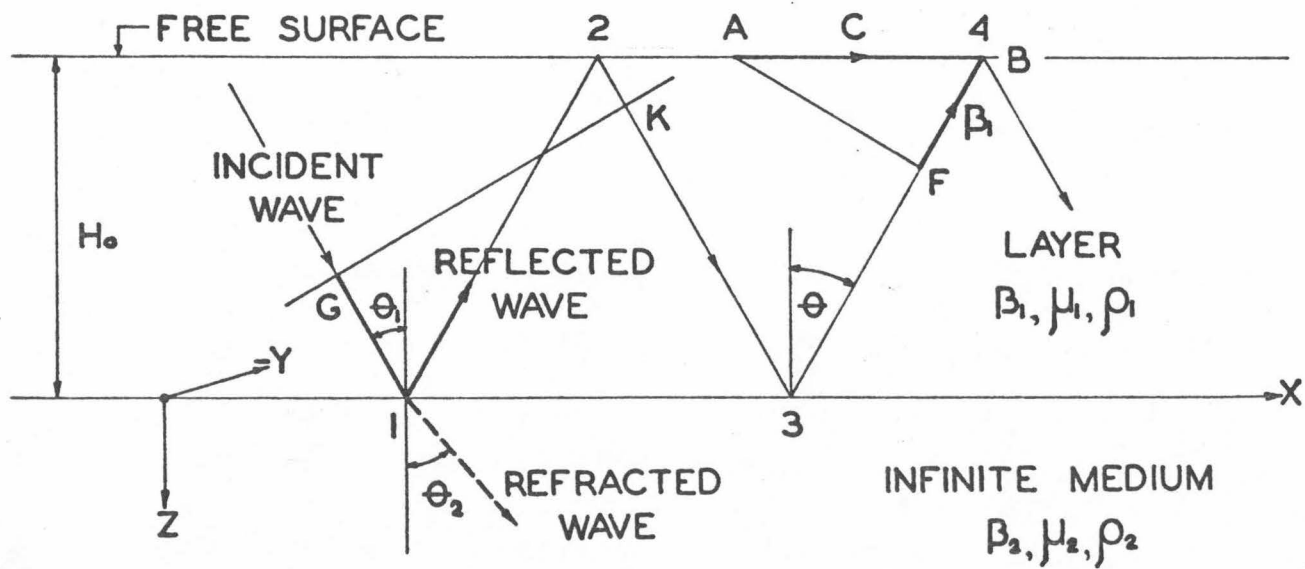
Figure 2.6. SH waves in the surface layer

$\sin \theta_2 \geq 1$. The limiting case of θ_1 denoted here θ_c is then given by

$$\sin \theta_c = \frac{\beta_1}{\beta_2} \quad \text{or} \quad \theta_c = \sin^{-1} \frac{\beta_1}{\beta_2} \tag{25}$$

Thus in order that the energy be preserved in the layer, θ has to be greater than θ_c and of course less than $\pi/2$. To see how this requirement is fulfilled in the expressions governing the Love wave motion in the layer, one can first observe the relationship between the phase velocity C and SH wave velocity β_1 in the layer and β_2 in the medium. Three points can be observed in Fig. 2.6, namely A, B and F. Point A represents the intersection of the plane wave front traveling along the ray path 3-4, and the free surface. By definition the velocity with which that point propagates in the positive x direction is given by C. The point F which lies on the same plane wave front moves along the ray path 3-4 towards B with the velocity β_1. From the geometry in Fig. 2.6 it follows then that

$$\sin \theta = \frac{\beta_1}{C} \tag{26}$$

Also from the geometry it may be seen that when $\theta \rightarrow \pi/2$, $\sin \theta \rightarrow 1$ and so $\beta_1/C \rightarrow 1$, i.e., $C \rightarrow \beta_1$. Thus the smallest value that C could attain in principle is β_1. On the other hand when $\theta \rightarrow \theta_c$, from (25) it follows that

$$\sin \theta_c = \frac{\beta_1}{\beta_2} \Rightarrow \frac{\beta_1}{\beta_2} = \frac{\beta_1}{C}$$

or $C \to \beta_2$ as $\theta \to \theta_c$. Thus from the simple geometry of the ray paths it can be concluded that if any successive reflection in the layer is to be realized, which will in turn lead to a conservation of energy in the layer the phase velocity C must lie in the interval $\beta_1 < C < \beta_2$ which is equivalent to the statement $\theta_c < \theta < \pi/2$. Simple geometry considerations also suggest that when $\theta = \pi/2$ it becomes impossible to set up a steady bouncing of the ray path 1, 2, 3, 4 ... in the layer (Fig. 2.6). In the other extreme case when $\theta = \theta_c$, as it will next be seen, p_2 (see (21)) becomes equal to zero and the wave amplitude does not decrease towards zero when z increases to infinity (see (22)). Thus there exists a wave in the infinite medium which is not confined to the proximity of the layer and the fourth boundary condition (6d) is violated. Therefore C has to be in the open interval (β_1, β_2) and θ in the open interval $(\theta_c, \pi/2)$.

In the solution of $Z(x,z)$ a requirement was given that $p_2 > 0$ (see (22)). Since from (21)

$$p_2 \equiv \omega \sqrt{\frac{1}{C^2} - \frac{1}{\beta_2^2}}$$

and from (26) $C = \beta_1/\sin \theta$ it follows

$$p_2 = \omega \sqrt{\frac{\sin^2 \theta}{\beta_1^2} - \frac{1}{\beta_2^2}}$$

Because ω is positive and real, condition that $p_2 > 0$ and real becomes

$$\frac{\sin \theta}{\beta_1} > \frac{1}{\beta_2}$$

which implies $\sin\theta > \beta_1/\beta_2$. As it may be seen, this statement is equivalent to (25) which defines the critical angle θ_c. It is thus demonstrated that the geometric or ray approach and the analytic formulation both lead to the same conditions for the existence of surface Love waves.

The requirement that the ray bounding in the layer along 1,2,3,4... etc., constructively interferes can be related to the distance along the ray path from say G to K (Fig. 2.6), and the phase shifts that are experienced at the points 1 and 2. This leads to the period equation for Love waves (e.g., see Ewing, Jardetsky and Press, 1957) in the surface layer with a constant thickness H_0, which is given by (see Appendix I)

$$\tan\left(\frac{\omega H_0}{\beta_1}\sqrt{1 - \frac{\beta_1^2}{C^2}}\right) = \frac{\mu_2}{\mu_1}\frac{\beta_1}{\beta_2}\sqrt{\frac{\dfrac{\beta_2^2}{C^2} - 1}{1 - \dfrac{\beta_1^2}{C^2}}} \tag{27}$$

and is the same as the equation obtained by introducing a solution in the form $v = X(x)Z(z)T(t)$ into the four boundary conditions given by (6a), (6b), (6c) and (6d). Defining $\xi \equiv \mu_2/\mu_1$ and $\chi \equiv \beta_2/\beta_1$ and also $\epsilon \equiv \beta_1/C$ equation (27) becomes

$$\tan\left(\frac{\omega H_0}{\beta_1}\sqrt{1 - \epsilon^2}\right) = \frac{\xi}{\chi}\sqrt{\frac{\chi^2\epsilon^2 - 1}{1 - \epsilon^2}} \tag{27'}$$

It can be further shown (see Appendix I) that this equation approximately gives characteristic values C also in the case of the layer with a variable thickness H(x) along the x axis. This can be done

provided that θ and η (see Fig. 2.4) are uniformly "small" on x in [a,b], by simply changing H_0 in (27') to $H_0\big(\alpha(x) - \psi(x)\big)$. For a chosen value of $(\omega H_0/\beta_1)\big(\alpha(x) - \psi(x)\big)$ the solution of equation (27') gives a denumerable set of the characteristic values C or equivalently ϵ belonging to the mode shapes $n = 0, 1, \ldots, N(\omega)$.

Since the phase velocity plays an important role in the variation of the amplitude of Love waves along the x direction (see (19)), diagrams showing the phase velocity dependence on the material properties expressed through the ratios ξ and χ, and the parameter $(\omega H_0/\beta_1)\big(\alpha(x) - \psi(x)\big)$, for the fundamental mode shape, have been plotted in Fig. 2.7 to Fig. 2.10. In addition, for completeness, group wave velocities were also calculated from (see Ewing, Jardetsky and Press, 1957)

$$U = \frac{C}{1 - \dfrac{\omega}{C}\dfrac{dC}{d\omega}} \tag{28}$$

where U is the group wave velocity. Introducing the ratio $\delta \equiv \beta_1/U$ one can write

$$\delta = \epsilon\left(1 - \frac{\omega}{C}\frac{dC}{d\omega}\right) \tag{29}$$

The dimensionless parameters ϵ and δ are given in Fig. 2.7 to Fig. 2.10 plotted versus the dimensionless factor $\omega H/\beta_1$ and for various values of $\chi = \beta_2/\beta_1$ and $\varkappa = \rho_2/\rho_1$.

Figure 2.7. Phase- (β_1/C) and group-velocity (β_1/U) curves corresponding to the fundamental mode of Love waves in the single surface layer for various ratios $\varkappa = \rho_2/\rho_1$

LOVE WAVE DISPERSION FOR FIRST MODE

Figure 2.8. Phase- (β_1/C) and group-velocity (β_1/U) curves corresponding to the fundamental mode of Love waves in the single surface layer for various ratios $\varkappa = \rho_2/\rho_1$

LOVE WAVE DISPERSION FOR FIRST MODE

$\dfrac{\beta_2}{\beta_1} = 2.5$

$\dfrac{\beta_1}{U}$

$\dfrac{\beta_1}{C}$

$\varkappa = 2.0$

$\varkappa = 1.5$

$\varkappa = 1.0$

$\varkappa = 1.0$

$\varkappa = 2.0$

$\dfrac{\omega H}{\beta_1}$

Figure 2.9. Phase- (β_1/C) and group-velocity (β_1/U) curves corresponding to the fundamental mode of Love waves in the single surface layer for various ratios $\varkappa = \rho_2/\rho_1$

LOVE WAVE DISPERSION FOR FIRST MODE

Figure 2.10. Phase- (β_1/C) and group-velocity (β_1/U) curves corresponding to the fundamental mode of Love waves in the single surface layer for various ratios $\varkappa = \rho_2/\rho_1$

LOVE WAVE DISPERSION FOR FIRST MODE

$\dfrac{\beta_2}{\beta_1} = 4.5$

$\dfrac{\beta_1}{U}$

$\dfrac{\beta_1}{C}$

$\varkappa = 2.0$

$\varkappa = 1.5$

$\varkappa = 1.0$

$\varkappa = 1.0$

$\varkappa = 2.0$
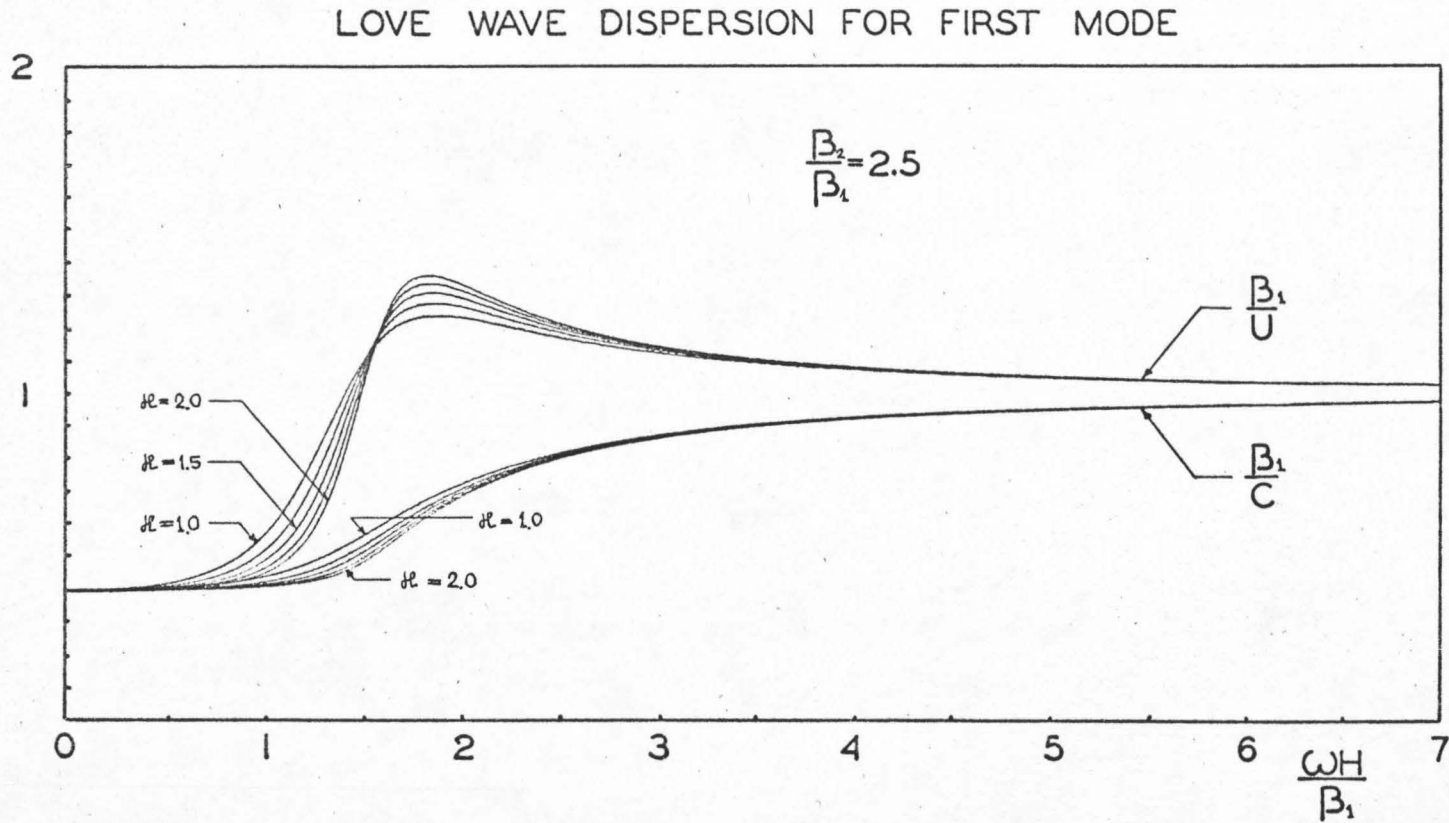
$\dfrac{\omega H}{\beta_1}$

D. VARIATIONS OF LOVE WAVE AMPLITUDES CAUSED BY CHANGING THICKNESS OF THE LAYER

One of the principal objectives of this work is to understand at least qualitatively the relationship between surface wave amplitudes and the thickness of the layer. The significance of the existence of the surface layer has already been considered and it has been shown that it leads to an increase of the energy flux in the vicinity of the surface. Considering the wave energy as "flowing" through the surface layer as a wave guide, the next question that can be asked is how the amplitudes of the wave motion change as a function of the layer thickness $H(x)$. It will be assumed in what follows, that the dissipation of wave energy caused by anelasticity, geometric scattering, and nonuniformity introduced by the variable boundary conditions are negligible.

It is assumed that the Love wave type motions in the layer with the variable thickness can be described by the function $v(x,z,t)$ such that $v(x,z,t) = X(x)Z(x,z)T(t)$. It should be pointed out here that in the precise sense Love waves are defined only for a layer of constant thickness. In this approach, the same name is assigned to the similar type of motion in the layer with the variable thickness. Since $T(t)$ is always bounded by 1 and since the maximum amplitude $Z(x,z)$ occurs on the surface when $\beta_1 < \beta_2$, the amplitude of $v(x,z,t)$ at $z = H_0 \psi(x)$ is the same as $X(x)$, if $Z(x,z)$, at $z = H_0 \psi(x)$, is normalized to unity. Therefore, if $v(x,z,t)$ is acceptable as a first approximation to the solution, the surface wave amplitude will be well

approximated by $A(x)$ as given by (19) in the section C, when ω is large.

By substitution of the trial solution $v(x,z,t) = X(x)Z(x,z)T(t)$ where $X(x)$, $Z(x,z)$ and $T(t)$ are given by (18), (22) and (9) in the section C, it can be shown (see Appendix II) that the differential equation (3) can not be satisfied identically along the layer thickness $H(x) = H_0\left(\alpha(x) - \psi(x)\right)$ but only within an error of the order

$$O\left(\frac{\omega^2 H^2(x)}{\beta_1^2} A\right)$$

(see Appendix II) where $A \equiv \max_{x\in[a,b]} [\theta(x), \eta(x)]$. A detailed consideration (see Appendix II) shows that this error is bounded above by

$$O\left(\frac{\omega^2 H^2(x)}{\beta_1^2} A\right)$$

and then decreases exponentially to zero when $z \to +\infty$. The character of the error shows that for $\frac{\omega^2 H^2(x)}{\beta_1} A$ small, the approximation to the solution of (3) of the section C is probably "reasonably good." However, it shows that a compromise must be made in restricting $\alpha(x)$ and $\psi(x)$ to be smooth so that $\theta(x)$ and $\eta(x)$ (see Fig. 2.4) together with their derivatives (see Appendix II) are sufficiently small. Then, when ω is large, which is required by the asymptotic solution for $X(x)$, and when $\frac{\omega H(x)}{\beta_1}$ is greater than 2-3, the factor

$$\frac{\omega^2 H^2(x)}{\beta_1^2} A$$

will still be small enough, provided A is sufficiently small.

The requirement that $\frac{\omega H(x)}{\beta_1}$ be greater than 2-3 is the result of the approximations made in the period equation (see Appendix I) by assuming that the phase velocity $C(x)$ at a given fixed x is approximately the same as the phase velocity for the layer of uniform thickness equal to the thickness $H(x)$. It is intuitively clear that $v(x,z,t) = X(x)Z(x,z)T(t)$ might be a "reasonable" approximation when variations of $H(x)$ away from H_0 are small, which will be the case if A is small.

If all requirements stated above are satisfied, one has from (19) of the section C that

$$A(x) \approx C^{1/2}(x)\left[1 + O\left(\frac{1}{\omega}\right)\right] \tag{1}$$

If two points on the surface of the layer defined by $x = x_1$ and $x = x_2$ are considered, the ratio of the maximum amplitudes of the ground motion at the two locations will be for high frequency waves

$$\frac{A(x_2)}{A(x_1)} \approx \sqrt{\frac{C(x_2)}{C(x_1)}} + O\left(\frac{1}{\omega}\right) \tag{2}$$

Since it is convenient to calculate ratios $\epsilon = \beta_1/C(x)$ as functions of the rigidity ratio $\xi = \mu_2/\mu_1$ and the velocity ratio $\chi = \beta_2/\beta_1$ together with the dimensionless parameter $\frac{\omega H(x)}{\beta_1}$, where $H(x) \equiv H_0\left(\alpha(x)-\psi(x)\right)$, one obtains

$$\frac{A(x_2)}{A(x_1)} \approx \sqrt{\frac{\epsilon(\underline{x}_1)}{\epsilon(\underline{x}_2)}} + O\left(\frac{1}{\omega}\right) \tag{3}$$

where by definition

$$\underline{x}_i \equiv \left(\varkappa, \chi, x, \frac{\omega H(x_i)}{\beta_1} \right)$$

and

$$\epsilon(\underline{x}_i) = \frac{\beta_1}{C(\underline{x}_i)}$$

Examination of Figs. 2.7 to 2.10 shows that for all $\varkappa$ and χ values considered, $\epsilon(\underline{x})$ increases towards 1 asymptotically as $\frac{\omega H(x)}{\beta_1} \rightarrow +\infty$. Thus if $H(x_2)$ is greater than $H(x_1)$, with all other parameters held fixed, $\epsilon(\underline{x}_2)$ will be greater than $\epsilon(\underline{x}_1)$ and so $A(x_2)/A(x_1) < 1$. This means that when the thickness of the layer increases, the amplitude of the Love waves decreases. It can also be seen that for $\frac{\omega H(x)}{\beta_1} > 2 \dot{-} 3$, the change in $\epsilon(\underline{x})$ for an appreciable increase in $\frac{\omega H(x)}{\beta_1}$ produces in general only a minor variation in $\epsilon(\underline{x})$ and so $A(x_2)/A(x_1)$ is less than one but is also very close to 1. The range $\frac{\omega H(x)}{\beta_1} > 2 \dot{-} 3$ perhaps covers almost all frequencies (corresponding to the fundamental mode shape) in which one is primarily interested in strong motion spectrum analysis. Most of the surface wave energy probably is contained in the fundamental mode of vibration and so it may be tentatively concluded that even in the case when all modes are considered the total resulting change in the spectrum amplitudes, even for considerable changes in the layer thickness, will be of the order of 1. The general trend will be that when the energy "flows" toward an increasing thickness of the layer, the amplitudes of the waves will decrease and conversely. This is in agreement with what one might expect for the case when essentially all energy is contained in the layer, because when $\frac{\omega H(x)}{\beta_1}$ is large and tends to $+\infty$ at the

same time $\alpha \to \pi/2$. It has already been shown (see Section B, and Fig. 2.5) that for α close to $\pi/2$ practically all high frequency energy is contained in the layer.

The restrictions imposed by the error estimates for approximations involved in the differential equation and the period equation, can be summarized as

$$A\frac{\omega^2 H^2(x)}{\beta_1^2} \ll 1 \tag{4}$$

and

$$\frac{\omega^2 H^2(x)}{\beta_1^2} \gtrsim 2 \tag{5}$$

Although these restrictions appear to be severe ones, particularly restriction (4) on A, there will be many cases in which the approximations described, may be used. This is because strong motion response spectrum analysis mostly involves high frequencies so that (5) will usually be satisfied. Furthermore, gradients along the free surface and lower boundaries of the layer are often smoothly and slowly changing functions for many actual geologic conditions.

To this point, the treatment of the variation of wave amplitudes has been formal and derived as a consequence of the properties of the period equation and the amplitude of the solution X(x) satisfying

$$X_{xx}(x) + \frac{\omega^2}{C^2(x)} X(x) = 0 \tag{6}$$

for large ω. Remembering that (see Fig. 2.6)

$$C(x) = \frac{\beta_1}{\sin \theta(x)} \tag{7}$$

and considering the layer represented in Fig. 2.11, it will be seen from a purely geometrical argument that when $H(x)$ increases along the x coordinate, $C(x)$ decreases and conversely. This is true if the layer thickness is a continuous and smoothly changing function of x, and if the slopes of the boundary surfaces of the layer are uniformly small, continuous and slowly changing along x. As was already pointed out, one of the necessary conditions for the existence of the surface wave is that $\theta_c < \theta(x) < \pi/2$. Thus as seen in Fig. 2.11, if energy is propagated from left to right, towards the increasing layer thickness, $\theta(x)$ will be slowly increasing and $C(x)$ will decrease. Consequently $\omega^2/C^2(x)$ will increase and as already mentioned, the amplitude of the solution $X(x)$ as given by (1) will decrease. Thus it becomes clear that when the ray propagates toward a gradually deeper alluvium, if $\theta(x)$ was initially in the interval $\theta_c < \theta(x) < \pi/2$, it will remain there. This also means that all of the energy belonging to that ray will be preserved in the layer. This is, however, not the case for all rays with $\theta_c < \theta(x) < \pi/2$ which propagate in the opposite direction, i.e., from the deep into the shallower alluvium or from right to the left in Fig. 11. Since $\theta(x)$ is decreasing from x_2 towards x_1, all rays with angles $\theta_c < \theta(x) < \theta_c + |\theta_1^2(x)|$ will reach the shallow alluvium with $\theta(x) \leq \theta_c$, where $|\theta_1^2(x)|$ is the amount of the decrease of $\theta(x)$ between x_1 and x_2. Therefore, for all angles with $\theta_c < \theta(x) < \theta_c + |\theta_1^2(x)|$ some fraction of the energy will be dissipated into the
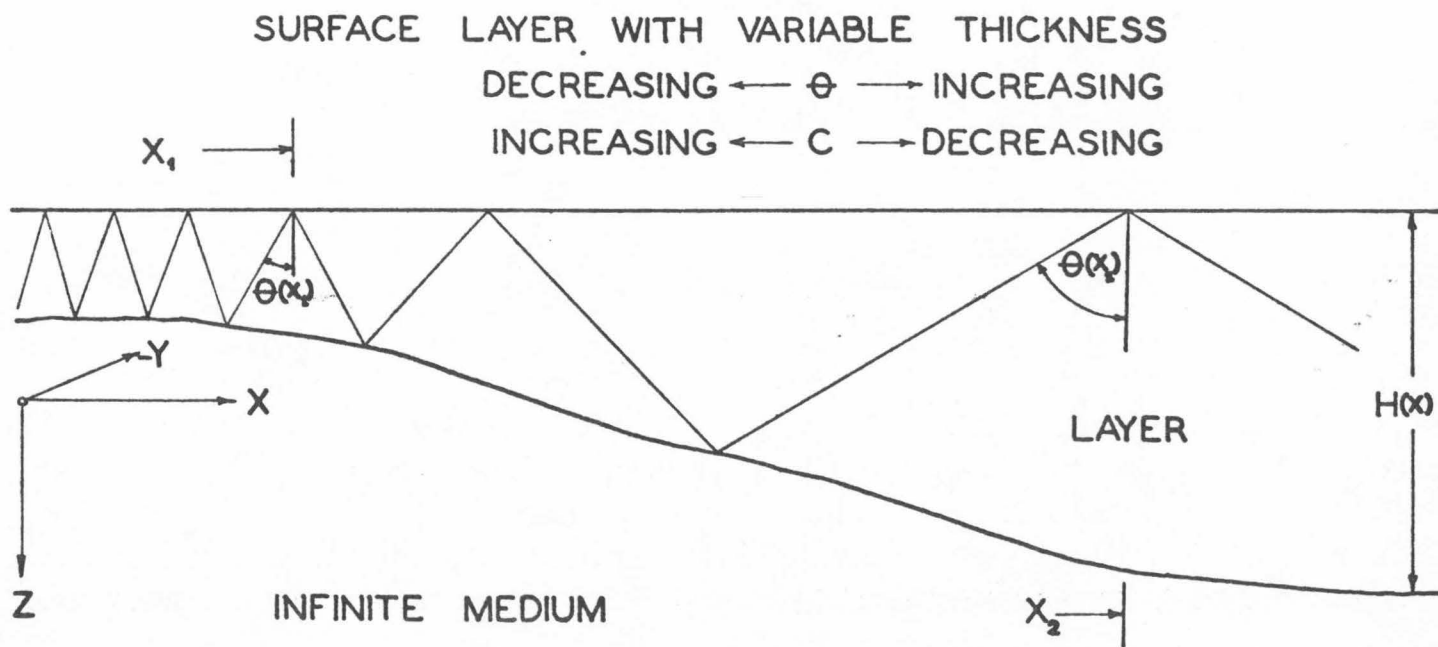
Figure 2.11. Surface layer with variable thickness

underlying infinite medium in the form of refracted waves. Because
of this behavior, the analysis and all conclusions will be applicable
for $\theta_c + |\theta_1^2(x)| < \theta(x) < \pi/2$ rather than for $\theta_c < \theta(x) < \pi/2$ when
the energy propagates from deep to shallow alluvium.

There have been several attempts in the past to solve the prob-
lem of surface Love waves propagating through a surface layer of
variable thickness. Homma (1952) analyzed a surface layer with
linearly changing thickness using a polar coordinate system. He con-
sidered SH type of motion, and found that "in a surface layer of
gradually and linearly varying thickness, a Love wave can be trans-
mitted in an approximate sense . . . the velocity and wave form are
the same as those in the case of a uniform thickness which is equal
to the general mean thickness in the region where the Love wave can
be propagated without much deformation." He found further that the
x dependence of the solution is described by cylindrical functions of
the third kind whose arguments are $\omega x/\beta_1$. Although Homma does not
point that out explicitly, it is easily seen that for $\omega x/\beta_1$ large, the
asymptotic expansions that he derives for these functions contain the
factor

$$\left(\frac{\omega x}{\beta_1}\right)^{-1/2}$$

where x is oriented towards the increasing thickness of the layer,
and this indicates that the amplitudes of waves decrease with the in-
crease in the layer thickness.

DeNoyer (1961) investigated the effect of a sinusoidal variation
of layer thickness on the propagation of Love waves. He used an

approximate period equation and postulated conservation of energy in the layer to obtain the variation of the wave amplitudes along the x direction. His findings appear to be in qualitative agreement with the present work, indicating that the increase in layer thickness leads to a decrease of the Love wave amplitudes and conversely.

Shelton (1963) used a mechanical model to study the effect of linearly increasing layer thickness on the propagation of Rayleigh waves. These waves are not analyzed in the present work, but it may be of interest to mention some of the qualitative results obtained by Shelton. The depth of his layer was 0.25 inch from 0 to 20 inches along the x axis, with a linear increase from 20 to 28 inches and of constant thickness 1 inch from 28 to 48 inches. Among other observations, he finds for the short period waves that "the usual inference of a greater average thickness where the phase velocity is lower seems valid." With respect to variations of wave amplitudes, he states that "the apparent attenuation for propagation downslope is less than for propagation up-slope, especially for the intermediate period range." Although these are findings based on only one model study, so that no generalizations can be made, it is interesting to observe that the qualitative behavior of the Rayleigh wave propagation in the model appears to be in many respects similar to the general behavior of Love waves described above.

E. ON THE SHIFTING OF SPECTRUM PEAKS AS A CONSEQUENCE OF A MODEL WITH HORIZONTALLY PROPAGATING ENERGY

It has been observed that the relative velocity response spectra calculated for the same strong motion station but for different

earthquakes often do not resemble each other. Also, for the same earthquake but when several stations were distributed along approximately a straight line some 3 to 5 miles apart (G. W. Housner and M. D. Trifunac, 1967) spectrum peaks were displaced from station to station although geological conditions were similar. Several reasons for such a behavior could be sought. For example, a variable thickness of the layers underlying the stations, treated from the point of view of a model with vertically incoming shear waves might be considered. Here another plausible explanation will be explored, involving the concept of horizontally propagating energy in the form of Love waves. Complete explanations will no doubt involve a combination of mechanisms. It must be kept in mind, of course, that the present analysis always assumes an infinite train of waves, whereas the actual earthquake problem is transient. However, since surface waves are a relatively long train of waves, there is reason to hope that the steady state solutions may be reasonable approximations in many cases.

It has been shown above that the ground motion resulting from the constructive interference of SH waves in a layer of constant thickness can be described by the product of three functions $X(x)$, $T(t)$ and $Z(x)$ each of which depends on only one variable. Since $T(t)$ is found to be sinusoidal, one can think of $X(x)Z(z)$ as an amplitude function of the wave motion describing the behavior of the wave envelope in the xz plane when waves are propagating in the x direction. Furthermore, since $Z(z)$, which is also called the mode shape function, is determined within a constant multiple for all x,

if one normalizes the maximum amplitude to be unity, at the surface of the layer, for a monotonically increasing SH wave velocity with depth, then the wave amplitude along the surface of the layer becomes $X(x)$. The behavior of this function along the x direction will be examined now for a layer of the constant thickness H_0. The differential equation whose solution is $X(x)$ was given as

$$X_{xx}(x) + \frac{\omega^2}{C^2} X(x) = 0 \tag{1}$$

First one can change the variable x to $x = H_0 \eta$, so that η will be dimensionless measure of distance along x in terms of the layer thickness H_0. Equation (1) then becomes

$$X_{\eta\eta}(\eta) + \frac{\omega^2 H_0^2}{C^2} X(\eta) = 0 \tag{1'}$$

Choosing now arbitrarily the initial conditions to be $X(\eta=0) = 1$, and $X_\eta(\eta=0) = 0$ for all $\omega \in [\,0,\infty)$ one can write the solution

$$X(\eta) = \cos \frac{\omega H_0}{C} \eta \tag{2}$$

This solution represents an oscillatory function with zeros at

$$\eta = \frac{C\pi}{\omega H_0} \left(\frac{1}{2} + n \right) ; \qquad n = 0,1,\dots \tag{3}$$

or in terms of the period of vibration T

$$\eta = \frac{CT}{2H_0} \left(\frac{1}{2} + n \right) = \frac{\ell}{2H_0} \left(\frac{1}{2} + n \right) \tag{4}$$

where $CT = \ell$ is the wave length along the x axis.

Because the amplitude of the final surface motion is obtained by multiplying X(x) by T(t) and since T(t) is also a sinusoidal function with amplitude equal to unity, in the spectrum computation amplitude variations along the x direction are observed as a variation of the absolute value of the X(x) function.

The relative velocity response spectrum, by definition, represents the maximum amplitude of the velocity response of a viscously damped one degree of freedom system during the time of the earthquake excitation. It can be shown that there is a close similarity in the shape of the zero-damped relative velocity response spectrum and the Fourier amplitude spectrum of the excitation function (D. E. Hudson, 1962) and that one can be used as an approximate representation of the other. For this reason both of these terms are used in this work sometimes interchangeably. Here, X(x) as the amplitude function is the same as the amplitude of the Fourier spectrum for the same frequency ω and for the same fixed value of x. It is customary to plot the relative response spectrum versus the natural period of vibration of a one degree of freedom system.

If one writes $X(\eta)$ function in terms of the period $T = 2\pi/\omega$ it follows that

$$X(\eta) = \cos \frac{2\pi H_0}{CT} \eta \tag{5}$$

if $X(\eta=0) = 1$ and $X_\eta(x=0) = 0$ for all T. This is of course in general not a realistic assumption, as it would be expected that at the source of the energy radiation of SH waves, each $X(\eta)$ function would involve different initial conditions depending on the period T. This

assumption however permits a simple qualitative insight into the problem of the shifting of the peaks along the different η locations without altering the basic phenomenon.

If one were to calculate the response spectrum always at the same strong motion station, generated by waves coming from the same fault system but each time with a different generating mechanism, it would be precisely this $X(\eta=0)$ and $X_\eta(\eta=0)$ that would determine the location of the peaks in the spectrum. There is no reason to expect that all earthquakes will generate the same numerical values of $X(\eta=0)$ and $X_\eta(\eta=0)$, within a constant multiple, depending on the source parameters. Therefore there is no reason that peaks in the response spectrum at the same station should be similar, at the same periods, for earthquakes occurring on the same fault system.

On the other hand, when considering a steady state excitation and analyzing the behavior of the response spectra for several stations distributed along the η direction, initial conditions for $X(\eta)$ are the same for all stations, the distance from the source of the energy release and the ground properties along the propagation path being the only variables. For the case of a single layer with a constant thickness H_0 and for a given and fixed period T^*, the dimensionless parameter $2\pi H_0/CT^*$ is the same for all stations. Depending on the value of η it is seen from (5) that the Fourier amplitude spectrum at some stations can have a local maximum while it can be zero at some other station for the same period T^*. If the layer thickness changes very

slowly so that the slope and the curvature of free surface and the contact surface are small, the analysis of the preceding section shows that for waves with $\frac{\omega H(x)}{\beta_1} \gtrsim 2$, the amplitudes of the oscillatory function $X(\eta)$ will not vary considerably along η and practically the same type of the behavior of the spectrum peaks, as for the constant layer case will probably take place.

If it is assumed now, for the sake of a qualitative analysis only, that the Fourier amplitude spectrum at $\eta = 0$ is given by $S_{F/0}(T)$ and that

$$\left(\frac{dS_{F/\eta}(T)}{d\eta} \right)_{\eta=0} = \left(\frac{2\pi H_0}{CT} \sin \frac{2\pi H_0}{CT} \varphi \right) S_{F/0}(T) \tag{6}$$

i.e., that

$$\varphi = \sin^{-1} \left\{ \frac{CT}{2\pi H_0} \left(\frac{dS_{F/\eta}(T)}{d\eta} \right)_{\eta=0} \right\} \frac{1}{S_{F/0}(T)} \tag{6'}$$

One can conclude from the above discussion that $S_{F/\eta}(T)$, i.e., the Fourier amplitude spectrum at location η will be given by

$$S_{F/\eta}(T) = S_{F/0}(T) \left| \cos \frac{2\pi H_0}{CT}(\eta + \varphi) \right| \tag{7}$$

The locus of the zero spectrum amplitudes will occur, as shown above, at

$$\frac{2\pi H_0}{CT} (\eta + \varphi) = \left(\frac{1}{2} + n \right) \pi \; ; \quad n = 0, 1, 2, \ldots \tag{8}$$

and for $\eta \epsilon [0, \infty)$ and $T \epsilon [0, \infty)$. The locus of the peak amplitudes

will occur at

$$\frac{2\pi H_0}{CT}(\eta+\varphi) = n\pi; \qquad n = 0, 1, 2, \ldots \tag{9}$$

The phase shift φ can be calculated in principle from (6') if $X(\eta=0)$ and $X_\eta(\eta=0)$ are known.

In order to illustrate the above described effect on the shifting of the spectrum peaks, the function $\left|\cos\frac{2\pi H_0}{CT}(\eta+\varphi)\right|$, with $\varphi \equiv 0$ for all T, is plotted in Fig. 2.12 for the set of dimensionless distances η, $\eta = 0., 2., \ldots, 8., 10.$. Each of the six functions is plotted versus the dimensionless period $\frac{CT}{2\pi H_0}$.

It may be seen from the previous discussion and from the conditions necessary for the successful application of the model with horizontally propagating energy, that the shifting of the peaks governed by the behavior of the $X(x)$ function will not be an appropriate explanation in every case. This is because the explanation is based on Love waves only, which may be an important part of the strong motion in some directions, but not necessarily in all directions. In the case, for example, of a simple vertical strike slip fault the above interpretation will probably describe reasonably well the predominant behavior of surface waves along the direction of the fault plane and in the perpendicular direction.

To show how a particular Fourier amplitude spectrum might change according to (7), for various values of η, an arbitrarily chosen model with a constant layer thickness was analyzed. The velocity of SH waves in the layer was taken to be $\beta_1 = 1.25$ km/sec and the layer thickness $H_0 = 0.30$ km. Ratios of the SH wave velocities and material
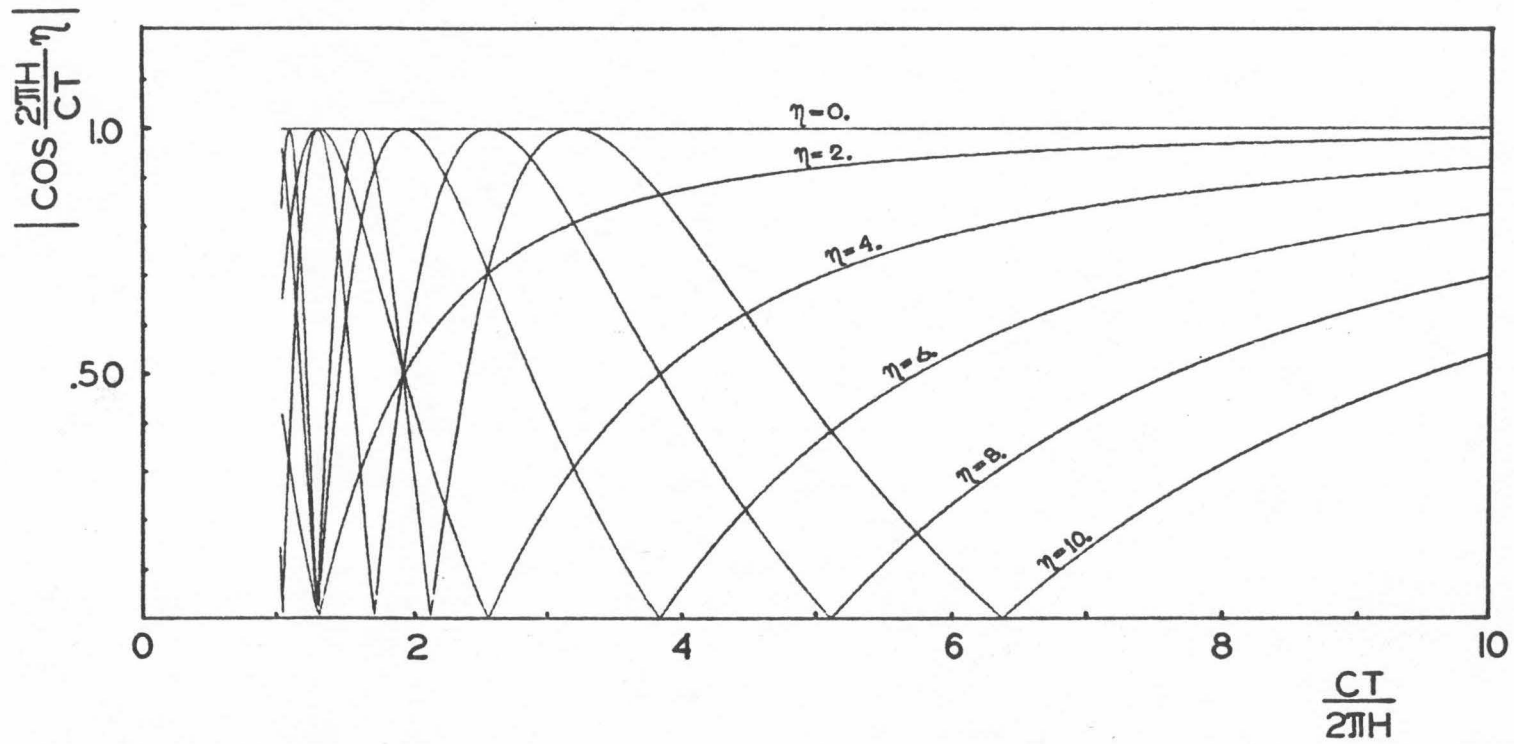
Figure 2.12. The function $\left| \cos \dfrac{2\pi H}{CT} \eta \right|$ for various values of η

densities in the infinite medium and the layer were taken as $\beta_2/\beta_1=2.24$ and $\rho_2/\rho_1=1.64$ respectively. An assumption was further made that all wave energy in this example is to be associated with the fundamental mode only. Using the above parameters one can construct the phase velocity C dependence for all periods T to be considered. If $S_{F/0}$ is assumed as given in Fig. 2.13 when $\eta=0.0$, then using (7) $S_{F/\eta}$ spectra for $\eta=2.0$, $\eta=4.0$, and $\eta=6.0$ can be easily constructed and are given in Fig. 2.13. The $S_{F/0}$ assumed in Fig. 2.13 at $\eta=0.0$ has the general appearance of an earthquake spectrum, although in this example it is of course the spectrum associated with an infinite train of waves. As may be seen, zeros and peaks in the spectra $S_{F/\eta}$ are continuously displaced toward the greater periods as η increases. It is also seen that the character of $\left|\cos\dfrac{2\pi H_0}{CT}\eta\right|$ function generates a large number of high frequency peaks in the low period region as η increases.

From the character of the spectra (Fig. 2.13) it may be found that peaks can occur at practically all periods if η variation is considerable. It can therefore be concluded that whenever a simplified interpretation in terms of horizontally propagating energy in the form of Love waves is acceptable, it may be quite erroneous to think in terms of "predominant periods of vibration" which are some intrinsic property of a local site.

It may be noted that the above considered solution of differential equation (3) (Section C) in the form $v(x,z,t)=Z(z)X(x)T(t)$ represents a standing wave. It can be shown that the general plane wave motion may be regarded as the result of superposing standing waves and that the
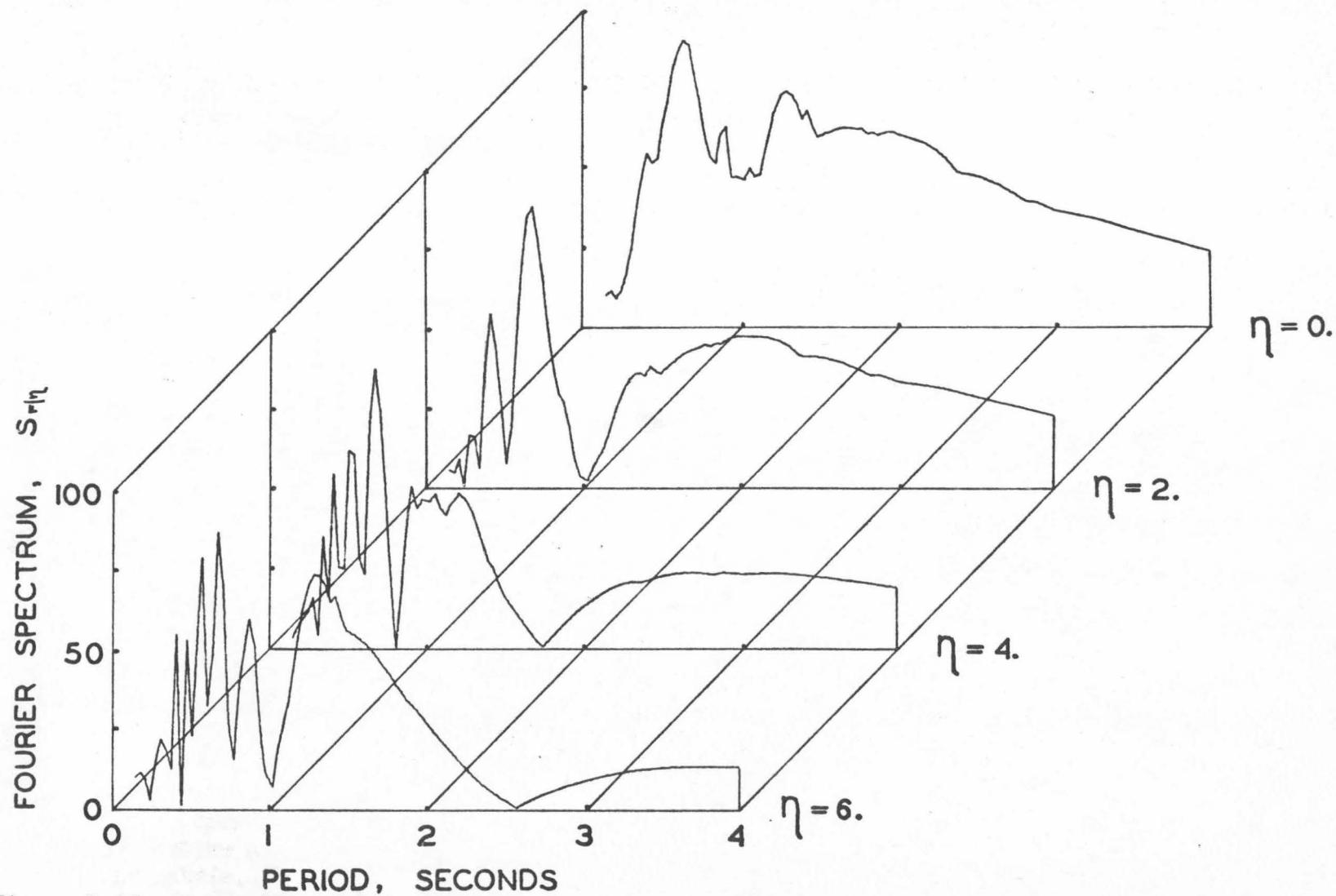
Figure 2.13. Dependence of the Fourier amplitude spectrum on the distance $x = \eta H_0$ for the surface layer with $H_0 = 0.30$ km, $\beta_2/\beta_1 = 2.24$ and $\rho_2/\rho_1 = .64$. $S_{F/\eta}$ is given for the arbitrary scale.

general result of such superposition is not itself a standing wave. This is because the sum of the terms like $v(x, z, t) = Z(z)X(x)T(t)$ is not in general expressible as a product of functions containing x and t alone.

F. CONCLUSIONS.

The model with horizontally propagating seismic energy in the form of SH waves through a single layer as a wave guide has been analyzed. Although the model and the theory which was applied to it were much simplified, many of the derived properties can be expected to illustrate well a number of the phenomena associated with strong earthquake ground motion. Some of these findings which are important from the point of view of earthquake engineering are:

1. If there exists a surface layer, or several layers, of considerable thickness, with low velocities of SH waves, and if in addition a near source of earthquake energy release occurs in or predominantly in the layer, then the main part of the high frequency radiated energy will be confined to the layer as a wave guide. A fraction of this energy will be fed into the buildings and other man-made structures on or near the surface of the layer. The presence of the surface wave guide will thus increase the amount of energy transferred into surface structures, for the same total amount of the energy released by the earthquake.

2. The surface amplitude of the guided SH waves will decrease if the energy of the wave is essentially confined to the layer and if the wave propagates toward an increasing layer thickness. Conversely,

when the wave propagates towards a decreasing layer thickness, the amplitude will increase. The model with horizontally propagating energy thus results in an opposite conclusion as to the relationship between layer thickness and surface wave amplitudes as inferred from the model with vertically propagating shear waves.

3. The constructive interference of SH waves bouncing in the surface layer will introduce the following features into the Fourier amplitude spectrum for the motion at the surface of the layer. The zeroes and the peaks in the Fourier amplitude spectrum for an infinite train of standing waves will be continuously displaced towards the longer periods as the distance between the recording station and the source of the energy release increases. Also, a larger number of the short period peaks will be generated as this distance increases. For this model the concept of predominant spectrum peaks at a fixed frequency depending on layer thickness and properties is not appropriate.

APPENDIX I

PERIOD EQUATION

The derivation of the period equation will be considered here, in detail, for the general case of a layer with a variable thickness $H(x)$ (Fig. 2.4). As was shown, z-dependence of the solution represented by the function $Z(x, z)$ can be written as:

$$Z(x, z) = \begin{cases} C \sin p_1 z + D \cos p_1 z & \text{in the layer} \qquad (1a) \\ F e^{-p_2 z} & \text{in the infinite medium} \qquad (1b) \end{cases}$$

where C, D and F are at this point assumed to be constants, independent of x and

$$p_1 \equiv \frac{\omega}{\beta_1} \sqrt{1 - \frac{\beta_1^2}{C^2(x)}} \qquad (2a)$$

$$p_2 \equiv \frac{\omega}{\beta_2} \sqrt{\frac{\beta_2^2}{C^2(x)} - 1} \qquad (2b)$$

where $C = C(x)$ is the phase velocity associated with a given frequency ω and mode shape and which varies in general with x. In the simple case of a layer of constant thickness $H(x) = H_0$, C is a constant (i. e. , does not depend on x.) and $Z(x, z)$ becomes $Z(z)$ a function of z only. One could proceed here by assuming that the solution corresponding to a given mode shape could be expressed as $v(x, z, t) = X(x)Z(x, z)T(t)$ and later show that this is approximately true close to the limiting case when $\psi(x) \rightarrow -1$ and $\alpha(x) \rightarrow 0$ (Fig. 2.4). This will be done in Appendix II.

The displacement solutions can be written as:

$$v_j(x, z, t) = X(x)Z_j(x, z)T(t) \tag{3}$$

with j=1 in the layer and j=2 in the infinite medium. The boundary conditions to be satisfied are (omitting arguments in the function v_j)

1. $v_1 = v_2$ at $z = f \equiv \alpha(x)H_0$ (4a)

2. $\dfrac{\partial v_1}{\partial s} = 0$ at $z = H \equiv \psi(x)H_0$ (4b)

3. $\mu_1 \dfrac{\partial v_1}{\partial s} = \mu_2 \dfrac{\partial v_2}{\partial s}$ at $z = f$ (4c)

where $\partial/\partial s$ indicates the rate of change of the corresponding function along the normal to the surface of the layer or along the normal to the welded contact between the layer and the infinite medium. Now, since (see Fig. 2.4)

$$\frac{\partial v_j}{\partial s} = \frac{\partial v_j}{\partial x}\frac{dx}{ds} + \frac{\partial v_j}{\partial y}\frac{dz}{ds} = \frac{\partial v_j}{\partial x}\sin\left(\begin{matrix}\theta\\\eta\end{matrix}\right) + \frac{\partial v_j}{\partial z}\cos\left(\begin{matrix}\theta\\\eta\end{matrix}\right) \tag{5}$$

and introducing a simplifying notation so that e. g.

$$X_1^f \equiv X_1(f) = X_1[\alpha(x)H_0]; \qquad X_{1_x}^H \equiv \frac{\partial}{\partial x}X_1[\psi(x)H_0]$$

and so on, boundary conditions 1, 2, and 3 give

1. $\left(C\sin p_1 f + D\cos p_1 f\right)X_1^f = Fe^{-p_2 f}X_2^f$ (6a)

2. $\left[X_{1_x}^H\left(C\sin p_1 H + D\cos p_1 H\right) + X_1^H Z_{1_x}^H\right]\sin\eta +$

    $+ X_1^H\left[Cp_1\cos p_1 H - Dp_1\sin p_1 H\right]\cos\eta = 0$ (6b)

3. $\mu_1 \left\{ \left[X^f_{1_x} \left(C \sin p_1 f + D \cos p_1 f \right) + X^f_1 Z^f_{1_x} \right] \sin \theta + X^f_1 \left[Cp_1 \cos p_1 f - \right. \right.$

$\left. \left. - Dp_1 \sin p_1 f \right] \cos \theta \right\} = \mu_2 \left[\left(X^f_{2_x} Fe^{-p_2 f} + X^f_2 Z^f_{2_x} \right) \sin \theta + \right.$

$$\left. + X^f_2 \left(-Fp_2 e^{-p_2 f} \cos \theta \right) \right] \tag{6c}$$

Introduce now, by definition, the following notation

$$X^H_1 Z^H_{1_x} = \left(C\epsilon(H) + D\delta(H) \right) X^H_1 \tag{7a}$$

$$X^f_1 Z^f_{1_x} \equiv \left(C\epsilon(f) + D\delta(f) \right) X^f_1 \tag{7b}$$

$$X^f_2 Z^f_{2_x} \equiv FX^f_2 \rho(f) \tag{7c}$$

Then the above given boundary conditions (6a), (6b), and (6c) can be represented as a system of homogeneous equations with the three unknowns C, D and F. The condition that these three unknowns possess a nontrivial solution is that the determinant of the coefficent matrix be zero. This gives

$$
\begin{vmatrix}
X_1^f \sin p_1 f & X_1^f \cos p_1 f & -X_2^f e^{-p_2 f} \\[2em]
\begin{pmatrix} X_{1_x}^H \sin p_1 H \sin \eta + \\[0.5em] + X_1^H \epsilon(\mathrm{II}) \sin \eta + \\[0.5em] + X_1^H p_1 \cos p_1 H \cos \eta \end{pmatrix} & \begin{pmatrix} X_{1_x}^H \cos p_1 H \sin \eta + \\[0.5em] + X_1^H \delta(H) \sin \eta + \\[0.5em] - X_1^H p_1 \sin p_1 H \cos \eta \end{pmatrix} & 0 \\[3em]
\mu_1 \begin{pmatrix} X_{1_x}^f \sin p_1 f \sin \theta + \\[0.5em] + X_1^f \epsilon(f) \sin \theta + \\[0.5em] + X_1^f p_1 \cos p_1 f \cos \theta \end{pmatrix} & \mu_1 \begin{pmatrix} X_{1_x}^f \cos p_1 f \sin \theta + \\[0.5em] + X_1^f \delta(f) \sin \theta - \\[0.5em] - X_1^f p_1 \sin p_1 f \cos \theta \end{pmatrix} & -\mu_2 \begin{pmatrix} X_{2_x}^f e^{-p_2 f} \sin \theta + \\[0.5em] + X_2^f \rho(f) \sin \theta - \\[0.5em] - p_2 e^{-p_2 f} X_2^f \cos \theta \end{pmatrix}
\end{vmatrix} = 0
$$

(8)

Now define

$$\frac{\mu_2}{\mu_1} \equiv \xi \tag{9}$$

$$\varkappa_H \equiv \frac{X_{1_x}^H}{X_1^H}; \qquad \varkappa_f \equiv \frac{X_{1_x}^f}{X_1^f} \tag{10a); (10b}$$

and since $X_1^f = X_2^f$ it follows that

$$\frac{1}{\xi}\varkappa_f = \frac{X_{2_x}^f}{X_1^f} \tag{10c}$$

assuming for the moment that X_1^f, X_2^f and X_1^H do not vanish at the point under consideration. Also define

$$a\binom{H}{f} \equiv \varkappa_H \sin p_1\binom{H}{f} + \epsilon\binom{H}{f} \tag{11a}$$

$$b\binom{H}{f} \equiv \varkappa_H \cos p_1\binom{H}{f} + \delta\binom{H}{f} \tag{11b}$$

$$c(f) \equiv -\varkappa_f - \xi\rho(f)e^{p_2 f} \tag{11c}$$

Now using the above definitions one can rewrite the determinant (8) in a simplified form

$$\begin{vmatrix} \sin p_1 f & \cos p_1 f & 1 \\ a(H)\tan\eta + p_1\cos p_1 H & b(H)\tan\eta - p_1\sin p_1 H & 0 \\ a(f)\tan\theta + p_1\cos p_1 f & b(f)\tan\theta - p_1\sin p_1 f & c(f)\tan\theta - \xi p_2 \end{vmatrix} = 0$$

$$\tag{12}$$

Expanding determinant (12) one obtains

$$\sin p_1 f \Big[b(H) \tan \eta \, c(f) \tan \theta - p_1 \sin p_1 H c(f) \tan \theta - b(H) \tan \eta \, \xi \, p_2 +$$

$$+ p_1 p_2 \, \xi \sin p_1 H \Big] - \cos p_1 f \Big[a(H) \tan \eta \, c(f) \tan \theta +$$

$$+ p_1 \cos p_1 H c(f) \tan \theta - p_1 \cos p_1 H \, \xi \, p_2 - a(H) \tan \eta \, p_2 \, \xi \Big] +$$

$$+ \Big[a(H) \tan \eta \, b(f) \tan \theta + p_1 \cos p_1 H b(f) \tan \theta - a(H) \tan \eta \, p_1 \sin p_1 f -$$

$$- p_1^2 \sin p_1 f \cos p_1 H - a(f) \tan \theta \, b(H) \tan \eta - p_1 \cos p_1 f b(H) \tan \eta +$$

$$+ a(f) \tan \theta \, p_1 \sin p_1 H + p_1^2 \sin p_1 H \cos p_1 f \Big] = 0 \qquad (13)$$

After some adding and rearranging of terms this equation can be rewritten as

$$p_1 \sin p_1 H \cos p_1 f - p_1 \sin p_1 f \cos p_1 H +$$

$$+ p_2 \, \xi \sin p_1 f \sin p_1 H + p_2 \, \xi \cos p_1 H \cos p_1 f + \Phi_0 = 0 \qquad (14)$$

where Φ_0 is given by:

$$\Phi_0 = \frac{\tan \eta}{p_1} \Big[-b(H) \sin p_1 f \, \xi \, p_2 + a(H) p_2 \, \xi \cos p_1 H - a(H) p_1 \sin p_1 f -$$

$$- p_1 b(H) \cos p_1 H \Big] + \frac{\tan \theta}{p_1} \Big[-p_1 \sin p_1 f \sin p_1 H c(f) -$$

$$- c(f) p_1 \cos p_1 H \cos p_1 f + p_1 b(f) \cos p_1 H + a(f) p_1 \sin p_1 H \Big] +$$

$$+ \frac{\tan \theta \tan \eta}{p_1} \Big[b(H) c(f) \sin p_1 f - a(H) c(f) \cos p_1 f +$$

$$+ a(H) b(f) - a(f) b(f) \Big] \qquad (15)$$

For the uniform layer on an infinite medium $\alpha(x) \equiv 0$ and $\psi(x) \equiv -1$ for all x and therefore $\tan \theta$ and $\tan \eta$ become zero and Φ_0 is then

identically zero for all x. In that special case the above equation (14) reduces to

$$p_1 \sin p_1 H_0 + p_2 \xi \cos p_1 H_0 = 0 \tag{16}$$

or

$$-\tan p_1 H_0 = \xi \frac{p_2}{p_1} \tag{17}$$

which in the expanded form becomes

$$-\tan \frac{\omega H_0}{\beta_1} \sqrt{1 - \frac{\beta_1^2}{C^2}} = \frac{\mu_2 \beta_1}{\mu_1 \beta_2} \sqrt{\frac{\frac{\beta_2^2}{C^2} - 1}{1 - \frac{\beta_1^2}{C^2}}} \tag{17$'$}$$

which is the same as the classical period equation for the uniform layer.

Now define

$$\frac{p_2}{p_1} \equiv \gamma; \qquad \xi = \frac{\mu_2}{\mu_1}; \qquad \frac{\beta_1}{C(x)} = \epsilon(x) \tag{18); (19); (20}$$

and

$$\frac{\beta_2}{\beta_1} \equiv \chi; \qquad \frac{\omega H_0}{\beta_1} \equiv \lambda \tag{21); (22}$$

Recall from (4a) and (4b) that $f \equiv \alpha(x) H_0$ and $H \equiv \psi(x) H_0$. Then

$$\gamma \equiv \frac{p_2}{p_1} = \frac{\beta_1}{\beta_2} \frac{\sqrt{\frac{\beta_2^2}{C^2} - 1}}{\sqrt{1 - \frac{\beta_1^2}{C^2}}} = \frac{1}{\chi} \sqrt{\frac{\chi^2 \epsilon^2 - 1}{1 - \epsilon^2}} \tag{23}$$

Let

$$p_1 H \equiv \lambda \psi(x) \sqrt{1-\epsilon^2(x)} \; ; \qquad p_1 f \equiv \lambda \alpha(x) \sqrt{1-\epsilon^2(x)} \qquad (24); \; (25)$$

Define

$$y \equiv \gamma \xi p_1 H = \frac{\xi}{\chi} \sqrt{\frac{\chi^2 \epsilon^2 - 1}{1 - \epsilon^2}} \; \lambda \psi(x) \sqrt{1 - \epsilon^2} = \frac{\lambda \psi(x) \xi}{\chi} \sqrt{\chi^2 \epsilon^2 - 1} \qquad (26)$$

Then

$$y^2 = \frac{\lambda^2 \psi^2(x) \xi^2}{\chi^2} \left(\chi^2 \epsilon^2 - 1 \right) \qquad (27)$$

or

$$\epsilon^2 = \frac{y^2}{\lambda^2 \psi^2(x) \xi^2} + \frac{1}{\chi^2} \qquad (28)$$

Now from the period equation as given by (14) one has

$$y \equiv p_1 H \gamma \xi = -p_1 H \left(\frac{\sin p_1 H \cos p_1 f - \sin p_1 f \cos p_1 H + \Phi_0/p_1}{\sin p_1 f \sin p_1 H + \cos p_1 H \cos p_1 f} \right) \equiv -p_1 H(\cdot) \qquad (29)$$

Also from (28) and (24)

$$1 - \left(\frac{p_1 H}{\lambda \psi} \right)^2 = \frac{y^2}{\lambda^2 \psi^2 \xi^2} + \frac{1}{\chi^2} \qquad (30)$$

or

$$\frac{y^2}{\xi^2} + \left(p_1 H \right)^2 = \lambda^2 \psi^2 \left(1 - \frac{1}{\chi^2} \right) \qquad (31)$$

which is the equation of an ellipse. Then using the above expression for y given by (29) and (24) one gets

$$\frac{(p_1 H)^2}{\xi^2} (\cdot)^2 + (p_1 H)^2 = \frac{(p_1 H)^2}{1 - \epsilon^2} \left(1 - \frac{1}{\chi^2} \right) \qquad (32)$$

or finally

$$\epsilon = \left[1 - \frac{1 - \dfrac{1}{\chi^2}}{1 + \dfrac{(.)^2}{\xi^2}} \right]^{1/2} \tag{33}$$

Examining the case of the uniform layer $(\Phi_0 \equiv 0)$, it is clear that, when $(.) \to 0$ which occurs, among other possible cases, when $\omega \to 0$, one obtains from (33), using also the definition for χ in (21), that $C \to \beta_2$. Also, when $(.) \to +\infty$, $\epsilon \to 1$ and therefore $C \to \beta_1$. Both limiting cases are as expected. For a layer with a variable thickness along the x-direction it would be expected that under certain restrictions $\Phi_0(x)/p_1$ could be small so that it can be neglected in its contribution to the term in $(.)$ given by (29). Defining $(.)^* = (.)_{\Phi_0 = 0}$ one can write

$$(.)^* \equiv \frac{\sin p_1 f \cos p_1 H - \sin p_1 H \cos p_1 f}{\sin p_1 f \sin p_1 H + \cos p_1 H \cos p_1 f} \tag{34}$$

and

$$(.) = (.)^* \left[1 - \frac{\Phi_0/p_1}{(\sin p_1 f \sin p_1 H + \cos p_1 H \cos p_1 f)(.)^*} \right] \tag{35}$$

Simple trigonometric transformation shows that

$$(.)^* \equiv \tan(p_1 f - p_1 H) = -\tan(p_1 H - p_1 f) \tag{34'}$$

and from definitions (24) and (25) for $p_1 H$ and $p_1 f$

$$p_1 H - p_1 f = p_1 H_0 \left(\Psi(x) - \alpha(x) \right) \equiv p_1 H(x) \tag{36}$$

also

$$\frac{p_1 H(x)}{\sqrt{1-\epsilon^2(x)}} = \frac{\omega H_0}{\beta_1}\Big(\psi(x) - \alpha(x)\Big) \tag{37}$$

Since

$$\tan\alpha = \tan(\alpha + n\pi) ; \qquad n = 0, 1, \ldots$$

identifying $p_1 H(x)$ with $\alpha + n\pi$ following can be written

$$\frac{\alpha + n\pi}{\sqrt{1-\epsilon^2(x)}} = \lambda\Big(\psi(x) - \alpha(x)\Big) \tag{38}$$

where $n = 0, 1, 2, \ldots$ corresponds to the fundamental, first, second and higher modes. The usual approach in many treatments of the period equation is to solve the transcendental equation (14) by some numerical method. It is proposed here, instead, to choose n first, which determines the mode to be considered and then to choose the value of α in the interval $0 < \alpha < \frac{\pi}{2}$. Using $\alpha + n\pi$ in place of $p_1 H(x)$ in equation (33) yields then the value of $\epsilon(x)$ for that α and n. Equation (38) then gives the resulting value of $\lambda(\psi(x) - \alpha(x))$, i.e., λ which is given by $\frac{\omega H_0}{\beta_1}$. Thus sweeping α in the interval $(0, \pi/2)$ will sweep out all values of $\lambda\epsilon(0, \infty)$ and all corresponding values of $\epsilon(x)$ in the interval $\left(\frac{1}{\chi}, 1\right)$. Since this can be done with great accuracy and for any spacing of the originally chosen value of α this approach may be much better than solving the transcendental equation (14) which must be done by a method of interpolation which may be very time consuming.

Consider again the expression

$$(\cdot) = (\cdot)^* \left[1 + \frac{\Phi_0 / p_1}{(\sin p_1 H \cos p_1 f - \sin p_1 f \cos p_1 H)} \right] \tag{35}$$

Since $\sin p_1 H \cos p_1 f - \sin p_1 f \cos p_1 H = \sin(p_1 H - p_1 f)$, (35) becomes

$$(\cdot) = (\cdot)^* \left[1 + \frac{\Phi_0}{p_1} \frac{1}{\sin(p_1 H - p_1 f)} \right] \equiv (\cdot)^* A \tag{35$'$}$$

where

$$A \equiv 1 + \frac{1}{\sin(\alpha + n\pi)} \frac{\Phi_0}{p_1} \tag{39}$$

So far, nothing has been said about Φ_0 except that one could hope that it is "small" for some values of the parameters. If that condition is satisfied in addition α must be close to $\pi/2$ so that $|\sin(\alpha + n\pi)|$ is close to 1 and consequently $A \approx 1$. Thus if Φ_0 is small for α in the proximity of $\pi/2$ it could be expected that the approximation to $\epsilon(x)$ calculated from (33) by interchanging $(\cdot)$ by $(\cdot)^*$ will be good.

It can be shown (using expression (6) in Appendix II) that $\varkappa_{H_f}$ is given by

$$\varkappa_{H_f} = \frac{1}{2} \frac{1}{C(x)} \frac{dC(x)}{dx} - \frac{\omega}{C(x)} \left(1 - \frac{x}{C(x)} \frac{dC(x)}{dx} \right) \tan \frac{\omega x}{C(x)} + O\left(\frac{1}{\cos \frac{\omega x}{C(x)}} \right) \tag{40}$$

Since

$$\epsilon(x) = \frac{\beta_1}{C(x)}, \qquad \frac{dC(x)}{dx} = -\frac{\beta_1}{\epsilon^2(x)} \frac{d\epsilon(x)}{dx}$$

and

$$|\varkappa_{H_f}| \lesssim \frac{1}{2} \frac{1}{\epsilon(x)} \frac{d\epsilon(x)}{dx} + \frac{\omega}{C(x)} \left(1 + \frac{xC(x)}{\beta_1} \frac{d\epsilon(x)}{dx} \right) \tan \frac{\omega x}{C(x)}$$
$$+ O\left(\frac{1}{\cos \frac{\omega x}{C(x)}} \right) \tag{41}$$

When α is close to $\pi/2$, $C(x) \sim \beta_1$ and $\frac{d\epsilon(x)}{dx} \to 0$ so that

$$\left| \underset{f}{\overset{\varkappa}{H}} \right| \cos \frac{\omega x}{C(x)} \lesssim \frac{\omega}{C(x)} \left(1 + x \frac{d\epsilon(x)}{dx} \right) + O(1) \tag{42}$$

From definitions (7a) and (7b) and using the result (29) from Appendix II one can write

$$\left| \epsilon \binom{H}{f} \right| = O\left[\frac{\omega H(x)}{\beta_1} \binom{\theta}{\eta} \right] = O\left[\frac{\omega H(x)}{\beta_1} A_0 \right] \tag{43}$$

$$\left| \delta \binom{H}{f} \right| = O\left[\frac{\omega H(x)}{\beta_1} \binom{\theta}{\eta} \right] = O\left[\frac{\omega H(x)}{\beta_1} A_0 \right] \tag{44}$$

Further, using (7c) and (11c), i.e.,

$$c(f) \equiv -\varkappa_f - \xi \rho(f) e^{P_2 f} \tag{45}$$

it can be shown that

$$\left| c(f) \right| = O\left[\frac{\omega H(x)}{\beta_1} A_0 \right] \tag{46}$$

where $A_0 \equiv \max [\theta, \eta]$ over $x\epsilon[a, b]$.

To avoid difficulty in the behavior of $\underset{f}{\overset{\varkappa}{H}}$ when $\frac{\omega x}{C(x)}$ becomes $\frac{\pi}{2} + n\pi$, and since $\underset{f}{\varkappa_H}$ were introduced for formal convenience only, the whole period equation (14) can be multiplied by $\cos^2 \frac{\omega x}{C(x)}$. This does not affect the previous results since the equation has to vanish for any x anyway. Then one may observe that $\Phi_0 \cos^2 \frac{\omega x}{C(x)} \equiv \Phi_0'$ will now be an appropriate error term to consider. Using (11a) and (11b) multiplied by $\cos^2 \frac{\omega x}{C(x)}$, the following can be written

$$\left|\cos^2 \frac{\omega x}{C(x)}\left[a\binom{H}{f}\right]\right|, \quad \left|\cos^2 \frac{\omega x}{C(x)}\left[b\binom{H}{f}\right]\right| \lesssim \frac{\omega}{C(x)}\left(1 + x\frac{d\epsilon(x)}{dx}\right) +$$

$$+ O\left[\frac{\omega H(x)}{\beta_1}\binom{\theta}{\eta}\right] \lesssim O\left[\frac{\omega H(x)}{\beta_1}\left(1 + \binom{\theta}{\eta}(1+x)\right)\right] \equiv M \quad (47)$$

using the result (obtained in Appendix II) that $\frac{d\epsilon}{dx} \sim \binom{\theta}{\eta}$ when α is close to $\pi/2$. Now using the above derived individual bounds on terms, that enter in the expression for Φ_0 in (15), one can bound Φ_0' using the following definitions:

$$A_\theta^\eta \equiv \max_{x\epsilon[a,b]} (\tan\theta, \tan\eta) \quad (48)$$

$$\xi p_2 \leq \frac{\xi\omega}{\beta_1\chi}\sqrt{\chi^2 - 1} \equiv N \quad (49)$$

Then from (15) it follows that

$$\left|\frac{\Phi_0 \cos^2 \frac{\omega x}{C(x)}}{p_1}\right| \leq \frac{A_\theta^\eta}{p_1^2}\left[2MN + 2Mp_1 + 4p_1M + 4A_\theta^\eta M^2\right] \quad (50)$$

Now remembering that $p_1 H(x) = \alpha + n\pi$ and using (47), (48) and (49), the following can be written

$$\left|\frac{\Phi_0'}{p_1}\right| = O\left\{A_\theta^\eta \frac{\omega^2 H^2(x)}{\beta_1^2(\alpha + n\pi)^2}\left[1 + \binom{\theta}{\eta}(1+x)\right]\right\} \quad (51)$$

Here, the term $\binom{\theta}{\eta}(1+x)$ is left explicitly in the order term in (51) only to illustrate the x dependence of the error. For $x\epsilon[a,b]$ this term could have been absorbed in the order constant in (51). With this result, relation (39) becomes

$$A = 1 + \frac{1}{\sin(\alpha + n\pi)} \; O\left[A_\theta^\eta \; \frac{\omega^2 H^2(x)}{\beta_1^2(\alpha + n\pi)^2} \left[1 + \left(\frac{\theta}{\eta}\right)(1+x) \right] \right] \tag{52}$$

The only possible way for A to be "close" to 1 is that α be away from zero and that order term defined by (51) be small. This can be achieved only if A_θ^η which is the maximum value of the slope of the surface of the layer or of the contact of the layer and the infinite medium is small. Therefore it should be required that A_θ^η be of the order

$$A_\theta^\eta = O\left\{ \frac{\beta_1^2(\alpha + n\pi)^2}{\omega^2 H^2(x)} \; \frac{1}{\left[1 + \left(\frac{\theta}{\eta}\right)(1+x) \right]} \right\} \tag{53}$$

Remembering that when $\alpha \to \frac{\pi}{2}$, the parameter $\frac{\omega H(x)}{\beta_1}$ tends to infinity, it is seen that a compromise must be made so that α is close to $\pi/2$ but still not "too close" so that the term $\frac{\omega H(x)}{\beta_1}$ does not become too large. These requirements are certainly very severe but it still may be expected that when (53) is satisfied the approximate solution can be used.

APPENDIX II

ERRORS OF THE APPROXIMATE SOLUTION

The form of the approximate solution associated with each modeshape frequency and corresponding characteristic value or phase velocity C has been shown to be the product of the three functions $X(x)$, $Z(x, z)$ and $T(t)$, so that

$$v(x, z, t) = X(x) Z(x, z) T(t) \tag{1}$$

It was also shown that for the arbitrarily chosen initial conditions

$$T(t) = \cos \omega t \tag{2}$$

$$X(x) = C^{1/2}(x) \cos \frac{\omega x}{C(x)} + O\left(\frac{C^{1/2}(x)}{\omega} \right) \tag{3}$$

and

$$Z(x, z) = \begin{cases} C \sin p_1 z + D \cos p_1 z, & \text{in the layer} \\ F e^{-p_2 z} & \text{in the infinite medium} \end{cases} \tag{4}$$

with

$$p_1 \equiv \frac{\omega}{\beta_1} \sqrt{1 - \frac{\beta_1^2}{C^2(x)}}$$

and

$$p_2 \equiv \frac{\omega}{\beta_2} \sqrt{\frac{\beta_2^2}{C^2(x)} - 1}$$

where $Z(x, z)$ is the form of the solution of the modal equation in the layer and in the infinite medium. Remembering that $H(x) \equiv - H_0(\alpha(x) - \psi(x))$ and normalizing modeshapes so that the surface amplitude equals unity,

one can write

$$Z(x, z) = \begin{cases} \cos p_1(z-\psi(x)H_0) & \text{in the layer} \\ \\ \cos p_1 H_0(\alpha(x)-\psi(x))e^{-p_2 z + p_2 \alpha(x)H_0} & \text{in the infinite medium} \end{cases} \quad (4')$$

when the boundary conditions 1, 2, 3 and 4 (Section C) have been used.

It will be useful to write down some derivatives of the above solutions.

$$T_{tt} = -\omega^2 \cos \omega t \quad (5)$$

$$X_x = \frac{1}{2}C^{-1/2}(x)\frac{dC(x)}{dx}\cos\frac{\omega x}{C(x)} - C^{1/2}(x)\left[\frac{\omega}{C(x)} - \frac{\omega x}{C^2(x)}\frac{dC(x)}{dx}\right]\sin\frac{\omega x}{C(x)} + O(1) \quad (6)$$

The first and second derivatives of $Z(x, z)$ with respect to x become, in the layer,

$$Z_x(x,z) = -(z-\psi(x)H_0)\frac{dp_1}{dx}\sin p_1(z-\psi(x)H_0) + H_0 p_1\frac{d\psi(x)}{dx}\sin p_1(z-\psi(x)H_0) \quad (7)$$

and

$$Z_{xx}(x, z) = \left[H_0\frac{dp_1}{dx}\frac{d\psi(x)}{dx} + H_0 p_1\frac{d^2\psi(x)}{dx^2} + H_0\frac{d\psi(x)}{dx}\frac{dp_1}{dx}\right.$$

$$\left. -(z-\psi(x)H_0)\frac{d^2 p_1}{dx^2}\right]\sin p_1(z-\psi(x)H_0) + \left[H_0 p_1\frac{d\psi(x)}{dx}\right.$$

$$\left. -(z-\psi(x)H_0)\frac{dp_1}{dx}\right]\cdot\left[(z-\psi(x)H_0)\frac{dp_1}{dx}\right.$$

$$\left. -H_0 p_1\frac{d\psi(x)}{dx}\right]\cos p_1(z-\psi(x)H_0) \quad (8)$$

Now since $\rho/\mu \equiv 1/\beta^2$, because the shear wave velocity of SH waves is given by $\beta = \sqrt{\mu/\rho}$, it then follows

$$\frac{\rho}{\mu} \frac{T_{tt}}{T} = -\frac{\omega^2}{\beta^2} \tag{9}$$

$$\frac{X_{xx}}{X} = -\frac{\omega^2}{C^2(x)} \tag{10}$$

where (10) comes directly from the differential equation for X, assuming that T and X do not vanish at this point.

From the differential equation for $Z(x, z)$, also directly, if $Z(x, z) \neq 0$, it follows that

$$\frac{Z_{zz}}{Z} = \begin{cases} -p_1^2 & \text{in the layer} \\ p_2^2 & \text{in the infinite medium} \end{cases} \tag{11}$$

Substitution of the assumed solution $v(x, z, t) = X(x)Z(x, z)T(t)$ into the differential equation (3) (Section C) gives (omitting the arguments in the functions)

$$XZT\left(\frac{\rho}{\mu} \frac{T_{tt}}{T} - \frac{X_{xx}}{X} - \frac{Z_{zz}}{Z}\right) - XZT\left(2\frac{X_x Z_x}{XZ} + \frac{Z_{xx}}{Z}\right) \stackrel{?}{=} 0 \tag{12}$$

For the layer of uniform thickness in the x direction, the second term in the brackets in equation (12) would vanish by virtue of the fact that $Z(x, z)$ would not be a function of x. The question mark on the equality sign in equation (12) indicates that if one had the exact solution to the problem then one would have equalities for all x, z and t. Since here only a trial solution $v(x, z, t)$ has been considered as suggested by a limiting case of a layer with a constant thickness, no equality can be expected to hold in general.

Now substituting relations (9), (10) and (11) into the first bracket on the left in equation (12) it follows

$$-\frac{\omega^2}{\beta_1^2} + \frac{\omega^2}{C^2(x)} + \frac{\omega^2}{\beta_1^2}\left(1 - \frac{\beta_1^2}{C^2(x)}\right) \equiv 0 \quad \text{in the layer}$$

and

$$-\frac{\omega^2}{\beta_2^2} + \frac{\omega^2}{C^2(x)} - \frac{\omega^2}{\beta_2^2}\left(\frac{\beta_2^2}{C^2(x)} - 1\right) \equiv 0 \quad \text{in the infinite medium.}$$

Thus the first term in equation (12) is always zero and so this shows that $v(x, z, t) = X(x)Z(z)T(t)$ indeed satisfies exactly the differential equation for the layer with $H(x) = H_0 = \text{const.}$

If the trial solution to equation (12) is to be acceptable at least in the asymptotic sense, then the contribution to the differential equation from the second term in brackets should be "small". That is

$$2X_x Z_z + X Z_{xx} = \text{error} \tag{13}$$

should be small.

Before interpreting the above error term it is necessary to consider first the behavior of the derivatives of p_1 along the x axis.

$$p_1 \equiv \frac{\omega}{\beta_1}\sqrt{1 - \frac{\beta_1^2}{C^2(x)}}$$

Here $C(x)$ is the velocity of the wave front along the surface of the layer (A in Fig. 2.6) while β_1 is the velocity of the SH wave in the layer. Denoting by φ the angle between the ray and the normal to the boundary of the layer, one has (here φ is used instead of θ as given in Fig. 2.6 to avoid ambiguity in notation, since $\frac{\partial \alpha(x)}{\partial x} = \tan\theta$ as given in Fig. 2.4)

$$\varepsilon(x) = \frac{\beta_1}{C(x)} = \sin\varphi \tag{14}$$

and from (14)

$$P_1 = \frac{\omega}{\beta_1}\sqrt{1-\sin^2\varphi} = \frac{\omega}{\beta_1}\cos\varphi \tag{15}$$

Now

$$\frac{dp_1}{dx} = \frac{\partial p_1}{\partial\varphi}\frac{d\varphi}{dx} = -\frac{\omega}{\beta_1}\sin\varphi\frac{d\varphi}{dx} \tag{16}$$

where $d\varphi/dx$ represents a change of φ along the x direction. Since the layer medium is uniform, this change can occur only on the boundary of the layer. If the boundary has a slope θ or η with respect to the horizontal, $d\varphi/dx$ will be equal to θ or η depending on the boundary in question (see Fig. 2.4). Thus

$$\frac{dp_1}{dx} = -\frac{\omega}{\beta_1}\sin\varphi\binom{\theta}{\eta} \tag{17}$$

Also

$$\frac{d^2p_1}{dx^2} = \frac{\partial^2 p_1}{\partial\varphi^2}\left(\frac{d\varphi}{dx}\right)^2 + \frac{\partial p_1}{\partial\varphi}\frac{d^2\varphi}{dx^2} = -\frac{\omega}{\beta_1}\cos\varphi\binom{\theta}{\eta}^2 - \frac{\omega}{\beta_1}\sin\varphi\begin{bmatrix}\dfrac{d\theta}{dx}\\[4pt]\dfrac{d\eta}{dx}\end{bmatrix} \tag{18}$$

Now since $\epsilon = \sin\varphi$ from (14)

$$\frac{d\epsilon}{dx} = \cos\varphi\frac{d\varphi}{dx} = \cos\varphi\binom{\theta}{\eta} \tag{19}$$

and also

$$\frac{d^2\epsilon}{dx^2} = -\sin\varphi\left(\frac{d\varphi}{dx}\right)^2 + \cos\varphi\frac{d^2\varphi}{dx^2} = \cos\varphi\begin{bmatrix}\dfrac{d\theta}{dx}\\[4pt]\dfrac{d\eta}{dx}\end{bmatrix} - \sin\varphi\binom{\theta}{\eta} \tag{20}$$

Define now

$$A \equiv \max_{x\epsilon[a,b]}\left[\theta(x),\eta(x)\right] \tag{21}$$

143

and

$$K \equiv \max_{x\epsilon[a,b]} \left[\frac{d\theta(x)}{dx}, \frac{d\eta(x)}{dx} \right] \tag{22}$$

If it is assumed that both A and K are snall, then neglecting squares of small quantities one can write

$$\max_{x\epsilon[a,b]} \left| \frac{dp_1}{dx} \right| = \frac{\omega}{\beta_1} A \tag{23}$$

$$\max_{x\epsilon[a,b]} \left| \frac{d^2 p_1}{dx^2} \right| \sim \frac{\omega}{\beta_1} K \tag{24}$$

Also, from Fig. 2.4 for small θ and η it follows that

$$\frac{d\alpha(x)}{dx} \approx \theta(x) \quad \text{and} \quad \frac{d\psi(x)}{dx} \approx \eta(x) \tag{25},(26)$$

so that

$$\max_{x\epsilon[a,b]} \left| \frac{d\psi}{dx} \right| \approx A \tag{27}$$

and

$$\max_{x\epsilon[a,b]} \left| \frac{d^2\psi}{dx^2} \right| \approx K \tag{28}$$

If now the above bounds given by (21) to (28) together with (15) are used in (7) and (8) one can write

$$\max_{x\epsilon[a,b]} |Z_x(x,z)| \leqslant H(x)A\left(1+\frac{\omega}{\beta_1}\right) \tag{29}$$

and

$$\max_{x\epsilon[a,b]} |Z_{xx}(x,z)| \leqslant H(x)\frac{\omega}{\beta_1}\left(2A^2+2K\right) + 4H^2(x)\frac{\omega^2}{\beta_1^2}A^2 \tag{30}$$

Recalling the expression for the derivative of X(x) function (6) and using the relation

$$\frac{dC(x)}{dx} = \frac{\partial C}{\partial \epsilon} \frac{d\epsilon}{dx} = -\frac{\beta_1}{\epsilon^2} \frac{d\epsilon}{dx} \tag{31}$$

together with bounds for $d\epsilon/dx$ given by (19), it can be shown by the direct substitution of (31) and (19) into the (6) that

$$\max_{x\epsilon[a,b]} |X_x(x)| = O\left[\frac{\omega}{\beta_1}(1 + xA)\right] \tag{32}$$

Now, expressions (29), (30) and (32) can be used to estimate the order of the error in the differential equation (12) given by (13). Since, the the error in the layer is given by

$$E \equiv 2X_x Z_x + XZ_{xx} \tag{13}$$

neglecting the contribution of the higher order terms, E becomes

$$E = O\left[\frac{\omega}{\beta_1}(1 + xA)\right] \cdot H(x)A\left(1 + \frac{\omega}{\beta_1}\right) + 4H^2(x)\frac{\omega^2}{\beta_1^2}A^2 \tag{33}$$

Here the first term in (30) was neglected because both A^2 and K are assumed to be second order small quantities. From (33) it follows that

$$E = O\left[\frac{\omega^2 H^2(x)}{\beta_1^2}A\right] \tag{34}$$

for $x\epsilon[a,b]$, where the interval $[a,b]$ is sufficiently small, i.e., at most

$$b-a = O\left(\frac{1}{A}\right) \tag{35}$$

This illustrates that the quality of the solution "becomes worse" as one goes "too far" along the x axis. This appears to be obvious also from simple physical insight into the problem.

The analysis of the error has been concentrated so far only on the part of the solution $v(x, z, t)$ in the surface layer, i.e., when $H_0 \psi(x) \leq z \leq H_0 \alpha(x)$. The form of the solution, given by $(4')$ in the infinite medium for $z \geq \alpha(x) H_0$ contains an exponential $e^{-p_2 z}$ where $p_2 > 0$. Continuity of the approximate solution across the boundary $\alpha(x) H_0$ indicates that the error has to be continuous also and of precisely the same order as (34) in the vicinity of the boundary $\alpha(x) H_0$. The presence of the exponential term $e^{-p_2 z}$ causes the error to exponentially decrease as $z \to \infty$. Thus it follows that the error in approximating the differential equation (12) by $v(x, z, t)$ is also of a "surface character" as are the waves considered.

It is interesting to observe that when $\alpha \to \pi/2$, $\frac{\omega H(x)}{\beta_1} \to \infty$. Thus in fact α may not attain exactly the value of $\pi/2$ because in the limit E would become infinite for any fixed A away from zero. This, however, does not mean that the solution developed is not useful in the fairly wide range of values of $\frac{\omega H(x)}{\beta_1}$ when $\alpha \epsilon \left(\frac{\pi}{2} \Omega, \frac{\pi}{2} \right)$, and where Ω is less than 1, but sufficiently far away from zero. In fact when $\frac{\omega H(x)}{\beta_1} \epsilon I$ and $I \equiv (\sim 2, M)$ where M is chosen so that $M^2 A \ll 1$, many practical cases of interest can still be successfully treated by this approximate approach.

REFERENCES

Aki, K. (1966). Generation and propagation of G waves from the
Niigata earthquake of June 16, 1964, Part 2. Estimation of the
earthquake moment release, energy, and stress-strain drop
from the G wave spectrum, Bull, Earthquake Res. Inst.,
Tokyo Univ., 44, 73-88.

Alford, J. L., G. W. Housner and R. R. Martel (1951). Spectrum
analysis of strong-motion earthquakes. Earthquake Eng. Res.
Laboratory, California Institute of Technology.

Allen, C. R., A. Grantz, J. N. Brune, M. M. Clark, R. V. Sharp,
T. G. Theodore, E. W. Wolfe and M. Wyss (1968). The
Borrego Mountain, California, Earthquake of 9 April 1968:
A Preliminary Report, Bull. Seism. Soc. Amer., 58,
1183-1186.

Ben-Menahem, A. and D. G. Harkrider (1964). Radiation patterns
of seismic surface waves from buried dipolar point sources in
a flat stratified earth. J. Geoph. Res., 69, 2605-2620.

Biehler, S. (1964). Geophysical study of the salton trough of
Southern California, Ph. D. Thesis, California Institute of
Technology.

Birch, F. (1961). The velocity of compressional waves in rocks to
10 kilobars, 2, J. Geoph. Res. 66, 2199-2224.

Brune, J. N. (1968). Seismic moment, seismicity and rate of the
slip along major fault zones, J. Geoph. Res., 73, 777-784.

Brune, J. N. and C. R. Allen (1967). A low-stress-drop, low
magnitude earthquake with surface faulting: The Imperial,
California, earthquake of March 4, 1965. Bull. Seism. Soc.
Amer., 57, 501-514.

Brune, J. N. and G. R. Engen (1968). Excitation of Mantle Love
waves and definition of mantle wave magnitude, in press.

Brune, J. N. and C. King (1967). Excitation of Mantle Rayleigh
waves of period 100 seconds as a function of magnitude, Bull.
Seism. Soc. Amer., 57, 1355-1365.

Buwalda, J. P. Unpublished field notes (original notebook and some
additional data were kindly supplied by Prof. C. R. Allen).

147

Byerly, D. and J. M. DeNoyer (1958). Energy in earthquakes as computed from geodetic observations [Chapter 2], Benioff, V. H., and other eds., Contributions in Geophysics: Internat. Ser. Mons. Earth Sci., v. 1, 17-35.

Courant, R. and D. Hilbert (1931). Methoden der Mathematischen Physik, Springer Verlag.

DeNoyer, J. (1961). The effect of variations in layer thickness on Love waves, Bull. Seism. Soc. Amer., 51, 227-235.

Eaton, J. P. (1967). Instrumental seismic studies — The Parkfield-Cholome, California, earthquakes of June-August 1966, U. S. Geol. Survey Prof. Paper 579, 57-65.

Ewing, M. W., Jardetzky, S. W. and Press, F. (1957). Elastic waves in layered media, McGraw-Hill.

Florensov, N. A. and V. P. Solonenko (1963). The Gobi-Altai Earthquake, Isdatel'stvo Akademii Nank S.S.R., Moscow, p. 392.

Gutenberg, B. (1957). Effects of ground on earthquake motion, Bull. Seism. Soc. Amer., 47, 221-250.

Hamilton, R. M. and J. H. Healy (1969). Seismic activity associated with nuclear explosions, in press.

Homma, S. (1952). Love waves in a surface layer of varying thickness, Geophys. Mag. (Tokyo), 24, 9-14.

Housner, G. W. and M. D. Trifunac (1967). Analysis of accelerograms — Parkfield Earthquake, Bull. Seism. Soc. Amer., 57, 1193-1220.

Hudson, D. E. (1962). Some problems in the application of spectrum techniques to strong-motion earthquake analysis, Bull. Seism. Soc. Amer., 52, 417-430.

Hudson, J. A. (1962). The total internal reflection of SH waves, Geophysical Journal, Royal Astr. Soc., 6, 509-531.

Knopoff, L. (1958). Energy release in earthquakes, Geophys. J., 1, 44-52.

Maruyama, T. (1963). On the force equivalent of dynamic elastic dislocations with reference to the earthquake mechanism, Bull. Earthquake Res. Inst., Tokyo Univ., 41, 467-486.

Richter, C. F. (1958). Elementary Seismology, N. H. Freeman.

Savage, J. C. (1965). The stopping phase on Seismograms, Bull. Seism. Soc. Amer., 55, 47-58.

Shelton, S. A. (1963). Surface wave propagation in the western
    United States, Ph. D. Thesis, California Institute of Technology.

Tsai, N. C. (1969). Influence of local geology on earthquake ground
    motion, Ph. D. Thesis, California Institute of Technology.

Whitman, R. V. (1968). Local soil condition upon seismic threat to
    Nuclear Power Plant, Report for Stone and Webster Eng. Corp.

Wu, F. T. (1968). Parkfield earthquake of June 29, 1966;
    Magnitude and source mechanism, Bull. Seism. Soc. Amer.,
    58, 689-709.

Wyss, M. and J. N. Brune (1967). The Alaska earthquake of
    28 March 1964; A complex multiple structure, Bull. Seism.
    Soc. Amer., 57, 1017-1023.

Wyss, M. and J. N. Brune (1968). Seismic Moment, Stress and
    Source Dimensions for Earthquakes in California-Nevada Region,
    J. Geoph. Res., 73, 4681-4694.